The role of Ciliary Neurotrophic Factor in hippocampal synaptic plasticity and learning

Die Rolle von Ciliary Neurotrophic Factor bei hippocampaler synaptischer Plastizität und Lernen

Doctoral thesis for a doctoral degree

at the Graduate School of Life Sciences,

Julius-Maximilians-Universität Würzburg,

Section Neuroscience

submitted by

Cora Freifrau Rüdt von Collenberg

from

Nürnberg

Würzburg, 2019

Submitted on:

……..……..

Office stamp

Members of the *Promotionskomitee*:

Chairperson: Prof. Dr. Thomas Dandekar

Primary Supervisor: Prof. Dr. Michael Sendtner

Supervisor (Second): PD Dr. Robert Blum

Supervisor (Third): Prof. Dr. Martin Korte

Members of the *defence committee*

Chairperson: Prof. Dr. Caroline Kisker

Prof. Dr. Esther Asan

Prof. Dr. Andreas Draguhn

Prof. Dr. Christian Rosenmund

Date of Public Defence: ……..……

Date of Receipt of Certificates:……..

Für meine Familie

Für meinen Mann

TABLE OF CONTENTS

Abstract

Ciliary neurotrophic factor (Cntf) acts as a differentiation and survival factor for different types of neurons and glial cells. It is expressed by peripheral Schwann cells and astrocytes in the central nervous system and mediates its effects via a receptor complex involving CntfRα, LifRß and gp130, leading to downstream activation of Stat3. Recent studies by our group have shown that Cntf modulates neuronal microtubule dynamics via Stat3/stathmin interaction. In a mouse model for motor neuron disease, i.e. *pmn*, Cntf is able to rescue axonal degeneration through Stat3/stathmin signaling. While these findings suggest a role of Cntf in controlling axonal functions in the neuromuscular system, additional data indicate that Cntf might also play a role in synaptic plasticity in the hippocampus. Electrophysiological recordings in hippocampal organotypic cultures and acute slices revealed a deficit in long-term potentiation (LTP) in *Cntf* $^{-/-}$ mice. This deficit was rescued by 24 h stimulation with Cntf, combined with an acute application of Cntf during LTP-measurements indicating that Cntf is both necessary and sufficient for hippocampal LTP, and possibly synaptic plasticity. Therefore, *Cntf* knockout mice were investigated to elucidate this possible role of Cntf in hippocampal LTP and synaptic plasticity.

First, we validated the presence of Cntf in the target tissue: in the hippocampus, Cntf was localized in Gfap-positive astrocytes surrounding small blood vessels in the fissure and in meningeal areas close to the dentate gyrus. Laser micro-dissection and qPCR analysis showed a similar distribution of Cntf-coding mRNA validating the obtained immunofluorescent results. Despite the strong LTP deficit in organotypic cultures, *in vivo* behavior of *Cntf* $^{-/-}$ mice regarding hippocampus-dependent learning and anxiety-related paradigms was largely inconspicuous. However, western blot analysis of hippocampal organotypic cultures revealed a significant reduction of pStat3 levels in *Cntf* $^{-/-}$ cultures under baseline conditions, which in turn were elevated upon Cntf stimulation. In order to resolve and examine synaptic structures we turned to *in vitro* analysis of cultured hippocampal neurons which indicated that pStat3 is predominantly located in the presynapse. In line with these findings, presynapses of *Cntf* $^{-/-}$ cultures were reduced in size and when in contact to astrocytes, contained less pStat3 immunoreactivity compared to presynapses in wildtype cultures.

In conclusion, our findings hypothesize that despite of a largely inconspicuous behavioral phenotype of *Cntf* $^{-/-}$ mice, Cntf appears to have an influence on pStat3 levels at hippocampal synapses. In a next step these two key questions need to be addressed experimentally: 1) is there a compensatory mechanism by members of the Cntf family, possibly downstream of

pStat3, which explains the *in vivo* behavioral results of *Cntf* $^{-/-}$ mice and can likewise account for the largely inconspicuous phenotype in CNTF-deficient humans? 2) How exactly does Cntf influence LTP through Stat3 signaling? To unravel the underlying mechanism further experiments should therefore investigate whether microtubule dynamics downstream of Stat3 and stathmin signaling are involved in the Cntf-induced modulation of hippocampal synaptic plasticity, similar to as it was shown in motoneurons.

Zusammenfassung

Ciliary neurotrophic factor (Cntf) wirkt als Differenzierungs- und Überlebensfaktor für verschiedene Arten von Neuronen und Gliazellen. Es wird von peripheren Schwann´schen Zellen und Astrozyten des zentralen Nervensystems exprimiert und vermittelt seine Effekte über einen Rezeptorenkomplex, der aus CntfRα, LifRß und gp130 besteht, und zu einer nachfolgenden Aktivierung von Stat3 führt. Jüngste Studien unserer Arbeitsgruppe haben gezeigt, dass Cntf neuronale Mikrotubulidynamik über Stat3/stathmin Interaktion modulieren kann. In *pmn* Mäusen, einem Mausmodell für Motoneuronenerkrankungen, ist Cntf in der Lage, durch Stat3/Stathmin Signaltransduktion die zugrundeliegende axonale Degeneration wieder aufzuheben. Während diese Ergebnisse eine Rolle von Cntf bei der Kontrolle axonaler Funktionen im neuromuskulären System postulieren, deuten zusätzliche Daten darauf hin, dass Cntf ebenfalls eine Funktion bei synaptischer Plastizität im Hippocampus ausübt. Elektrophysiologische Messungen in hippocampalen organotypischen Kulturen und akuten Schnitten zeigen ein Defizit in der Langzeitpotenzierung (LTP) bei *Cntf* $^{-/-}$ Mäusen. Dieses Defizit konnte durch eine 24 stündige Stimulation mit Cntf, in Kombination mit akuter Zugabe von Cntf während der LTP Messungen, kompensiert werden. Dies weist darauf hin, dass Cntf sowohl notwendig als auch ausreichend für hippocampale LTP und möglicherweise synaptische Plasizität ist. Deshalb wurden Cntf knockout Mäuse untersucht, um diese putative Rolle von Cntf bei hippocampaler LTP und synaptischer Plastizität zu untersuchen.

Zunächst haben wir die Lokalisation von Cntf in unserem Zielgewebe bestätigt: im Hippocampus war Cntf sowohl in Gfap-positiven Astrocyten lokalisiert, die kleine Blutgefäße in der Fissur umschließen, als auch in Gfap-positiven Astrocyten nahe des *Gyrus dentatus*. Lasermikrodissektion und qPCR-Analysen zeigten eine ähnliche Verteilung von Cntf kodierender mRNA, und bestätigten somit die durch Immunoflureszenz-Färbung erworbenen Ergebnisse. Trotz des starken LTP Defizits in organotypischen Kulturen zeigten jedoch *Cntf* $^{-/-}$ Mäuse in Hippocampus-abhängigen lern- und angstbedingten Verhaltensparadigmen keinen offensichtlichen Phänotyp. Allerdings zeigten Western Blot Analysen hippocampaler Kulturen eine signifikante Reduktion der pStat3 Level in *Cntf* $^{-/-}$ Kulturen unter Kontrollbedingungen, die nach Cntf Zugabe wieder erhöht werden konnten. Um synaptische Strukturen besser darstellen und evaluieren zu können, wurden hippocampale Neurone *in vitro* kultiviert, in denen Stat3 überwiegend in Präsynapsen lokalisiert war. In Übereinstimmung mit diesen Beobachtungen zeigten *Cntf* $^{-/-}$ Präsynapsen eine geringere

Größe und enthielten, verglichen zu Präsynapsen in Wildtypkulturen, weniger pStat3 Immunreaktivität, gerade dann, wenn sie sich in Kontakt mit Astrozyten befanden.

Zusammenfassend weisen unsere Befunde darauf hin, dass Cntf – trotz eines weitgehend unaufälligen Verhaltensphänotyps bei *Cntf* $^{-/-}$ Mäusen – einen Einfluss auf den Level von pStat3 an hippokampalen Synapsen zu haben scheint. In einem nächsten Schritt sollten die folgenden zwei Schlüsselfragen experimentell geklärt werden: 1) gibt es einen kompensierenden Mechanismus, über welchen Mitglieder der Cntf Familie wirken könnten – möglicherweise nachfolgend von pStat3 – und welcher das Verhalten der *Cntf* $^{-/-}$ Mäuse, sowie den größtenteils unauffälligen Phänotyp bei CNTF defizienten Menschen erklären könnte? 2) Wie genau wirkt sich Cntf induziertes pStat3 auf LTP aus? Um diesen zugrundeliegenden Mechanismus aufzuklären, sollten weitere Experimente untersuchen, ob pStat3 und Stathmin abhängige Mikrotubulidynamik in der durch Cntf induzierten Modulation hippocampaler Plastizität eine Rolle spielt – ähnlich, wie es in Motoneuronen bereits gezeigt wurde.

1 Introduction

1.1 Neurotrophic factors

Neurotrophins constitute a specific family of conserved proteins (Gotz and Schartl, 1994), which can promote development and survival of distinct types of neurons (Barde, 1994; Thoenen, 1995) and which also affect cellular and synaptic plasticity (McAllister et al., 1999; Huang and Reichardt, 2001; Park and Poo, 2013). The first discovered neurotrophic factor, nerve growth factor (Ngf), was identified in 1954 as a target-derived factor that promotes nerve fiber outgrowth of sympathetic and sensory spinal ganglia in the chick embryo (Levi-Montalcini et al., 1954; Yivgi-Ohana et al., 2009). Brain-derived neurotrophic factor (Bdnf) was the second neurotrophic factor of this family discovered in 1982 (Barde et al., 1982). Bdnf promoted the survival of cultured chick embryonic ganglia neurons but differed from NGF in function and antigenic properties (Barde et al., 1982). Bdnf has become one of the most investigated neurotrophic factors in a wide number of fields including neurological and neuropsychiatric diseases (Huang and Reichardt, 2001; Park and Poo, 2013). The structural similarities between Ngf and Bdnf (Leibrock et al., 1989) facilitated the finding of two more neurotrophic factors: neurotrophic factor 3 (Nt3) and 4 (Nt4) in 1990 and 1991, respectively (Maisonpierre et al., 1990; Hallbook et al., 1991). These neurotrophic factors are similar in structure (Leibrock et al., 1989) and bind to different subtypes of the same receptor family: the tropomyosin receptor kinase (Trk) family (Martin-Zanca et al., 1986; Patapoutian and Reichardt, 2001; Chao, 2003; Park and Poo, 2013). However, there are other families of neurotrophic factors which do not bind to receptors of the Trk family, for example members of the Gdnf family that bind to receptors involving the c-ret protein kinase (Lin et al., 1993; Ibanez and Andressoo, 2017) and members of the Cntf/Lif/Cardiotrophin family that bind to receptors involving gp130 which has originally been identified as the signal transducing receptor component of Interleukin-6 (Taga et al., 1989a; Murakami et al., 1991). Ciliary neurotrophic factor (Cntf) was originally discovers as a neurotrophic factor in embryonic chic eye tissue (Adler et al., 1979). It does not share similarities in structure and receptor interaction with neurotrophins (Davis et al., 1991), but can also induce neuronal survival (Helfand et al., 1976; Adler et al., 1979; Arakawa et al., 1990; Ip et al., 1991; Sendtner et al., 1994).

1.2 Ciliary Neurotrophic factor

1.2.1 Discovery and first findings

Ciliary Neurotrophic factor (Cntf) was first discovered in 1979 in embryonic chick eye tissue, where it was identified as a survival factor for isolated neurons of the ciliary ganglion (Helfand et al., 1976; Adler et al., 1979; Nishi and Berg, 1981). It was first partially purified from the same tissue (Barbin et al., 1984) and later purified from adult rat sciatic nerves in 1986 (Manthorpe et al., 1986). Cntf is a small, cytosolic (Rudge et al., 1987) molecule of 22 kDa, composed of ~200 amino acids (Lin et al., 1989; Stockli et al., 1989). The corresponding gene is located on chromosome 19 in the mouse (Kaupmann et al., 1991). The Cntf mRNA is expressed in myelinating Schwann cells and astrocytes, where the Cntf protein was also detected in the supernatant of cultures *in vitro* (Lillien et al., 1988; Stockli et al., 1989; Friedman et al., 1992; Rudge et al., 1992; Sendtner et al., 1992a; Sendtner et al., 1994). Further *in vitro* studies revealed that Cntf induces astrocyte type II differentiation (Hughes et al., 1988), and cholinergic differentiation of sympathetic neurons (Ernsberger et al., 1989; Saadat et al., 1989), suggesting a more multifaceted role than exclusively acting on the survival of ciliary neurons. Its manner of secretion is yet unclear, since it lacks the classical N-terminal leader sequence that drives proteins into the secretory compartment within the endoplasmic reticulum (Lin et al., 1989; Stockli et al., 1989). The observation that Cntf is localized in the supernatant of cultured astrocytes (Lillien et al., 1988; Rudge et al., 1992) indicates that it is secreted via a non-classical secretion pathway.

1.2.2 Cntf as member of the Il-6 cytokine family

Cntf shares many features concerning its structure and receptor components with the interleukin 6 (Il-6) cytokine family (Bazan, 1991; Davis et al., 1991; Ip et al., 1991). Cytokines of the Il-6 family are a divergent family of small proteins which are involved in cell signaling and inflammation (Zhang and An, 2007). The Il-6 family is comprised of interleukin-6 (Il-6), interleukin-11 (Il-11), leukemia inhibitory factor (Lif), oncostatin M (Osm), cardiotrophin 1 (Ct-1). Cardiotrophin-like cytokine (Clc) and Cntf (Patterson, 1992; Hibi et al., 1996; Taga and Kishimoto, 1997; Rose-John, 2018). They all share the same core structure of a bundle of four alpha helices and interact with receptor complexes involving gp130 (Murakami et al., 1991; Simpson et al., 1997). The second transmembrane component of this receptor is the LifRß protein (Davis et al., 1991). For Cntf, Lif and Ct-1 receptor complexes, the functional interaction with the transmembrane glycoprotein of 130 kDa (gp130) is important for the signal transduction (Taga et al., 1989a; Hibi et al., 1990; Davis et

al., 1991; Ip and Yancopoulos, 1992). For Cntf, a third signaling component is needed which does not bind LIF and CT-1 and thus mediates specificity for Cntf: the Cntf receptor alpha (CntfRα) (Davis et al., 1991; Ip and Yancopoulos, 1992; Ip et al., 1993d). This receptor is usually bound by a GPI anchor to the outer part of the cell membrane (Davis et al., 1991). However, it has been reported that Cntf can interact with different compositions of its receptor complex, including binding to a soluble form of CntfRα (Davis et al., 1993; Panayotatos et al., 1994) or binding in combination with Lif (Pasquin et al., 2015). Binding of Cntf is also facilitated by the protein sorting receptor sortilin (Larsen et al., 2010; Pasquin et al., 2015). Sortilin was suggested to have at least two functions on Cntf signaling: One is to provide rapid endocytosis and the removal of Cntf from its receptor, and the second function is to facilitate Cntf signaling through the gp130/ LifRß heterodimeric complex (Larsen et al., 2010). The complex receptor binding properties of Il-6-like cytokines and Cntf specifically complicates predictions about the impact of Cntf signaling as well as possible compensational or additive effects within members of the same cytokine family (Pasquin et al., 2015). Although Cntf shares cytokine features concerning structure and receptor complexes, it behaves in many ways like a neurotrophic factor (Arakawa et al., 1990; Sendtner et al., 1991; Sendtner et al., 1994). In particular, it is only found at very low quantities in the circulation, has a very short half-life in blood and is quickly removed by the liver (Dittrich et al., 1994).

1.2.3 The role of Cntf in motoneurons

In vitro studies following the discovery of Cntf demonstrated, that Cntf is not only a survival factor for neurons in the ciliary ganglion (Helfand et al., 1976; Adler et al., 1979) but for a wide range of neurons (Manthorpe et al., 1982; Barbin et al., 1984) including motoneurons (Arakawa et al., 1990). It has been shown that exogenous Cntf can promote the survival of cultured hippocampal neurons (Ip et al., 1991). Cntf is mostly found in the nervous system where expression is most prominent in the peripheral nerves like the sciatic nerve (Stockli et al., 1991; Sendtner et al., 1992a). In line with Cntf distribution, mRNA of the CntfRα is also most prominently expressed in the nervous system (Davis et al., 1991; Ip et al., 1993d) but also, unlike Cntf itself (Stockli et al., 1989), in skeletal muscle. Within the brain, CntfRα shows highest expression levels in the cerebellum (Davis et al., 1991). Cntf expression in the sciatic nerve peaks at around 4 weeks postnatally which coincides with the myelination of Schwann cells (Stockli et al., 1991; Jessen and Mirsky, 1992). Creating a full Cntf knockout (*Cntf*$^{-/-}$) mouse model allowed the first insight into the physiological role of Cntf. The *Cntf*$^{-/-}$ proved to be viable and fertile and Cntf did not seem to play a major role in embryonic development (Masu et al., 1993). In contrast, CntfRα knockout mice die already perinataly

(DeChiara et al., 1995). With respect to motoneuron physiology, *Cntf*$^{-/-}$ mice showed a reduction in the number of motoneurons in postnatal week 28. Subsequent reduction in forelimb grip strength is observed in parallel (Masu et al., 1993). It had been shown before that Cntf has a strong effect on motoneuron survival and axon growth *in vitro* (Arakawa et al., 1990; Sendtner et al., 1991) as well as in young Wistar rats *in vivo* (Sendtner et al., 1990) after nerve lesion. In a mouse model for motoneuron disease, the so called *pmn* mouse model (Schmalbruch et al., 1991), Cntf treatment *in vivo*, via grafting of stable D3 cell line expressing Cntf under the CMV promotor, rescued the phenotype of axonal degeneration (Sendtner et al., 1992e). Later studies revealed that the signaling pathway responsible for the rescue in the *pmn* mouse model is transmitted via the Jak2/Stat3 pathway (Selvaraj et al., 2012).

1.2.4 The Jak2/Stat3 pathway and microtubule dynamics

Upon binding to its receptor, Cntf can induce phosphorylation of the janus kinase 2 (Jak2) which in turn can phosphorylate signal transducer and activator 3 (Stat3) (Stahl and Yancopoulos, 1993; Darnell et al., 1994; Zhong et al., 1994; Heim et al., 1995; Stahl et al., 1995). Stat3 plays an important role in Il-6 like cytokine signaling (Stahl and Yancopoulos, 1993; Stahl et al., 1995). Once phosphorylated, Stat3 (pStat3) can either dimerize and act as transcription factor in the nucleus or act locally on many targets (Gough et al., 2009; Wegrzyn et al., 2009; Camporeale et al., 2014; Meier and Larner, 2014; Liu et al., 2018; Sala et al., 2019). It also interacts locally with stathmin (Shuai, 1994; Shuai et al., 1994; Ng et al., 2006). Stathmin is a small protein of 17 kDa involved in the regulation of the cytoskeleton via influencing microtubule dynamics (Sobel et al., 1989; Gavet et al., 1998). It binds the alpha/beta tubulin heterodimers of which microtubules are comprised which can lead to microtubule catastrophe *in vitro* (Belmont and Mitchison, 1996). Upon phosphorylation of stathmin at Ser ^{16} however, the binding affinity to the tubulin heterodimers decreases (Di Paolo et al., 1997; Larsson et al., 1997; Manna et al., 2009). These dimers are subsequently released which can in turn lead to increased microtubule assembly or stability (Belmont and Mitchison, 1996; Marklund et al., 1996; Curmi et al., 1997; Jourdain et al., 1997; Gavet et al., 1998). Notably, in cultured motoneurons of the *pmn* mouse model, Cntf application leads to axonal stabilization in motoneurons and a rescue of the cellular phenotype by acting through the Stat3-stathmin signaling pathway to tubulin dynamics (Selvaraj et al., 2012).

1.2.5 Cntf in the hippocampus

Cntf did not only show a beneficial role in motoneuron survival and maintenance, but also on hippocampal neurons *in vitro* (Ip et al., 1991). In *in vivo* mouse and rat studies, Cntf was mostly found in the peripheral nerve system related to muscle innervation. Only small quantities were found in the brain, in particular in the optic nerve and olfactory bulb (Stockli et al., 1991; Sendtner et al., 1992a). However, Cntf and its receptor were also found to play a role in the maintenance of the forebrain neural stem cells in the subventricular zone of the lateral ventricle both, *in vitro* and *in vivo* (Ip et al., 1993d; Shimazaki et al., 2001; Emsley and Hagg, 2003; Gregg and Weiss, 2005). This zone and the subgranular layer of the dentate gyrus (DG) in the hippocampus are the only known areas in the brain where adult neurogenesis takes place (McKay, 1997; Gage et al., 1998; Gage, 2000; Kempermann and Gage, 2000). The DG is part of the trisynaptic circuit in the hippocampus, a structure which is important for formation and processing of contextual and spatial memory (Deng et al., 2010). Layers II and III in the prefrontal cortex mostly project onto the granule cell layer of the DG, which is supposedly involved in pattern separation and pattern completion (Gilbert and Kesner, 2006; Knierim and Neunuebel, 2016). The granule neurons project onto the *Cornu Ammonis* area 3 (CA3) where large mossy fiber boutons form connections onto glutamatergic excitatory pyramidal cells as well as *en passant* boutons onto Gabaergic inhibitory neurons (Acsady et al., 1998; Galimberti et al., 2006). Furthermore, the form strong bouton synapses with mossy cells in the hilus, a pathway supposed to mediate ipsi- and contralateral information processing. This complex network innervation of the mossy fibers onto the CA3 area ensures memory precision (Ruediger et al., 2011). Neurons in the CA3 area project onto the pyramidal excitatory neurons in the CA1 via the so called Schaffer-collateral (Deng et al., 2010). The CntfRα, which is mostly expressed in skeletal muscle and motoneurons, is present in almost all parts of the brain, including the hippocampus (Davis et al., 1991). *Cntf*$^{-/-}$ mice showed a dramatic decrease in doublecortin (Dcx)-positive cells, in the subgranular zone of the DG (Muller et al., 2009). Dcx-positive immature neurons reflect a transient neuronal state in adult neurogenesis and therefore Dxc-labeling is commonly used to investigate experience-dependent cellular plasticity in the adult hippocampus (Gage et al., 1998). Using *Cntf*$^{-/-}$ mice it was shown that Cntf signaling via Stat3 can regulate the extent of hippocampal neurogenesis (Muller et al., 2009). On a behavioral level however, no phenotype related to this finding has been reported yet.

1.2.6 CNTF in humans

CNTF has been mapped to chromosome 11 in the human genome (Negro et al., 1991a; Negro et al., 1991b; Giovannini et al., 1993). Notably, about 3% of the world wide population lack CNTF, due to a point mutation in the intron between exon 1 and 2 that leads to the insertion of four additional base pairs (CCAG) creating an new splice acceptor site within the coding region (Takahashi et al., 1994). This RNA splicing mutation predicts a 62 amino acid long protein, which is not detectable, probably due to instability or rapid degradation (Takahashi et al., 1994) or simply the absence of a suitable antibody. CNTF deficiency has not been causally associated with any neurological diseases (Takahashi et al., 1994; Thome et al., 1996e; Thome et al., 1996a, c; Gelernter et al., 1997; Munzberg et al., 1998; Grunblatt et al., 2006). However, associative studies have shown an involvement of CNTF in motoneuron disease (Giess et al., 1998), amyotrophic lateral sclerosis (ALS) (Giess et al., 2002a; Giess et al., 2002e) or as a protective factor in a demyelinating CNS disease (Linker et al., 2002). In a RNA-seq study which was performed in 27 tissues from 95 human individuals, highest expression levels of CNTF on the transcript level were found in bone marrow, but also in brain tissue as well as nervous system unrelated tissue like heart, kidney, lung and testis (Fagerberg et al., 2014). Considering its role in rodents as a survival and maintenance factor for motoneurons, first studies focused on this area of research. CNTF was indeed found in human sciatic nerve (Takahashi et al., 1996) and elevated levels of CNTFRα were found in denervated human skeletal muscle (Weis et al., 1998). *In vivo* and *ex vivo* experiments followed the line of CNTF as a maintenance factor for motoneurons (Sendtner et al., 1990; Sendtner et al., 1992e) and showed endogenous levels of CNTF after peripheral nerve injury (Anand et al., 1997). CNTF is not causally linked to amyotrophic lateral sclerosis (ALS) (Takahashi, 1995) but an earlier onset of ALS has been observed in CNTF knockout individuals (Giess et al., 2002a). Treatment of ALS patients with subcutaneous systemic application of CNTF did not lead to a desired positive outcome and instead lead to a series of negative side effects including fever and cachexia (ACTS, 1995, 1996; Miller et al., 1996). These clinical studies might have failed due to limited knowledge of pharmacokinetics then and difficulties of systematical administration of CNTF to the motoneurons (Dittrich et al., 1994; Dittrich et al., 1996; Thoenen and Sendtner, 2002). The side effects that occurred in the clinical studies led to the discovery that CNTF shows leptin-like properties in food intake reduction - without side effects like hunger or stress (Xu et al., 1998; Lambert et al., 2001). Clinical trials in obesity with a modified recombinant version of CNTF however, lead only to a minor effect in weight loss (Ettinger et al., 2003). Following CNTF back to the roots of its

discovery in the ciliary ganglion in the chicken and its beneficial role in survival and protections of these neurons (Adler et al., 1979; Jo et al., 1999; van Adel et al., 2003), studies in humans investigated the role of CNTF in the human eye (Sieving et al., 2006; Talcott et al., 2011; Zhang et al., 2011; Wen et al., 2012). Endogenous CNTF and its receptor were found in the human optical nerve head (Liu et al., 2007) and clinical studies reported protective effects of cone photoreceptors (Sieving et al., 2006; Talcott et al., 2011). On the basis of the protective effects of CNTF on photoreceptors across several species (Lavail et al., 1992; Wen et al., 2012), investigations concerning a possible beneficial effect of CNTF in *Retinitis pigmentosa* in humans have reached clinical trials (Birch et al., 2013; Pilli et al., 2014; Birch et al., 2016). Although clinical trials revealed only minor or controversial effects so far (Birch et al., 2013; Pilli et al., 2014; Birch et al., 2016; Ghasemi et al., 2018), CNTF is still one of the most commonly used neurotrophic factors to investigate neuroprotective effects of the human retina (Wen et al., 2012); (for an overview visit: https://clinicaltrials.gov/ct2/home and search for "Cntf"). Taken together, CNTF is a polyfunctional protein which is residing somewhere between a cytokine and a neurotrophic factor. It is hard to find its clinical relevance in humans with its many implications and involvements in different fields. Anyhow, almost 3% of humans are CNTF-deficient and seem largely inconspicuous (Takahashi et al., 1994).

1.3 Starting point for this thesis: Cntf and synaptic plasticity

Unpublished data by collaboration partners (Prof. Dr. Martin Korte, Braunschweig) suggest a role for Cntf in synaptic plasticity in the hippocampus of the mouse. Electrophysiological measurements in hippocampal slices of 8-week old mice and organotypic cultures of the hippocampus revealed a deficit in long-term potentiation (LTP) in *Cntf* $^{-/-}$ mice (Fig. 1).

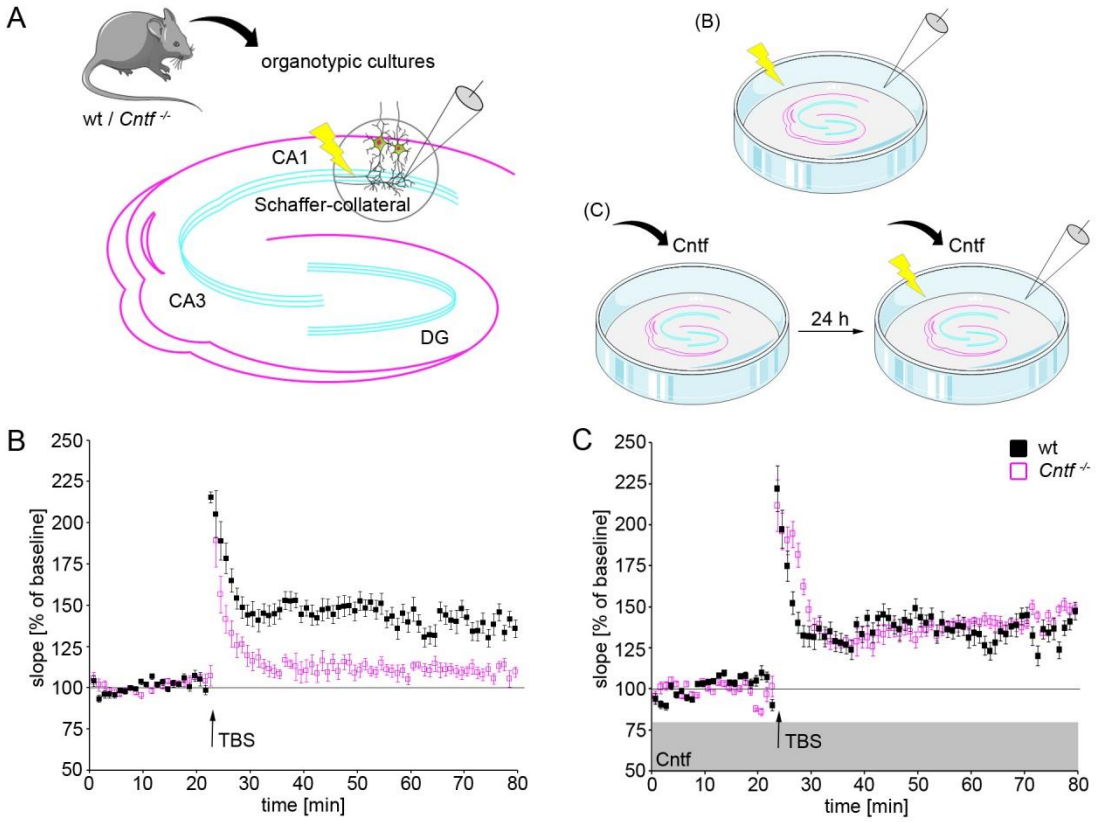

Figure 1. Electrophysiological measurements in organotypic cultures. (A) Schematic illustration of the experimental procedures. Schaffer collaterals between CA1 and CA3 were stimulated with TBS and EPSPs were measured in dendrites of CA1 pyramidal neurons (left). Stimulation and rescue experiment (right). **(B)** Organotypic cultures of *Cntf* $^{-/-}$ mice display deficits in LTP. **(C)** These deficits can be rescued by 24h pre-incubation with CNTF in addition to acute application of Cntf. Data acquired and provided by Prof. Dr. Martin Korte (TU, Braunschweig). CA1, cornu ammonis , CA3, cornu ammonis 3, DG, dentate gyrus, TBS, theta burst stimulus, LTP, long term potentiation, Cntf, ciliary neurotrophic factor. Error bars are presented as ±SEM. Graphical desing elements were provided by Servier Medical Arts.

1.3.1 Long term potentiation

LTP is believed to be a cellular correlate of learning which is characterized by coincident activation of the pre- and postsynapse that results in a prolonged increase in synaptic strength (Bliss and Lomo, 1973; Bliss and Collingridge, 1993; Nicoll and Malenka, 1995; Nicoll, 2017). In general, there are N-methyl-D-aspartate (NMDA) receptor-dependent and independent forms of LTP (Harris et al., 1984; Grover and Teyler, 1992; Cavus and Teyler, 1996). In brief, in NMDA-dependent LTP, glutamate is released from presynaptic vesicles and binds to two types of ionotropic glutamate receptors, the α- amino-3-hydroxy-5-methyl-4-isoxazolepropionic acid (AMPA) receptors and the NMDA receptors (Collingridge et al., 1983; Nicoll et al., 1988; Bashir et al., 1990). At rest, NMDA receptors (NMDAR) are blocked by Mg^{2+} ions, and this so-called magnesium block is voltage-dependent. In case of strong activation of AMPA receptors (AMPAR), the subsequent depolarization relieves the Mg^{2+} block and NMDAR can become active. The calcium ions can enter the postsynapse

through the non-specific, ionotropic NMDAR (Lynch et al., 1983; Mayer et al., 1984; Nowak et al., 1984; Ascher and Nowak, 1988; Nicoll et al., 1988). The Ca^{2+} ions, also provided by co-activated additional calcium-permeable ion channels such as voltage-gated calcium channels, now bind intracellularly to the calcium/calmodulin-dependent protein kinase II (CaMKII). By this basic mechanism, a complex interaction of downstream pathways can be responsible for functional and structural plasticity (Kennedy et al., 1983; Kelly et al., 1984; Malenka et al., 1989; Lisman, 1994). One important consequence of LTP can be that even more AMPAR are transported along the actin skeleton (Allison et al., 1998; Kim and Lisman, 1999; Hanley, 2014; Esteves da Silva et al., 2015) or diffuse from the synaptic membrane towards the active zone of the postsynapse, where they are anchored in the postsynaptic density (PSD) (Kennedy, 1993; Isaac et al., 1995; Liao et al., 1995; Penn et al., 2017). AMPAR trafficking to the PSD is also essential when previously silent postsynapses become active in an activity-dependent way. The increase in AMPAR in the PSD also increases the reactivity to the presynaptically released glutamate and thus contributes to an increase of the postsynaptic response (Isaac et al., 1995; Liao et al., 1995; Matsuzaki et al., 2004; Harvey and Svoboda, 2007; Huganir and Nicoll, 2013). LTP is a complex, structurally and timely organized process, which involves many players and phases and is not yet fully understood (Herring and Nicoll, 2016; Nicoll, 2017). However, recent results showed that there is a causal link between synaptic processes attributed to LTP and a specific form of memory (Nabavi et al., 2014).

1.3.2 The role of the cytoskeleton in LTP and spine dynamics

During LTP stimulation, the postsynapse can undergo structural plasticity (Engert and Bonhoeffer, 1999; Maletic-Savatic et al., 1999; Yuste and Bonhoeffer, 2001; Matsuzaki et al., 2004; Herring and Nicoll, 2016). This process is time-dependent and characterized by a volume increase of spine head and neck, accompanied by an increase in number of AMPAR during early LTP (0-60 min) (Herring and Nicoll, 2016). This rapid increase of AMPAR is a direct result of CaMKII activation via Ca^{2+} influx through the NMDAR during LTP induction (Lisman et al., 2012). It is suggested that during late LTP, i.e. after 60 min, the size of the PSD also increases (Bosch et al., 2014; Herring and Nicoll, 2016). These structural changes are most likely based on actin dynamics (Fischer et al., 1998; Kim and Lisman, 1999; Nimchinsky et al., 2002; Honkura et al., 2008; Bosch and Hayashi, 2012; Fortin et al., 2012) since inhibition of actin dynamics abolishes NMDAR-dependent spine enlargement (Matsuzaki et al., 2004; Harvey et al., 2008). The remodeling of the actin cytoskeleton in turn is most likely mediated by Rho GTPases, which are downstream targets of the CaMKII

(Nakayama et al., 2000; Murakoshi et al., 2011). LTP in the Schaffer-collateral at CA1 is also NMDAR-dependent (Collingridge et al., 1983).

However, increasing evidence suggests that also microtubule dynamics are involved in spine plasticity: microtubules can polymerize from their dynamic plus end retro-and anterogradely along the length of dendrites *in vivo* and *in vitro* (Stepanova et al., 2003; Yau et al., 2016). They enter dendritic spines sporadically under baseline conditions (Hu et al., 2008; Jaworski et al., 2009). Notably, these events seem to occur very scarcely since less than 10% of spines were targeted by microtubules and Hu *et al* calculated a likelihood of finding an invasion by randomly choosing one frame out of a 1 h time lapse of 0.88% only (Hu et al., 2008). However, microtubule entry into spines has also been observed in an activity-dependent manner (Hu et al., 2011; Merriam et al., 2011) which is assisted by actin remodeling at the base of the spine (Schatzle et al., 2018). Also under NMDA stimulated conditions, the number of spine entries per spine per hour was only increased to 1.5 in contrast to 1 under control conditions (Schatzle et al., 2018). One role of microtubule invasion into the dendritic spine during LTP could be direct cargo delivery, like GluA2 subunits of the AMPA receptor by the Kif5 transporter which drive LTP (Uchida et al., 2014; Esteves da Silva et al., 2015; McVicker et al., 2016).

Not only dynamics at the postsynapse, but also presynaptic transmitter release is involved in LTP (Watkins and Jane, 2006; Herring and Nicoll, 2016; Nicoll, 2017). Presynaptic strength and release probability depend on the readily releasable pool of vesicles, which in turn is linked to synaptic size (Harris and Sultan, 1995; Dobrunz and Stevens, 1997; Murthy et al., 2001; Schikorski and Stevens, 2001; Atwood and Karunanithi, 2002). These presynaptic vesicles containing transmitter in turn are transported anterogradely along microtubules by members of the kinesin transporter family (Del Castillo and Katz, 1954; Okada et al., 1995; Chia et al., 2013; Rizzoli, 2014; Wilhelm et al., 2014; Kevenaar et al., 2016; Guedes-Dias et al., 2019) which implies a role for microtubule dynamics in presynaptic synaptic plasticity.

Experiments showing that LTP is affected in *Cntf* $^{-/-}$ mice now raised the question how a neurotrophic factor can influence the potency of a synapse to undergo synaptic strengthening.

1.3.3 Effects of Jak2/Stat3 on synaptic plasticity

Jak/Stat interaction, which describes interaction between members of the Jak family (Jak1/2/3 and Tyk2) and the Stat family (Stat1/2/3/4/5a/5b/6), is involved in several physiological as well as pathological pathways in the CNS, as review by Nicolas *et al* (Nicolas et al., 2013).

When Stat3, which has been shown to play an important role in cytokine signaling (Stahl and Yancopoulos, 1993; Stahl et al., 1995), is inactivated in the germline, embryonic death occurs by day E6.5 (Takeda et al., 1997). Conditional knockout of Stat3 post gastrulation led to enhanced death of cytokine-signaling dependent sensory neurons (Alonzi et al., 2001). A neuron-specific conditional knockout of Stat3 did not lead to an increased death of motoneurons during the embryonic period but to a significantly reduced survival of motoneurons after nerve crush lesion in the adult mouse (Schweizer et al., 2002). These works suggest an involvement of Stat3 in the survival of different types of neurons at different stages of development.

Moreover, immunoelectron microscopic investigation revealed the presence of Stat3 in the PSD of postsynapses in the rat brain (Murata et al., 2000). Western blot and immunoprecipitation experiments confirmed the presence of pStat3 and pJak2 in the PSD (Murata et al., 2000), suggesting an involvement of both players in postsynaptic plasticity. Indeed, involvement of Jak2 activity has been shown in growth hormone (GH) mediated enhancement of EPSPs in the CA1 area of the rat hippocampus (Mahmoud and Grover, 2006). In a knockout mouse for cytoplasmic polyadenylation element binding protein 1 (CPEB-1), levels of GH as well as pJak2 and pStat3 were reduced and GH application to hippocampal slices led to induced Jak2 phosphorylation in wt animals, but not in CPEB-1 knockouts (Zearfoss et al., 2008). In later work, pStat3 has also been localized to the DG and CA1 region of the hippocampus in young mice where a function for Jak2/Stat3 signaling in spatial working memory was proposed (Chiba et al., 2009). More evidence for direct involvement in synaptic plasticity in the hippocampus came from experiments which investigated the role of Jak2/Stat3 in LTD and LTP (Nicolas et al., 2012). Phosphorylation of Stat3 via Jak2 was involved in NMDAR dependent LTD, but not in LTP. Intriguingly, this was independent of the translocation of pStat3 to the nucleus, suggesting a cytosolic function of pStat3 in synaptic plasticity (Nicolas et al., 2012). Since pStat3 can interact with stathmin in the cytosol and thus influence microtubule dynamics (Ng et al., 2006), the question arises whether the Jak2/Stat3 pathway exerts its function on synaptic plasticity via influencing microtubule dynamics. In fact, an involvement of microtubule dynamics in hippocampal LTD has already been shown (Kapitein et al., 2011).

1.4 Research question- Aim of the thesis

The observed LTP deficit - the absence of an increased rate of excitatory postsynaptic potentials (EPSPs) after LTP stimulation - was measured in CA1 dendrites in response to tetanic stimulation of the Schaffer collateral axons. The effect was rescued by 24 h pre stimulation in addition to acute application of Cntf during the LTP measurements. Baseline physiological properties were not affected.

The most intruiging question certainly is, why there is this immense LTP deficit in acute slices and organotypic cultures of *Cntf* $^{-/-}$ mice while CNTF-deficient humans behave largely inconspicuous (Takahashi et al., 1994). A study in *Cntf/Lif/Ct-1* knockout mice revealed that these mice displayed a higher decrease in grip strength than *Cntf* $^{-/-}$ mice alone (Masu et al., 1993; Sendtner et al., 1996; Holtmann et al., 2005). This indicates that, concerning motoneuron function, other members of the Il-6 cytokine family can compensate for Cntf – at least to a certain degree. This compentational mechanism does not seem to take place in the hippocampus, since Cntf-deficiency alone is able to interfere with LTP integrity.

These observations and the fact that LTP requires a tightly organized restructuring of the postsynaptic site, which involves actin as well as microtubule dynamics (Kapitein et al., 2010; Schatzle et al., 2018), combined with the previous finding that Cntf can influence microtubule dynamics in motoneurons (Selvaraj et al., 2012) and that the Jak2/Stat3 interaction is involved in synaptic plasticity (Nicolas et al., 2012), led to the hypothesis that Cntf affects the structural and functional plasticity of CA1 pyramidal neurons on the level of single glutamatergic synapses.

Therefore, this study aimed to answer the following key questions:

1.) Is Cntf involved in hippocampal synaptic plasticity by influencing microtubule dynamics in spines, mediated via the Jak/Stat pathway?
2.) Does Cntf-deficiency affect hippocampus-dependent memory processing?

We addressed this question by immunohistological and behavioral approaches as well as by investigations of Cntf signaling in organotypic cultures and in cultured hippocampal neurons *in vitro*.

Our findings highlight a possible new role for Cntf in hippocampal synaptic plasticity mediated via Stat3.

2. Material and Methods

2.1 Material

2.1.1 Chemicals and other substances

Products	*Company*	*Article Number*
5-Fluoro-2´-Deoxyuridin	Sigma	F0503
Acetic acid	Chem.Solute	2234
Agarose	Biozym	840004
Ammoniumpersulfate	Sigma	A6387
Aquapolymount	Polyscienes Inc.	18606
B27 X50	Gibco	17504-044
Betaine	Sigma	61962
BME	Gibco	41010-026
Bovine Serum Albumin – fatty acid free, low endotoxin (BSA)	Merck/Sigma Aldrich	A8806
Bromphenolblue	Sigma	B-8026
Cntf	in house preparation, purified recombinant rat Cntf from E.coli.	
cOmplete Tablets mini	Roche	4693132001
Cytosin β-D-arabinofuranoside hydrochloride	Sigma	C6645
DAPI (4',6-diamidino-2-phenylindol)	Sigma-Aldrich	D9542
Di-potassium hydrogen phosphate	Sigma-Aldrich	P9666
Di-sodium hydrogen phosphate	Merck	106580

DNase	Roche	10104159001
dNTP set	Fermentas	dNTP set
DTT	Thermo Fisher	along with SS III
EDTA (Ethylenediaminetetraacetic acid)	Sigma-Aldrich	E-6511
Ethanol	Sigma-Aldrich	32205
Ethyleneglycol	Merck	100949
Fetal calf serum	Linaris	
First strand buffer 5×	Thermo Fisher	along with SS III
Gene ladder1 kb -100 bp	Fermentas	SM0242
Glucose	Sigma	G7021-100G
Glutamax X100	Gibco	35050-038
Glycerol	Merck	104093
Glycine	Sigma	68898
Glycogen	Thermo Scientific	R0551
Hank’s Balanced Salt Solution	Sigma-Aldrich	H6648
Heparin-sodium 25000	Ratiopharm	
HEPES	Roth	H4034-25G
Horse serum	Linaris	SHD3250KYA
Immobilon Western	Millipore	P90720
Kynureic acid	Sigma	K3375
Luminaris HiGreen qPCR Master Mix	Thermo Scientific Fisher	K0992
Midori green	Nippon Genetics	Midori green

Neurobasal medium	Gibco	21103-049
Nonidet 40	Applichem	A1694
Paraformaldehyde	Merck	A113 13
Penicillin-Streptomycin (5,000 U/mL)	Gibco/Life technologies	15070-063
Phalloidin	Invitrogen	A12379
Polyacrylamide 30 %	Biorad	161058
Poly-L Lysine hydrobromide	Sigma	P2636
Potassium chloride	Sigma-Aldrich	P-5405
Potassium di-hydrogen phosphate	Merck	104873
Pre stained protein ladder	Thermo Scientific	26616
RNase away	Molecular Bioproducts	7002
RNasin Plus RNase Inhibitor	Promega	N2611
Sakura Finetek™ Tissue-Tek™ O.C.T. Compound	Fisher Scientific	12351753
SDS	Applichem	A7249
Sodium-ortho-vanadate	Sigma	S6508
Sodium-pyruvate X100	Gibco	11360-039
Sterile water	Ampuwa	Sterile water
Stripping buffer Restore Plus Western	Thermo Scientific	46430
Superscript III RT	Thermo Fisher	18080093
Taq DNA polymerase	5-Prime	2200020
Taq enhancer 5×	5-Prime	along *Taq* poly.
TEMED	Merck	UN2372

Toluidin blue	Sigma	M4159
Tris Base	PanReac Applichem	A2264,1000
Tris HCl	PanReac Applichem	Tris HCl
Triton X100	Carl Roth	3051.2
Trypsin	Worthington	53B14071
Trypsin inhibitor	Gibco/Life technologies	T6522
Tween 20	PanReac Applichem	A7932,0500
Uridine	Sigma	U3750
β-Mercaptoethanol	Sigma	M7 154

2.1.2 Antibodies

Primary antibodies	*Concentration*	*Company*	*Catalogue*
Guinea pig anti NeuN	1:400	Synaptic System	266004
Guinea pig anti-vGLUT	1:400	Synaptic Systems	135304
Mouse anti GAPDH (6C5)	1:3000 (WB)	MerckMillipore	CB1001
Mouse anti GFAP	1:2000	Sigma	G3893
Mouse anti Map2 (AP20)	1:1000	Sigma	M1406
Mouse anti STAT3 (124H6)	1:2000 (IF) 1:3000 (WB)	Cell Signaling	9139
Phalloidin-Alexa488	1:300	Invitrogen	A12379
Rabbit anti cFOS	1:10 000	Synaptic System	226 003
Rabbit anti CNTF (K10)	1:10.000/20.000 (IF) 1:10.000 (WB)	Inhouse (Stockli et al., 1991)	-
Rabbit anti pCREB (Ser133)	1:1000 (IF) 1:3000 (WB)	Cell Signaling	9198

Rabbit anti pSTAT3 (D3A7)	1:400 (IF) 1:2500 (WB)	Cell Signaling	9145

Secondary Antibodies	*Concentration*	*Dye Label*	*Company*	*Catalogue*
Donkey anti-guinea pig IgG (H+L) affiniPure	1/600 (0.44µg/µl)	Cy5-650	Jackson	706-175-148
Donkey anti-guinea pig IgG affiniPure	1/800 (0.44µg/µl)	Alexa 488	Jackson	706-545-148
Donkey anti-rabbit IgG affiniPure (H+L)	1/800 (0,5µg/µl)	Cy3-550	Jackson	711-165-152
Donkey anti-rabbit IgG H+L	1/10000 (0.4µg/µl)	HRP	Jackson	711-035-152
Goat anti-mouse IgG affiniPure (H+L)	1/800 (0.5µg/µl)	Cy5-650	Jackson	115-175-146
Goat anti-mouse IgG affiniPure (H+L)	1/800 (0.5µg/µl)	Alexa 488	Invitrogen	A11029
Goat Anti-Mouse IgG affiniPure (H+L)	1/10000 (0.4µg/µl)	HRP	Jackson	115-035-003

2.1.3 Buffers, solutions and media

Buffer/solution/medium	*Composition*
100 mM Tris HCl	157.6g in 1 litre dH_2O, pH 7.5
10 × Phosphate buffered saline	80 g NaCl, 2 g KCl, 2 g KH_2PO_4, 11.75 g $Na_2HPO_4 \times 2H_2O$ in 1 litre dH_2O
1 M HEPES	23.8 g in 100 ml sterile dH20, pH 7.3, sterile filter.
1 M Phosphate buffer	13.61 g KH_2PO_4, 17.42 g K_2HPO_4 in 100 ml dH_2O, pH 6.5

1 M Sodium chloride	58.44 g in 1 litre of dH_2O
50% Sucrose	50 g Sucrose in 100 ml 1X PBS
20% Triton X100	10 ml Triton X100 in 40 ml dH_2O. Stir for 30 min.
20% Tween 20	50 ml Tween 20 in 250 ml dH_2O. Stir for 5 min.
4% Paraformaldehyde	40 g Paraformaldehyde in 500 ml dH_2O with few drops of 5 M NaOH, stir for 20-30 min at 60°C till paraformaldehyde dissolves. Pass through a filter paper and add 410 ml of Buffer A (0.2M $Na_2PO_4x2H_2O$ in dH_2O) and 90 ml Buffer B (0.2M $NaH_2PO_4x2H_2O$ in dH_2O). pH 7.4
5% SDS	2.5 g in 50 ml dH_2O
50 × TAE buffer	242 g Tris Base, 292 g EDTA in 1 l dH_2O, pH 8.0
6 × Gel loading dye	40% Glycerol, 0.02% Bromophenol blue, 0.06% Xylene-cyanol, 1 × TAE in dH_2O
10 × RT	7 µl Tris HCl pH 8.00 (10 mM stock), 1 µl dNTPs (20 mM stock), 2 µl random primer N6 (5 mM stock)
4 × Lämmli sample buffer	4 ml 1 M Tris HCl pH 6.8, 8 ml 20% SDS, 5 ml Glycerol, 1.6 ml β-Mercaptoethanol, 1.4 ml H_2O, 10 mg Bromphenolblue, adds up to 20 ml
Blocking buffer	0.5% Triton X100 (from 20% Triton X100 stock), 0.1% Tween 20 (from 20% Tween 20 stock), 10% Horse serum in 1 × PBS
Elution buffer	10 mM Tris HCl pH 8.5, BSA (1mg/ml);
Cryoprotectant solution	30% Ethyleneglycol, 25% Glycerol, 0.4 M Phosphate buffer in dH_2O, pH. 7.4
Dissection medium for primary hippocampal cultures	0.1% Glucose (from 20% Glucose), 1 × Sodium-Pyruvate (from Sodium-Pyruvate X100) and 10 mM Hepes pH 7.3

	(from 100mM Hepes) in Hank's Buffered Salt Solution, incubate at 37°C
Dissection medium for organotypic cultures (GBSS)	Stock solution: 8 g, NaCl, 1 g D-Glucose, 0.37 g KCl, 0.03 g KH_2PO_4, 0.21 g $MgCl_2$ ×6 H_2O, 0.07 g $MgSO_4$ ×7 H_2O, 0.227 g $NaHCO_3$, 0.12 g Na_2HPO_4, 0.22 g $CaCl_2$, ad to 1 l and adjust pH to 7.2 with 0.5 M HCl, store at 4°C. For dissection, prepare freshly: 98 ml of stock solution and add 1 ml 5 mM Kynureic acid (in 1 M NaOH) and 1 ml of 50% Glucose (in H_2O). Store in fridge for 1-2 weeks.
10 × Electrophoresis buffer	30.5 g Tris Base, 144 g Glycine, 10 g SDS, ad 1 l
LTP +	To prepare 1 l: 6.721 g NaCl, 0.969 g KCl, 5.958 g HEPES, 0.441 g $CaCl_2$, 0.172 g NaH_2PO_4 × 2 H_2O, adjust to pH 7.4 and store at 4°C. Add freshly to 9.8 ml stock solution: 200 µl of 0.5 M Glucose and 1.1 µl of 1 M glycine
LTP -	To prepare 1 l: 7.305 g NaCl, 0.244 g KCl, 5.958 g HEPES, 0.294 g $CaCl_2$, 0.172 g NaH_2PO_4 × 2 H_2O, 0.246 g $MgSO_4$ × 7 H_2O, adjust to pH 7.4 and store at 4°C. Add freshly to 9.8 ml stock solution: 200 µl of 0.5 M Glucose
Maintenance medium for primary hippocampal cultures	1× B27 (from 50 × B27), 1× Glutamax (from 100 × Glutamax) and 1 × Pen/Strep in Neurobasal medium, incubate at 37°C
Maintenance medium for organotypic cultures	25 ml HS, 50 ml BME, 25 ml HBSS, 500 µl Glutamax, 1 ml 50% Glucose
Mitosis block for organotypic cultures	Prepare stock solutions of: 2,422 mg Uridin in 10 ml MilliQ (1 M); 2,797 mg Cytosin β-D-Arabinofuranosid*Hydrochlorid in 10 ml MilliQ (1 M) and 2,462 mg 5-Fluoro-2´-Deoxyuridin in 10 ml MilliQ (1 M). Mix stock solutions 1:1, sterile filter and aliquot in

	500 µl fractions to store at -20°C
PBS/Heparine	0.4% Heparin in 1 × PBS
Quenching solution	33 mM Glycin, 13.3 mM Tris in 1 × PBS, pH 7.4, osmolarity: 309 Osm
10 × TBS	12.1 g Tris Base, 87.7 g NaCl, adjust to pH 8.0, ad 1 l
TBST	100 ml TBS, 10 ml 20% Tween, ad 1 l
Transfer buffer	100 ml Electrophoresis buffer, 700 ml H_2O, 200 ml Methanol
Washing buffer	0.1% Triton × 100 (from 20% Triton × 100 stock), 0.1% Tween 20 (from 20% Tween 20 stock) in 1 × PBS
0.5 M EDTA	380.2 g in 1 litre dH_2O, pH 8.0

2.1.4 Consumables

Material	*Company*
4-well plates	Greiner
6-well/24-well plates – 128 x 86 mm	Thermo Scientific
Cell bottles 50ml	Greiner
Cover glass – 24 x 40 mm, 24 x 50 mm	R. Langenbrick
Coverslips (Ø 10mm)	Hartenstein
Cryomold biopsy – 15mm x 15mm x 5 mm	Sakura
Immersion oil IMMOIL-F30CC	Olympus
Millicell inserts	Millipore
Mini Protean Western System	BioRad
Neubauer chamber	Hartenstein

Objective slides – 70 x 26 mm	R. Langenbrick
Pasteur pipette	Brand
PVDF membrane	GE Healthcare
RNase-free soft tubes	Biozym
Roti coll 1, cyanoacrylate basis one component-instant glue	ROTH
T75 Cell culture flasks	Greiner
Venofix Safety winged IV needle 25Gx3/4" (0.5 × 19 mm)	B Braun
Vibratome injector blades – Single edges	Leica Microsystems
X-ray films	Fujifilm/Hartenstein

2.1.5 Equipment

Equipment	*Company*
Binocular	Zeiss
Cell culture CO_2 Incubator	Binder
Centrifuge Rotofix 32A	Hettich
FluoView FV1000 Confocal microscope	Olympus
Hood	Heraeus
Hot Bead Sterilizer	Fine Synaptic tools
Incubator	Heraeus
Labpump	Neolab
Laser Micro Dissection DM6000B	Leica
Lauda Ecoline water bath	Lab Commerce
LightCycler 1.5	Roche

Mc Ilwain Tissue Chopper	The Mickle Laboratory Engineering Co. LTD.
PCR-Mastercycler	Eppendorf
Rocking platform -Duomax 1030	Heidolph
Thermomixer comfort	Eppendorf
Ultrasonic Processor	Hielscher
Vibratome-VT1000S	Leica Microsystems

2.1.6 Software

Fluoview, version 4.1.a (Olympus).

FIJI ImageJ (WS Rasband, ImageJ, US NIH, Bethesda, Maryland, USA)

Leica Microsystems Laser Microdissection LMD 6.7.2.4295

Microsoft Office

Multi Conditioning System from TSE (256060 series)

Photoshop CS5 (Adobe)

Prism 6 (GraphPad)

TSE MCS FCS – SQ MED (TSE)

Video Mot 2 (TSE Germany)

2.2 Methods

2.2.1 Animals

Mice were bred in the animal facility of the Institute of Clinical Neurobiology, University Hospital of Würzburg. Mice were housed in groups of 3 to 5 animals under standard laboratory conditions (12h/12h light/dark cycle, access to food and water ad libitum). Animals were quarterly tested according to the Harlan 51M profile (Harlan Laboratories, Netherlands). Yearly pathogen-screening was performed according to the Harlan 52M profile. All mice were healthy and pathogen-free, with no obvious behavioral phenotypes. The following mouse lines were used:

- C57Bl6/J *Cntf* $^{-/-}$ (Cntf^{tm1Mpin}) (Masu et al., 1993)
- C57Bl6/J (Jackson laboratories)

2.2.2 Behavior

2.2.2.1 Animals

All animal experiments were carried out in accordance with European regulations on animal experimentation and protocols were approved by the local authorities (Regierung von Unterfranken, 55.2-2531.01-95/13). Mice were housed individually and kept at a 12-hour dark-light cycle with access to food and water *ad libitum*. The cages (Tecniplast, 1264C Eurostandard Typ II, 267 x 207 x 140 mm) were kept in a Scantainer (Scanbur Ltd. Denmark) assuring stable conditions by maintaining a temperature of about 21°C and air humidity of about 55% through constant air flow. For behaviour, four different cohorts were investigated where wildtype littermates served as internal control. Mice were around 8 weeks old when the experiments started:

Table 1 Overview over mouse cohorts investigated in behavioral paradigms

genotype	gender	cohort 1	cohort 2	cohort 3	cohort 4	sum
wildtype	male	3	8	6	10	27
	female	-	6	6	-	12
Cntf $^{-/-}$	male	10	3	6	8	27
	female	-	4	4	-	8
experiments		NOR, DL, FC, MWM	HP, OF, DL, EPM, NOR, FC, MWM	OF, EPM, FC, MWM	NOR, FC, MWM	

NOR, novel object recognition; DL, dark/light, FC, fear conditioning, MWM, Morris water maze, HP, hot plate, OF, open field, EPM, elevated plus maze

2.2.2.2 General procedure

Experiments were carried out during day time and therefore during the light phase of the cycle. Before every experiment, mice were transferred to another room in their home cages and were given half an hour for acclimatization. Mice were handled by the experimenter for 2-3 days prior to experiments to avoid any possible influence on the behavior. For the experiments, mice were transferred individually to a second room where the experiment would take place. Generally, males were tested before females to avoid distraction by female pheromones, which could also influence the behavior. The temperature was kept to around 22°C and the air humidity ranged between 35-55%.

2.2.2.3 Open field

A white square box made of frosted plastic (48 × 48 cm, height 50 cm) evenly illuminated with ca. 40 lux was used as open field arena. Mice were placed in the middle of the arena and were monitored for 10 or 30 min using a web cam-based system (camera: Logitech). Animal movements were tracked and analysed with the Video Mot Software (TSE, Germany). For analysis, the floor of the box was divided into different fields of interest and the following parameters were measured and compared between the centre of the arena (24 × 24 cm) versus the periphery: total distance travelled over time, travelling speed, time spent in the centre or periphery of the arena, number of entries to the centre and into the periphery.

2.2.2.4 Dark/light transition

The dark/light transition test was performed in the open field arena. For this purpose, a red acrylic glass box of 47 × 16 × 25 cm was positioned in the box covering approximately one half of the arena with a square opening serving as entrance for the mouse to enter the dark compartment. Mice were placed in the light compartment and their movements were tracked for 10 min using the Video Mot Software (TSE Germany, camera: Logitech). The following parameters were recorded and analysed: distance travelled in the light compartment and time spent in each compartment.

2.2.2.5 Elevated plus maze

The elevated plus maze consisted of a cross with two closed and two open arms made of white frosted plastic (TSE Germany, length of arm: 30 cm, width: 5 cm, height of closed arm: 15 cm, height above ground: 48 cm, luminosity adjusted to ca. 60 lux). Mice were placed on one of the open arms and their movement was tracked for 10 min using the Video Mot Software (TSE Germany, camera: Logitech). The following parameters were analysed and

compared between open and closed arms: distance travelled and time spent in open and closed arms.

2.2.2.6 Novel object recognition

The novel object recognition test was carried out in the open field arena (Leger et al., 2013). Two objects were presented: a cell culture flask (T75 Greiner, height about 16 cm) filled with water to the top and a 14.5 cm tower built of Lego bricks. Objects were placed in two diagonally opposing corners of the box 12 cm from each wall. During the first day, two identical objects were presented in a randomized fashion. Mice were observed and tracked for 10 min using the Video Mot Software (TSE Germany, camera: Logitech). The time the mice spent with their head in the fields of interest (2 cm distance surrounding each object) was measured manually. On the second day, mice were confronted with a familiar and a novel object. Here, a triplicate of the objects was used to avoid olfactory cues or influence. Position of objects was randomized to avoid position bias. The discrimination rate is calculated from the time difference spent between the objects in relation to the total time spent investigating either object: [(novel – familiar)/(novel + familiar)[s]]. The DR ranges from -1 (total time spent at familiar object) to +1 (total time spent at the novel object) and classifies animals with values above 0 as learners.

2.2.2.7 Hot plate

The hot plate setup (custom made) consisted of a viewing jar, a hollow acrylic glass cylinder (18.7 cm high and 14.2 cm wide) placed on a heatable metal block fixed on a magnetic stirrer hot plate (IKA, RCT basic). The temperature was monitored with a thermometer (IKA, ETS-D5) connected to the metal block. Mice were placed in the viewing jar with the metal block heated up to 54°C (±1°C). The time until the mice licked their hind paws, was measured and the mice were immediately removed from the plate. If the mice started jumping or vocalizing they were likewise immediately removed from the plate. If none of these criteria were met mice were taken off the hot plate after a maximum of 30 s to prevent tissue damage or other injuries.

2.2.2.8 Pavlovian fear conditioning

For Pavlovian fear conditioning, the Multi Conditioning System from TSE (256060 series) was used. The animals were monitored and tracked with the TSE MCS FCS – SQ MED software. Two different contexts were used: context A, a square clear acrylic box placed on a

metal grid and context B, a clear acrylic cylinder placed on black, rough plastic. After each mouse, the defaecation was removed and the contexts were wiped down with water.

Cohort 1 and 2

On the first day, mice were placed in context A. After a habituation time of 60 s, a tone (conditioned stimulus, CS, intensity 85 dB SPL, 10000 Hz) that lasted 10 s was presented three times with an inter stimulus interval (ISI) of 20 s. The CS was associated with a foot shock of 0.7 mA (unconditioned stimulus, US). The US was delivered via the electric grid during the last second of tone presentation. After an additional time of 30 s, mice were transferred back to their home cage. To test for cue memory the next day, mice were placed in context B. After an initial time of 60 s, the CS (tone) was delivered again for three times for 10 s with an ISI of 20 s, without administration of the US. On the third day, mice were replaced in the fear conditioning context (training Context A) for 6 min without CS presentation to recall contextual memory.

Cohort 3

Mice in cohort 3 underwent a renewal fear conditioning paradigm. On the first day, mice were conditioned in context A: after 60 s of habituation, 3 tone- shock pairings were administered with an ISI of 20 s. Tone presentation (intensity 85 dB SPL, 10000 Hz) took 10 s and the last second was accompanied by an electric foot shock of 0.7 mA. After additional 30 s, mice were transferred to their home cage. On the second day and third day, mice underwent extinction training in context B. Mice were presented with the tone 12 times with ISI of 20 s and a 60 s habituation phase before the first, as well as additional 30 s after the last tone. On day 4, mice were placed in context A to test for fear renewal. After 60s of habituation to the context, the tone was presented for 4 times with an ISI of 20s, followed by 30 s before transferring mice back to the home cage. To stress the difference between the two contexts, context A was wiped down with 75% of Ethanol, whereas context B was wiped down with 1% acetic acid.

Cohort 4

Mice in cohort 4 underwent contextual fear conditioning paradigm. Experiments took place in context A only (AAA paradigm). On day 1, after 60 s of habituation, mice received 5 electric foot shocks of 0.7 mA with ISI of 60 s. After additional 30 s, mice were transferred to their home cage. Over the course of the next 3 days, mice underwent one retrieval trial and 5

additional extinction trials, 2 trials each day. In each trial, mice were placed in context A for 6 min. This was repeated 2 hr later. On day 14, mice were again placed in context A for 6 min, to test for spontaneous recovery of conditioned fear.

2.2.2.9 Morris water maze

The Morris water maze (MWM) basin was made of frosted white plastic with a diameter of 120 cm. The maze was filled with tap water, which was adjusted to ~21°C. Lighting was kept dim at around 40 lux. Mice underwent five training days with four runs per mouse per day, starting once from each starting point in a randomized fashion named: “N”, “S”, “NE”, “SE” (Fig. 2). The platform consisted of clear plastic and had a diameter of 10 cm. It was placed in the middle of the “W” quadrant, around 1-2cm below the surface so that mice were able to stand. Mice were removed from the maze if they failed to find the platform within 60 s. On the sixth day, the platform was removed and mice were released once from the “E” starting point and removed from the maze 30 s or 60 s later. For reversed learning, the platform was positioned in quadrant “E” and mice were trained for 5 days and tested on day 6 as described above. Mice in cohort 3 and 4 underwent a reminder session before the reversal training. 2 or 6 runs were performed with the platform placed at the familiar position in quadrant “W” before the platform was moved to the new position in quadrant “E”. Mice were tracked with a webcam based system (Logitech) and the time spent in a quadrant and the number of wrong platform visits was analyzed using the Video Mot Software (TSE Germany). Latency to find the platform was measured manually with a stop watch. In between runs, mice were kept in front of an infrared light to allow warming up. On a separate day after testing day, a visual cue was placed on the platform and mice were released from the opposite quadrant to where the platform was located, to test for correct visual perception (flag test).

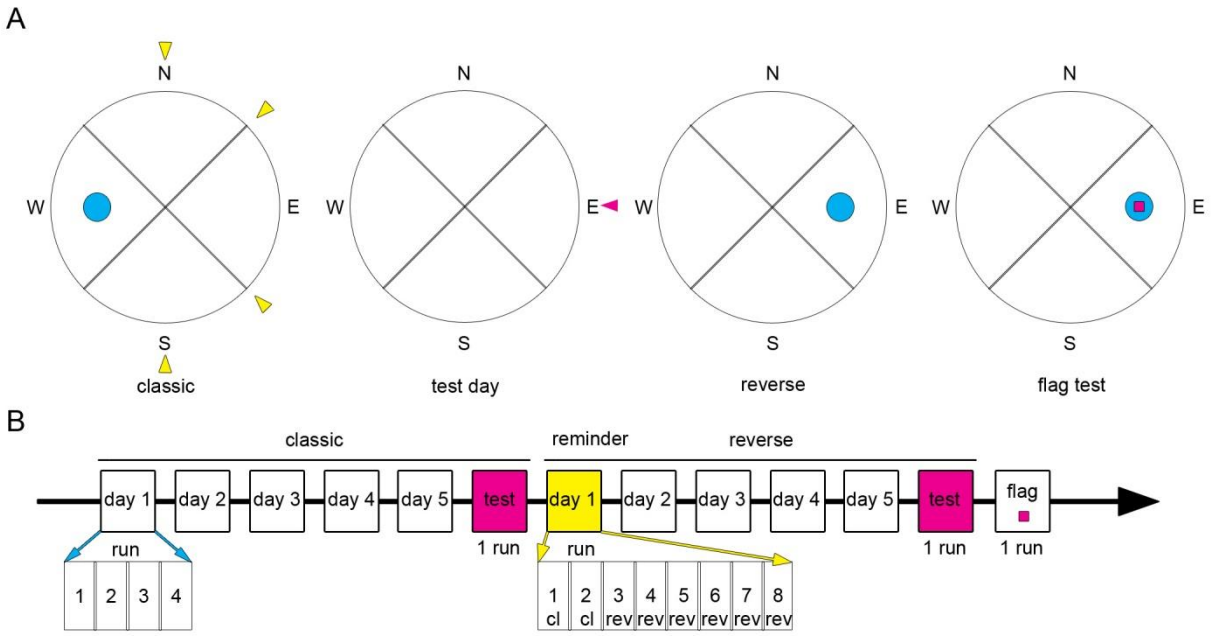

Figure 2. Schematic illustration of the Morris water maze (MWM) test procedure. (A) Top view onto the MWM in the different test situations. In the classic MWM the platform, illustrated by a blue circle, is located in the "W" quadrant. Yellow arrows illustrate starting points for classic MWM. On the test day, the platform is removed and animals start from the opposite quadrant to the former location of the platform, illustrated exemplary for the classic MWM by the magenta arrow. In the reverse MWM, the platform is located to the "E" quadrant. Starting points are mirrored accordingly from classic MWM. During flag test, a visible cue is placed on the platform and mice are released from the opposite quadrant. The visible cue is illustrated by the magenta square. **(B)** Illustration of the timeline of the MWM experiments. Classic and reverse MWM consist of 5 training days each. Each training day consist of 4 runs, one run from each starting point. On the test day, 1 run is performed only. The first day of the reverse MWM can include a reminder of the previous platform location. The reminder schedule of cohort 3 is depicted exemplary which includes 2 runs towards the classic MWM platform location and 6 runs with the relocated platform. The flag test is performed after the reverse MWM test day. W = west, N = north, E = east, S = south, cl = classic, rev = reverse.

2.2.3 Cell culture

2.2.3.1 Primary hippocampal neurons

Cover glasses as well as cell culture dishes were coated one night prior to preparation with 0.1% PLL, washed with HBSS and incubated with 100 µl of NB medium 2 hours before plating. Primary hippocampal neurons were obtained from C57Bl6/J and *Cntf* $^{-/-}$ mice at postnatal day 1 (P1). Hippocampi were dissected in HBSS and stored on ice during preparation. Per culture, hippocampi of five P1 mice were collected from both hemispheres and transferred to preparation solution under the hood. Hippocampi were washed twice with preparation solution before 500 µl of 2.5% trypsin was added. After 20 min in the incubator (37°C and 5% CO2), 500 µl of 0.1% DNase was added. An additional 5 min later,

hippocampi were washed twice with preparation solution. 200 µl of 0.1% of trypsin-inhibitor was added and hippocampi were triturated 10-15 times with a 1 ml pipette, before spinning down for 3 min at 1400 rpm in the centrifuge. Supernatant was removed and the trituration and centrifugation step was repeated. Cells were resuspended in NB medium with a 200 µl pipette and counted in a Neubauer-chamber. Hippocampal neurons were plated at a density of 20.000 cells per cover glass for staining and 200.000 cells per dish for western blotting. Approximately 2 hours after plating, cells were flooded with NB medium containing 0.1% FCS or HS to an end volume of 3 ml per dish. Four days following preparation half of the medium was substituted with FCS/HS free NB medium, which was repeated again four additional days later. Hippocampal neurons were cultured for 21-24 days and 500 µl of fresh medium was added once a week.

2.2.3.2 Stimulation of primary hippocampal cultures

After 21-24 days in culture, hippocampal neurons were stimulated with either chemical long term potentiation solution (+LTP), a HEPES buffered ACSF (-LTP) which served as control for the +LTP, Cntf (100ng/ml with 0.1% BSA) or 0.1% BSA. For the +LTP and –LTP stimulation, almost all of the culture medium was removed with a pump and 2 ml of the respective solution was added. BSA (vehicle control) and Cntf-containing solutions were simply added to the culture medium. Hippocampal neurons were returned to the incubator. After 15 min, the cultures were fixed with PBS-buffered 4% PFA (pH 7.4) for another 15 min at 37°C. Then, PFA was removed and the cultures were washed twice with 1 × PBS. Fixed cells were stored at 4°C until the immunofluorescence staining was performed.

Hippocampal cultures which were cultured for western blot analysis were stimulated as described above. The lysis took place on ice. After stimulation, the respective solution or medium was removed with a pump and 150 µl of ice-cold lysis buffer was added to the dish. Cells were scraped off the dish with a cell scraper and the mix of lysis buffer and cells was transferred to a 0.5 ml reaction tube. Samples were stored on ice for 30 min before undergoing two rounds of sonification (MS1 sonotrode, Hielscher, 5 pulses, 0.5 s, 80% amplitude). After additional 10 min on ice, followed by a 10 min centrifugation step at 14.000 rpm at 4°C, 75 µl of samples were mixed with 37.5 µl of 4 × Lämmli sample buffer and after 5 min at 95°C were stored at -20°C. The rest of the samples was stored at - 80°C.

2.2.3.3 Organotypic hippocampal cultures

Organotypic cultures were prepared from wt and *Cntf* knockout mice at P5-P7. 6-well dishes prefilled with 1.1 ml of maintenance medium and kept in the incubator. Hippocampi from

both hemispheres were carefully dissected in preparation medium on ice and cut into 400 µm thick sections with a tissue chopper. Four sections per well were transferred onto Millicell membrane inserts which were placed into the prewarmed 6-well dishes. Sections were cultured in the incubator at 37°C and 5% CO2 for 2 to 4 weeks. After three days in culture, 15.4 µl of mitosis block solution was added to the medium in each dish. 24 hr later, the Millicell membranes were transferred to fresh 6-well dishes containing culture medium. 500 µl of medium was exchanged twice a week.

2.2.3.4 Stimulation of organotypic cultures

Organotypic cultures were stimulated with chemical LTP solution (+LTP), -LTP, Cntf (100ng/ml with 0.1% BSA) and BSA (0.1%). For stimulation with +LTP and –LTP, Millicell membrane inserts were transferred into fresh 6-well dishes containing 1.1 ml of the respective solution. Cntf and BSA were simply added to the culture medium. Cultures were stimulated for 15 min in the incubator. For lysis, all four slices on one Millicell membrane were scratched off with a spatula and transferred immediately into 150 µl ice-cold lysis buffer. Samples were stored on ice for 30 min before undergoing two rounds of sonification (8 pulses, 0.5 s, 80% amplitude). After additional 10 min on ice, followed by a 10 min centrifugation step at 14.000 rpm at 4 °C, 75 µl of samples were mixed with 37.5 µl of 4 × Lämmli sample buffer and after 5 min at 95°C were stored at -20°C. 5 µl of samples were added to 45 µl of 1 × PBS and stored at - 20°C for BCA analysis. The rest of the samples was stored at - 80°C.

2.2.4 Molecular biology

2.2.4.1 Polymerase Chain Reaction (PCR)

Genomic DNA was isolated from ear punches and used as a template for genotyping. The following primer pairs were used to identify either wildtype mouse: CNTF E1S + CNTF/1A or a *Cntf* knockout mouse: CNTF E1S + 5'NEO.

Table 2 PCR primers and sequences for genotyping

primer	sequence
CNTF E1S	5´– GAG CAA TCA CCT CTG ACC CTT – 3´
CNTF/1A	5´– CAG GCT GGA TGA AGA CAG TAA G – 3´
5´NEO	5´– AGC CGA TTG TCT GTT GTG CCC – 3´

The master mix was prepared as follows and 1 µl of DNA was added to each tube. The PCR was running at the following conditions:

Table 3 PCR master mix and cycle conditions for genotyping

component	volume [µl]	PCR cycle conditions	duration	
Taq buffer	3	94°C	5 min	
dNTP (2 mM)	3	94°C	30 s	34 cyles
Primer 1 (20 pMol)	0.3	64°C	30 s	
Primer 2 (20 pMol)	0.3	72°C	60 s	
Betaine (5M)	6	72°C	7 min	
Taq	0.3	15°C	hold	
H_2O	16.1			

PCR samples were separated on a 2% agarose gel (in 1 × TEA) with 4 µl of Midori green to visualize the DNA fragments. The gel was run for 40 min at 120 V. Products for wildtype and knockout ran at 321 bp and 450 bp, respectively.

2.2.4.2 Tissue lysis for Western blot

Fresh brain tissue of wt or *Cntf* $^{-/-}$ mice was collected in 200 µl of lysis buffer and kept on ice for 30 min. Then two rounds of 8 sonification pulses (MS1 sonotrode, 0.5 s, 80%) were applied followed by 10 more minutes on ice. After a 10 min centrifugation step at 4°C, 14.000 rpm, 75 µl of supernatant were diluted with 37.5 µl of 4 ×Lämmli sample buffer and stored at -20°C for Western blot. 5 µl of sample were diluted in 45 µl of PBS for the BCA assay. The composition of the lysis buffer is listed below:

Table 4 Lysis buffer composition for western blot

component	concentration	volume for 4.25 ml [µl]
EDTA	0.5 M pH 8.0	100
Na-flouride	100 mM	40
Na-pyrophosphate	100 mM	200
Na-ortho vanadate	100 mM	40
NP 40	10 %	400
protease inhibitor mini tablet (Roche)	x	1 [piece]
HEPES, NaCl, Glycerol	50 mM, 150mM, 10 %	3600

2.2.4.3 BCA essay and western blot

The BCA assay was carried out using and following the BCA kit from Thermo Scientific. Western blotting was performed with the Mini Protean Western System from BioRad. For western blotting of fresh brain tissue or organotypic culture lysates, 40 µg of sample was used. For *in vitro* lysates, 25 µl of each sample was used. The samples were loaded on a 15% SDS page gel (composition see below) and run at 200 V. For band size control, 5 µl of the prestained protein ladder was loaded in each gel and the gel was run for about 90 min until the lowest band indicating a size of 15 kDa was run out. Wet blotting onto PVDF membrane took place at 4°C at 25 V (constant) for 15 hr. 5 % milk powder in TBST was used for blocking for 30 – 60 min. The membranes were cut between the 55 kDa and the 75 kDa band. The following proteins or epitopes were probed with the corresponding antibodies (see above):

Table 5 Overview western blot probing

upper part of membrane								
day 1			**day 2**					
protein	size	detection	epitope	size	detection			
pSTAT3	88 kDa	15 -30 s	STAT3	88 kDa	5-10 s			
lower part of membrane								
day 1			**day 2**			**day 3**		
protein	size	detection	epitope	size	detection	epitope	size	detection
pCREB	44 kDa	15 s	CNTF	22 kDa	30-60 s	GAPDH	36 kDa	1 s

Primary antibodies were applied for 1.5 – 3 hr and after three washing steps for 10 – 15 min in TBST, the secondary antibody was applied for 1.5 hr. Primary and secondary antibodies were applied in the 5% milk TBST blocking solution. After secondary antibody incubation, blots were washed twice for 10-20 min in TBST. The blots were developed with Immobilon Western HRP substrate, which was applied for 5 min prior to development and detected by a developing machine on x-ray films. After detection, blots were shortly washed in TBST, and then stripped for 10 min in stripping buffer followed by at least two washing steps in TBST. Membranes were stored in TBST at 4°C over night. Quantitative analysis was performed with FIJI(Image J).

Table 6 Gel composition for western blotting

stacking gel 5 %		**loading gel 15 %**	
component	**volume**	**component**	**volume**
30% Polyacrylamide	0.68 ml	30% Polyacrylamide	4 ml
1 M Tris (pH 6.8)	0.5 ml	1.5 M Tris (pH 8.8)	2 ml
10% Ammoniumpersulfate	40 µl	10% Ammoniumpersulfate	80 µl
10% SDS	40 µl	10% SDS	80 µl
TEMED	4 µl	TEMED	3.2 µl
H_2O	2.79 ml	H_2O	1.84 ml
total	4 ml	total	8 ml

2.2.4.4 Cryostat cutting and Toluidine blue staining of fresh frozen brain tissue

Fresh tissue was snap frozen in tissue tec on dry ice and stored at -80°C degrees. The Cryostat was set to – 16 to – 17°C, both, chamber and table. The lateral ventricles, dorsal and ventral hippocampus were cut into 20 µm sections and transferred immediately onto membrane-coated slides. When up to 8 sections were collected, the slide was placed in 70% ethanol for 30 s and allowed to dry at 40°C for 10 min. Sections were stored over night at 4°C and stained on the next day in 0.02% Toluidine blue prepared in DEPC water for 2-3 min on sight. Sections were then washed in DEPC water for around 5 s, and placed in 75% ethanol for around 60 s, depending on the preferred staining intensity. Sections were dried at 40°C for around 10 min and stored in 50 ml falcons filled with silica gel orange.

2.2.4.5 Laser microdissection

Slides with sections were kept on ice until cutting. The setup was wiped down with RNase Away. The following areas were selected for cutting: lateral ventricles, CA1, CA3, DG, SR, hippocampal fissure, area below the dentate gyrus at the interface to thalamus regions. Samples were collected from both hemispheres from 8-16 sections. When samples from one area were collected, 4.7 µl of lysis buffer was added onto the samples, spun down immediately and kept on ice until sample collection for all areas was completed. Microscope settings and lysis buffer composition are listed below:

Table 7 Microscope settings and lysis buffer composition for LMD

microscope settings		**lysis buffer**		
objective	× 20	**component**	**concentration**	**volume for 5 samples [µl]**

cutting mode	draw and cut	first strand buffer	5 ×	5
	single unit	RT	10 ×	2.5
laser settings		DTT	100 mM	2.5
power	35	glycogen	20 mg/ml	5
speed	20	NP 40	10% stock	1.45
aperture	6	RNasin	-	1.25
speciman balance	21	H_2O	-	5.8

2.2.4.6 Reverse Transcriptase quantitative Polymerase Chain Reaction (RT-qPCR)

LMD samples were incubated at 72°C for 2 min, followed by 1 min incubation on ice. After a 1 min centrifugation step, 0.5 µl of reverse transcriptase was added to each sample and RT took place for 2 hr at 37°C followed by a 5 min cooking step at 95°C. Finally, cDNA samples were stored at -20°C until further processing. Samples were purified with DNA-binding matrix according to the Qiagen kitII protocol. The qPCR was run in the LightCyler 1.5 from Roche using 6 µl cDNA template of purified sample for Cntf and 2 µl cDNA template for the 18S RNA subunit as control. The following primer pairs, master mix composition and program setups were used:

Table 8 Primer pairs and master mix component for qPCR

primer pairs	
name	**Sequence**
CNTF1-279f	5’ GGG ACC TCT GTA GCC GCT CTA T 3’
CNTF1-419r	5’ TCA TCT CAC TCC AGC GAT CAG T 3’
18S rRNA for	5’ CGC GGT TCT ATT TTG TTG GT 3’
18S rRNA rev	5’ AGT CGG CAT CGT TTA TGG TC 3’
master mix composition per sample	
component	**volume [µl]**
Luminaris HiGreen master mix (x2)	10
per primer (20pmol/µl)	0.8
H_2O	6.4
DNA	6 (Cntf), 2 (18 S)

Table 9 Lightcycler program conditions

Lightcycler program conditions				
18 S				
program	**temperature [°C]**	**hold time [s]**	**slope [°C/s]**	**cycles**
denaturation	50	120	20	1
	95	600	20	
amplification	95	15	20	30
	60	30	20	
	72	30	20	
	80	5	20	
melting curve	95	0	20	1
	60	15	20	
	95	0	0.1	
cooling	40	40	20	1
Cntf				
program	**temperature [°C]**	**hold time [s]**	**slope [°C/s]**	**cycles**
denaturation	95	600	20	1
amplification	95	15	20	50
	58	30	20	
	72	30	20	
	78	5	20	
melting curve	95	0	20	1
	60	15	20	
	95	0	0.1	
cooling	40	40	20	1

2.2.5 Immunohisto/cytochemical methods

2.2.5.1 Perfusion of mouse brains

Mice were killed with an overdose of CO_2 and perfused transcardially with first 0.4% heparin in 1 × PBS followed by 4% PFA in 1 x PBS. Roughly 50 -70 ml of heparin/PBS and 50 ml of PFA/PBS were used per animal. Pump speed was set to 25 (arbitrary units). The brain was removed and stored in 4% PFA/PBS at 4°C for overnight post fixation. PFA was exchanged with 1 x PBS 24 hr after perfusion. Brains were stored at 4°C until cutting.

2.2.5.2 Vibratome cutting of perfused mouse brains

Brains were embedded in 6% agarose in 1 x PBS and coronal sections of 40 µm were obtained using the Leica VT 1000S vibratome and collected free floating in 1 x PBS. Sections were kept at 4°C for short term storage. After one or two weeks, sections were transferred to cryoprotectant and transferred to -20°C for long term storage.

2.2.5.3 Immunofluorescent staining in vivo, in vitro and ex vivo

In vivo immunofluorescent staining was performed on free floating sections. Sections were first washed in 1 x PBS. After 30 min in 500 µl blocking solution at room temperature (RT), primary antibodies were applied in 300-500 µl blocking solution over night at 4°C. For Cntf staining, an extra 15-20 min quenching step in 500 µl quenching solution was included before blocking and primary antibody incubation was elongated to two times overnight. Sections were washed three times for 10 min in 500 µl washing solution followed by secondary antibody incubation in 300-500 µl blocking buffer for 3 hr at RT. After three further rounds of washing in 500 µl washing solution, sections were washed twice shortly with 500 µl 1× PBS. After 5 min DAPI (2 mg/ml; 1/5000 in 1× PBS) staining in 500 µl, sections were washed with 1× PBS, mounted on slides and fixed with Aquapolymount.

Immunofluorescent staining *in vitro* proceeded as described above but with shortened time periods of only 1.5 hr per antibody incubation. Washing sessions were performed by applying and removing the washing solution rapidly for eight times. Phalloidin staining preceded the DAPI staining and took 20 min. All steps were carried out at RT and with a volume of 70 µl for the respective solutions.

For staining of *ex vivo* organotypic cultures, the single slices were cut out from the Millicell membrane and four slices were stained in one well in 500 µl of the respective solutions. Immunofluorescent staining was performed similarly to the proceedings mentioned above. However, time spans were elongated: primary antibody incubation lasted for 3 times overnight at 4°C, washing steps took 30 min each, secondary antibody incubation at RT took 3 hr and DAPI staining was performed for 25 min.

2.2.5.4 Confocal microscopy

Images were obtained by confocal microscopy. An inverted IX81 microscope equipped with an Olympus FV1000 confocal laser scanning system and a FVD10 SPD spectral detector was used. Lasers were exciting at 405, 473, 559 and 635 nm. The following objectives were used:

Table 10 Overview over objectives for confocal microscopy

magnification factor	numerical aperture	immersion medium	z level step-size [µm]
× 10 UPlan SAPO	0.4	Air	1-2
× 20 UPlan SAPO	0.75	Air	1
× 40 UPlan FLN	1.30	Oil	0.7 -1
× 60 UPlan FLN	1.25	Oil	0.3 - 0.5

High-resolution images were taken in a sequential manner at high speed, with a maximum pixel resolution of about 2.5 - 3 pixels per feature. Z-stacks of 12 bit images (4095 grey values) were acquired and further processed with FIJI (Image J), where images were converted to RGB 8-bit images. Final processing, linear adjustments of brightness and contrast and figure arrangements were carried out in Adobe Photoshop CS5.

2.2.5.5 Quantitative analysis of indirect immunofluorescent signals in vitro

For all *in vitro* analysis, Phalloidin coupled to Alexa 488 dyes was used to identify the postsynapse. Immunoreactivity (IR) against vGluT was used as a marker for the presynapse (Cy5).

Analysis of colocalization between pStat3, vGluT and Phalloidin were perfomed in FIJI (Image J). The channels were split when opened in FIJI (Image J) and the "Coloc2" analysis was run by FIJI (Image J) for all channel pairings.

For quantitative analysis of pStat3 levels (Cy3) in spines *in vitro*, images of spines with a size of 46 x 46 pixels were randomly chosen in images of wildtype and *Cntf* $^{-/-}$ cultures. Roughly, three areas with spines per cell and 3 to 4 cells in 3-5 different cultures were chosen, adding up to around 40 spines per genotype per condition. The following conditions were analyzed: control, + LTP, Cntf, +LTP and Cntf. The experimenter was blinded for analysis in FIJI (Image J). RGB images were split into the respective channels and the post-and presynapse were marked manually using the freehand selection tool. Selected areas were added to the ROI manager and both were displayed in the channel showing the pStat3 staining. The following parameters were measured by FIJI (Image J): area, mean intensity, minimum and maximum intensity, integrated density and further analyzed in Excel.

Difference in presynaptic area and pStat3 amount between spines contacting astrocytes versus spines that are not in contact with astrocytes was analyzed. For each culture, three cells were evaluated the following way: within each image, three subareas were selected. The vGluT

channel was opened and the threshold was set as suggested. Then particles were analyzed setting the circularity to 0.0 and the arbitrary size from 0.1-5. All selected particles were added to the ROI (region of interest) manager and displayed in the channel showing pStat3 IR. FIJI (Image J) read out the following parameters: area, mean intensity, minimum and maximum intensity, integrated density. Further analysis took place in Excel.

2.2.6 Statistical analysis

Statistical analyses were performed with GraphPad Prism 6. Data are presented with standard error of the means (± SEM). Column statistics were run to check for Gaussian distribution to decide whether to use parametric or non-parametric tests. If one of the groups to be analysed failed the normality test or if value number was too small to run the normality test, non-parametric tests were chosen for further analysis. To account for statistical differences between genotypes and conditions depending on the experiment, one-way/two-way ANOVAs with post hoc multiple comparisons test or unpaired or paired *t*-tests as well as linear regression analyses were performed. Results were considered statistically significant at $p < 0.05$.

3 Results

3.1 Cntf protein and Cntf-coding mRNA is present in the mouse hippocampus

Cntf expression in the central nervous system has previously been detected in the optic nerve, olfactory bulb and in the subventricular zone of the lateral ventricles (Stockli et al., 1991; Sendtner et al., 1992a; Emsley and Hagg, 2003), and at low levels in cortex and hippocampus (Stockli et al., 1991; Ip et al., 1993d). To test whether Cntf is also present in the hippocampus and to identify the cell type that expresses Cntf, immunofluorescent stainings were carried out on PFA-fixed mouse brain sections. First, to confirm the staining technique, the lateral ventricles were investigated which showed Cntf-positive immunoreactivity (IR) in cells along the ventricles (Fig. 3 A). Anti-Cntf IR was absent in *Cntf* $^{-/-}$ animals (Fig. 3 B).

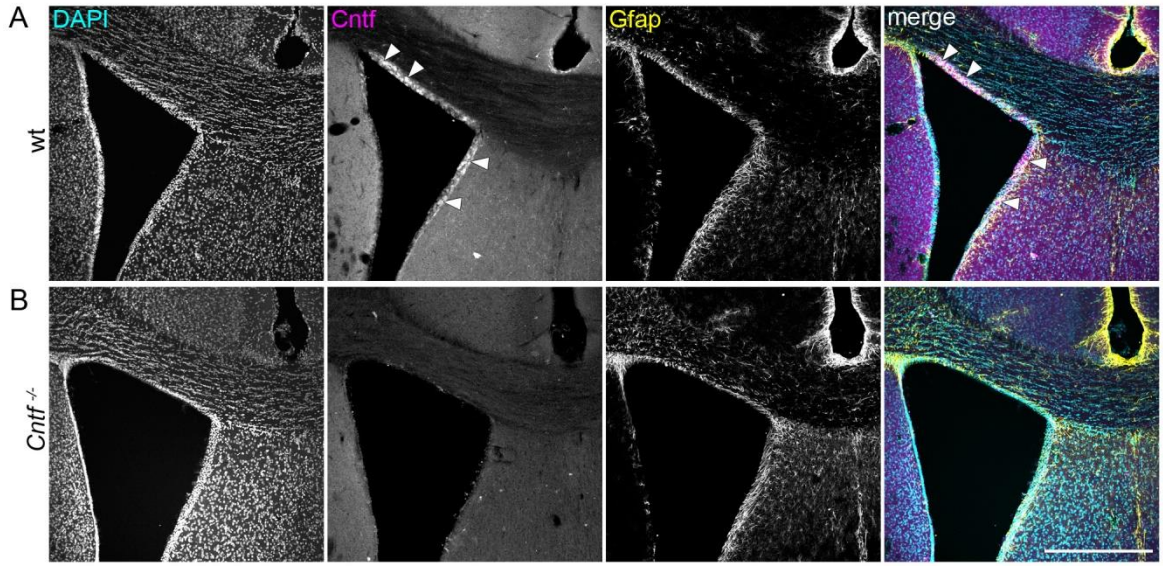

Figure 3. Cntf immunoreactivity is located to cells along the lateral ventricles. Immunofluorescent staining of Cntf in 40 µm thick coronal vibratome slices. **(A)** As indicated by arrows, Cntf immunoreactivity is located in ependymal cells, along the lateral ventricles of wt animals. **(B)** The anti-Cntf immunoreactivity is not present in *Cntf* $^{-/-}$ animals. Scale bar: 300 µm.

Within the hippocampus, Cntf signals were most prominent in the area below the dentate gyrus (DG), which most likely represents meningeal regions. Notably, Gfap-positive astrocytes surrounding vessels along the fissure also showed a pronounced anti-Cntf label (Fig. 4 A). The specific IR for Cntf was absent in *Cntf* $^{-/-}$ animals (Fig. 4 B).

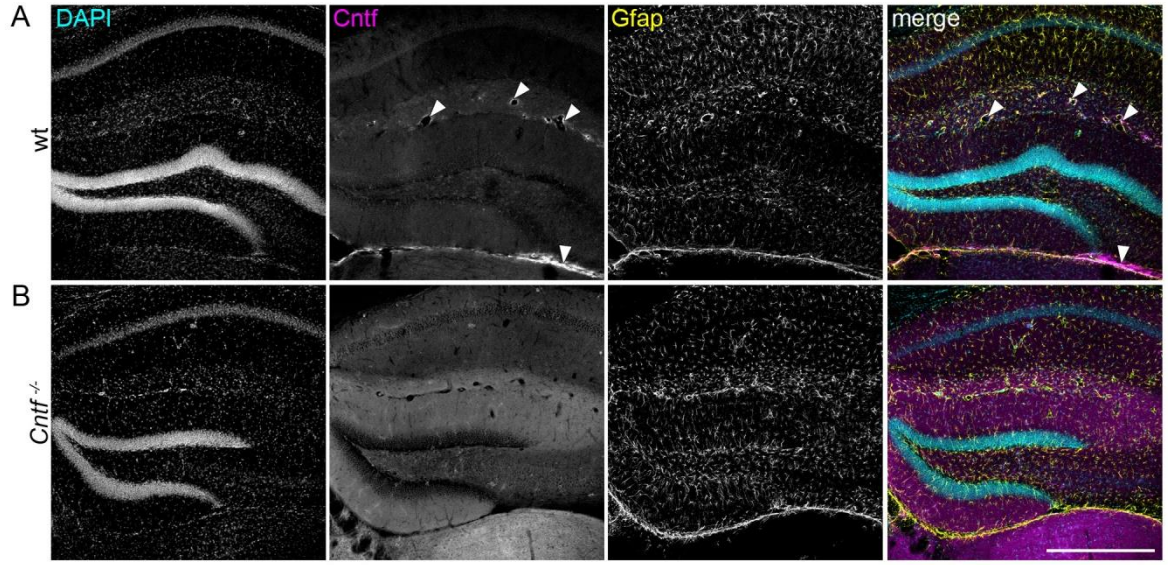

Figure 4. Cntf protein is present in astrocytes of the dorsal hippocampus. Immunofluorescence staining of Cntf in 40 µm thick coronal vibratome slices. **(A)** Immunoreactivity for Cntf is most prominent in the area below the dentate gyrus and in Gfap-positive astrocytes surrounding small blood vessels along the fissure. Arrows indicate positive immunoreactivity. **(B)** Anti-Cntf immunoreactivity is absent in *Cntf* $^{-/-}$ animals. Scale bar: 300 µm

Cntf was also present in Gfap-positive astrocytes in the fimbria including the meninges surrounding the fimbria. Lack of the corresponding IR in *Cntf* $^{-/-}$ animals again confirmed the specificity of the label (Fig. 5 A, B).

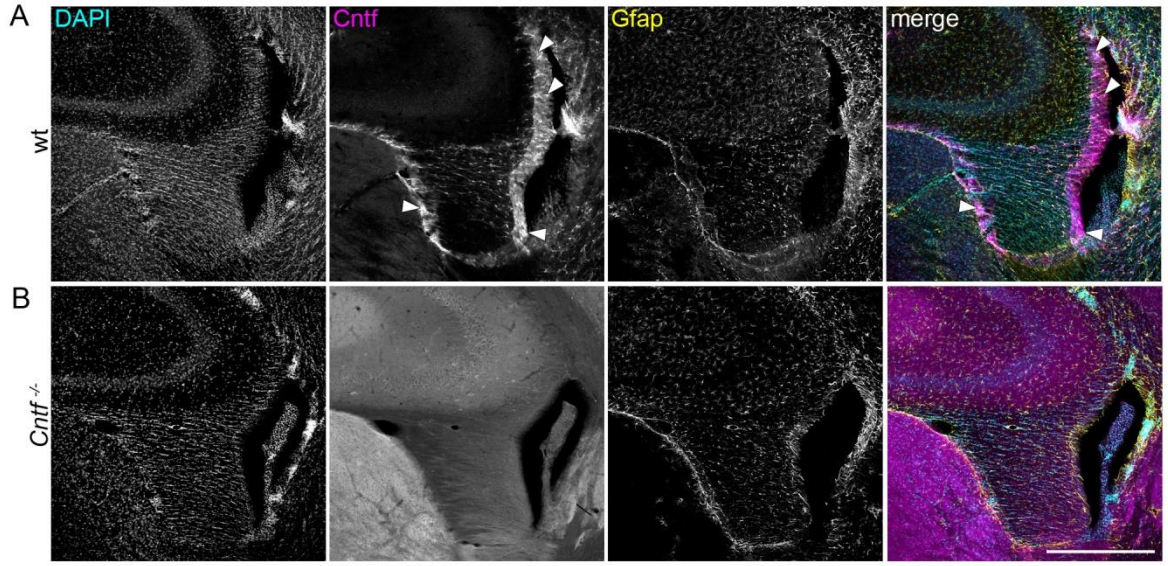

Figure 5. Cntf is located in meninges along the fimbria. Immunofluorescence staining of Cntf in 40 µm thick coronal vibratome slices. **(A)** Cntf immunoreactivity is present in Gfap positive astrocytes in the fimbria and the meninges surrounding the fimbria. **(B)** Specific Cntf staining is not present in *Cntf* $^{-/-}$ animals. Scale bar: 300 µm.

A closer look at the area below the DG confirmed that Cntf-positive cells were Gfap-positive astrocytes (Fig. 6 A, B). Again, the observed IR was absent in *Cntf* $^{-/-}$ animals (Fig. 6 C, D).

Interestingly, no specific staining was detected in granule or mossy cells within the DG, where Cntf was reported to influence neurogenesis (Muller et al., 2009).

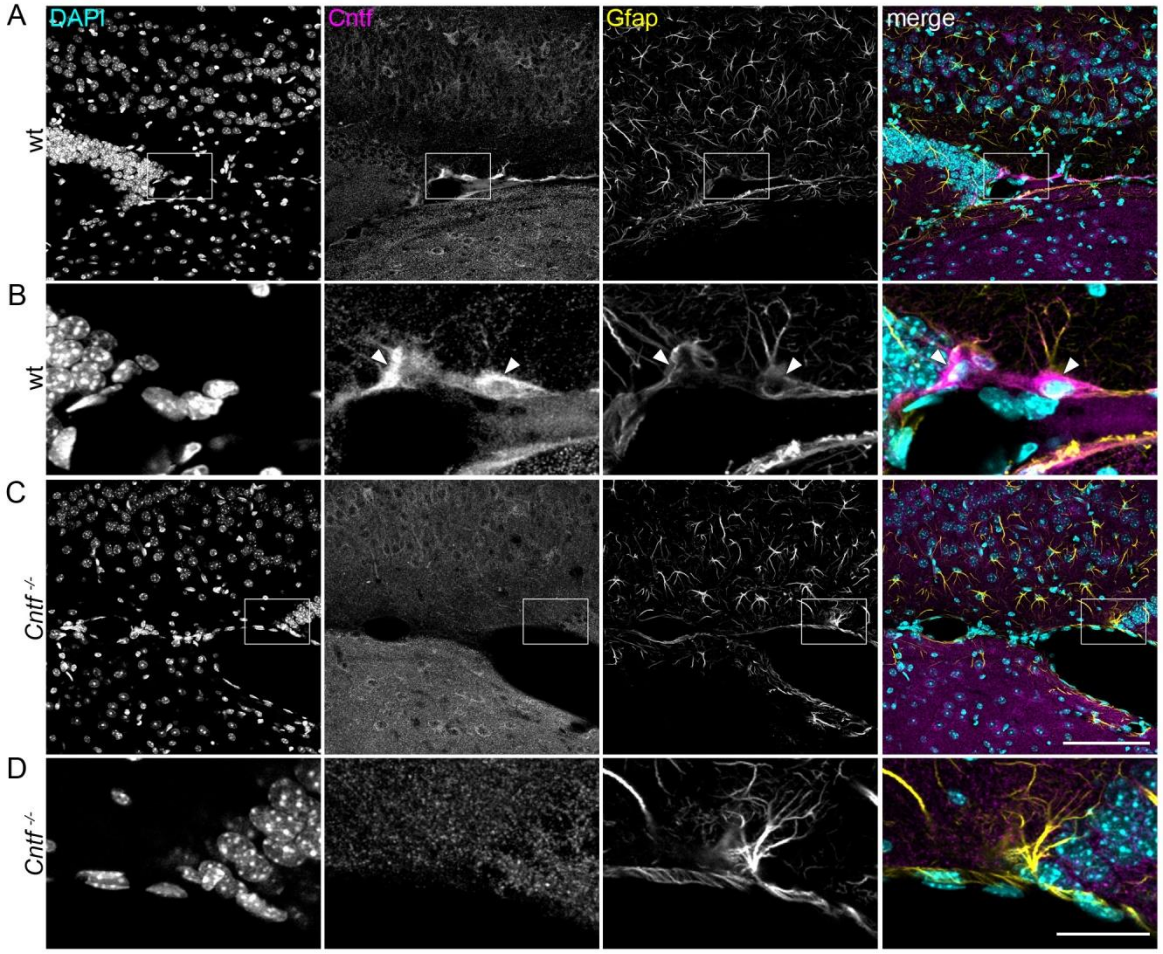

Figure 6. Cntf immunoreactivity is located in Gfap-positive astrocytes. Immunofluorescence staining of Cntf in 40 µm thick coronal vibratome slices. **(A)** Immunoreactivity of Cntf in the area below the dentate gyrus. Cells that are positive for Cntf are also positive for Gfap **(B)**. **(C, D)** The specific staining for Cntf is absent in *Cntf* $^{-/-}$ animals. Scale bar in C: 100 µm and D: 50 µm.

To investigate whether Cntf is also present on the RNA level, laser micro dissection was performed, followed by RT – qPCR analysis. The following areas were dissected from fresh frozen wildtypic mouse brain tissue. Due to the different connectivity profile, RNA was isolated from dorsal and ventral hippocampus and included the DG, CA3, CA1, the hippocampal fissure, the SR and the area surrounding the meninges below the DG (Fig 7 A, B). Highest levels of Cntf-coding mRNA were found in areas around the lateral ventricles. This area was therefore used as reference (Fig. 7 C). Aside from the ventricles, in both dorsal and ventral sections alike, RNA was most abundant in tissues around the meninges. Second highest Cntf-coding mRNA levels were found in the DG. This was surprising since specific immunoreactivity against Cntf in this region was not detectable. The RNA levels in CA3,

CA1 and the fissure were lower than in the DG and comparable amongst each other. The lowest amount of RNA was present in the SR.

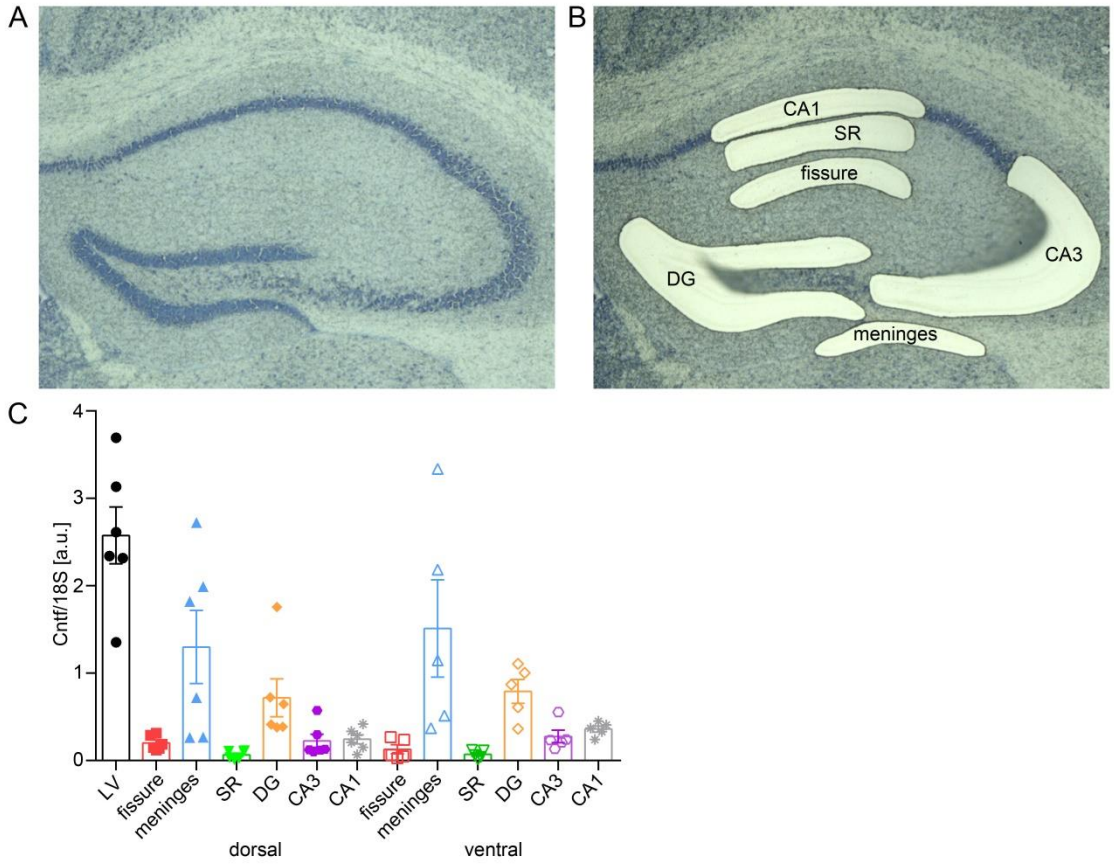

Figure 7. Cntf-coding mRNA is expressed in different areas of the hippocampus. Laser microdissection and qPCR from coronal sections of wt mice. Representative image of a section of a dorsal hippocampus **(A)** before and **(B)** after laser microdissection. **(C)** qPCR analysis shows highest Cntf/S 18 ratio in the lateral ventricles, followed by dorsal and ventral area surrounding the meninges and the DG. CA3, CA1 and the fissure show a similarly low ratio followed by the SR with the lowest RNA amount. Dorsal n = 6, ventral n = 5. LV = lateral ventricles, DG = dentate gyrus, CA3 = cornu ammonis 3, CA1, cornu ammonis 1, SR = stratum radiatum, meninges = area surrounding the meninges. Error bars are presented as ± SEM.

Overall, the results of the RNA analysis reflect the findings of the immunofluorescent stainings. Exception is the DG, which did not show immunoreactivity but revealed the highest levels of Cntf-coding mRNA within the hippocampus. We conclude that Cntf is expressed in the hippocampus of adult wildtype mice.

3.2 Cntf $^{-/-}$ mice do not show a pronounced behavioral phenotype

The observed differences in LTP performance on an electrophysiological level were measured in *ex vivo* hippocampal slices. This could predict functional alterations associated with defective LTP at Schaffer collateral synapses in the CA1 region of the hippocampus. We therefore wanted to know whether *Cntf* $^{-/-}$ mice show behavioral alterations in tasks known to involve this brain structure. Four cohorts of mice, which differed in number of animals and of

which two included female mice (cohort 2 and 3) were used for testing behavioral performance. This experimental approach was used to avoid over-standardization and to verify tendencies or effect sizes over several samples. In addition, some of the behavioral approaches, like the Morris water maze and some fear conditioning paradigms, had to be established in the course of this thesis. The validity of the anxiety-related and locomotor specific tests like open field, elevated plus maze and dark/light test within our animal facility was verified by studies on other mouse lines subjected to these tests (Deckert et al., 2017; Luningschror et al., 2017; R von Collenberg et al., 2019). Subsequent statistical analysis of cohort 2 and 3 showed that behavior in both cohorts, of male as well as female mice, was significantly different from another regarding some of the experiments (statistical details in Table 12). Although the results were similar on a qualitative level, an arithmetic grouping of the two cohorts was not feasible for the respective experiments. Therefore, results are then shown qualitatively but without statistical analysis due to the low n-numbers within the different samples.

3.2.1 Cntf $^{-/-}$ mice show no obvious phenotype in the novel object recognition task

In the novel object recognition task (NOR), mice are presented with two identical objects which they are allowed to explore freely (Fig. 8 A). After a certain amount of time, mice are exposed to the same situation but this time, one of the objects is substituted by a novel one (Ennaceur and Delacour, 1988; Antunes and Biala, 2012). Since the mice have to process the properties of the objects and recall them for comparison when they face the novel object, this task is well suited to investigate basic memory function (Ennaceur, 2010). At least the memory consolidation is believed to be hippocampus-dependent and the hippocampus seems to be responsible for long-term object recognition in rodents (Reger et al., 2009; Antunes and Biala, 2012).

One measure of recognition memory which is commonly used in the NOR is the discrimination ratio (DR) (Winters et al., 2008; Denninger et al., 2018; Sivakumaran et al., 2018). It is calculated from the time difference spent between the objects in relation to the total time spent investigating either object: [(novel – familiar) / (novel + familiar) [s]]. The DR ranges from -1 (total time spent at familiar object) to +1 (total time spent at the novel object) and classifies animals with values above 0 as learners. Cohort 1 was excluded from analysis, since the DR of the wt animals did not differ significantly from 0 (wt: $t(6) = 0.7647$, $p = 0.4734$, one sample t-test *vs*. 0). Likewise, wt and *Cntf* $^{-/-}$ mice females in cohort 2 did not

classify as learners (wt: t (5) = 0.7782, p = 0.4716; *Cntf* $^{-/-}$: t (3) = 1.565, p = 0.2154 one sample t-test *vs*. 0).

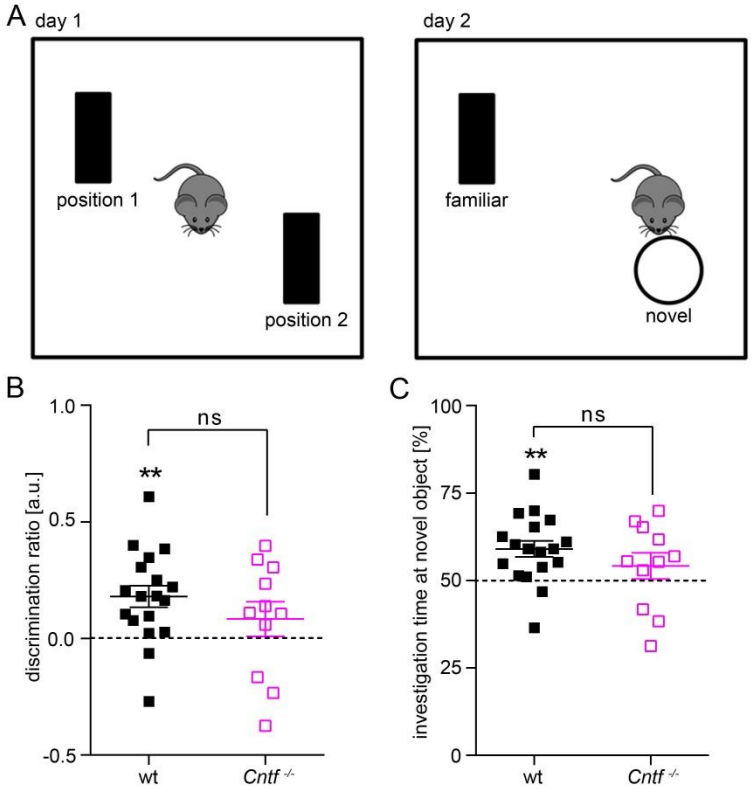

Figure 8. Wt and *Cntf* $^{-/-}$ mice of cohort 2 and 4 perform similar in the novel object recognition (NOR) task. (A) Schematic depiction of the NOR experimental procedure. Mice were presented with two identical objects on day 1 of which one is substituted with a novel object 24 h later. **(B)** Discrimination ratio (DR) of wt mice differs significantly from 0 whereas this is not the case for *Cntf* $^{-/-}$ mice. Wt and *Cntf* $^{-/-}$ mice do not differ significantly from each other. Mice with a DR above 0 are considered learners. Therefore 2 wt and 3 *Cntf* $^{-/-}$ mice are defined as non-learners. **(C)** The same relations between wt and *Cntf* $^{-/-}$ mice are present when the results are presented as the percentage of time spent at the novel object in relation to the total time spent at either of the objects. Male wt: n = 18, male *Cntf* $^{-/-}$: n = 11. ns $p < 0.05$ ** $p < 0.01$, error bars are presented as ± SEM.

In the remaining group of male mice of cohort 2 and 4, the DR of wt mice differed significantly from 0 (Fig. 8 B, t (17) = 3.892, p = 0.0012, one sample t-test *vs*. 0) whereas this was not the case for *Cntf* $^{-/-}$ mice (Fig. 8 B, t (10) = 1.116, p = 0.2903, one sample t-test *vs*. 0). 88.8% of wt male mice and 72.7% of *Cntf* $^{-/-}$ mice are therefore defined as learners. However in a separate analysis to compare between the groups, no overall statistical difference between wt and *Cntf* $^{-/-}$ mice was calculated (p = 0.2523, unpaired t-test). The same p-values were achieved when the percentage of time spent at the novel object in relation to the total time spent at either of the objects was determined (Fig. 8 C, respective p-values, one sample t-tests *vs*. 50%).

3.2.2 Cntf $^{-/-}$ mice perform normal in the Morris water maze

The Morris Water Maze (MWM) was originally invented in 1981 by Richard Morris to study place navigation in rodents (Morris, 1984). In brief, animals have to escape a circular swimming pool onto a platform that is hidden just beneath the surface, by using distal visual cues for orientation. These investigators showed that in case of lesion of the hippocampus, rats showed drastic impairment in place navigation (Morris et al., 1982). Blocking of NMDA receptors in the hippocampus also affected place learning in the MWM, which suggests that NMDA-dependent forms of LTP might be involved in hippocampal place learning (Morris et al., 1986).

Here, three cohorts of mice, two of which included female mice, were used to establish the MWM test and to investigate a possible consequence of Cntf-deficiency on spatial learning. One cohort was excluded from further analysis because these mice did not learn to find the location of the platform. The remaining two cohorts 2 and 3 did not behave significantly different from other cohorts regarding the classic MWM (see Table 12) and were therefore grouped. These cohorts also helped to establish the reverse MWM test, as indicated by the qualitative results. Both genotypes and genders reduced the latency to find the platform over the five training days (Fig. 9 A, B). Genotypes did not differ significantly from another (Fig. 9 A; $F(1, 21) = 0.3752$, $p = 0.5467$, 2way ANOVA genotype male; Fig. 9 B, $F(1, 17) = 1.131$, $p = 0.3024$, 2way ANOVA genotype female). On the test day when the platform was removed female and male mice spent most time in the target quadrant, independently of the genotype (Fig. 9 C; $F(1, 76) = 0.00108$, $p = 0.9739$, 2way ANOVA genotype male; Fig. 9 D, $F(1, 17) = 1.131$, $p = 0.3024$, 2way ANOVA genotype female).

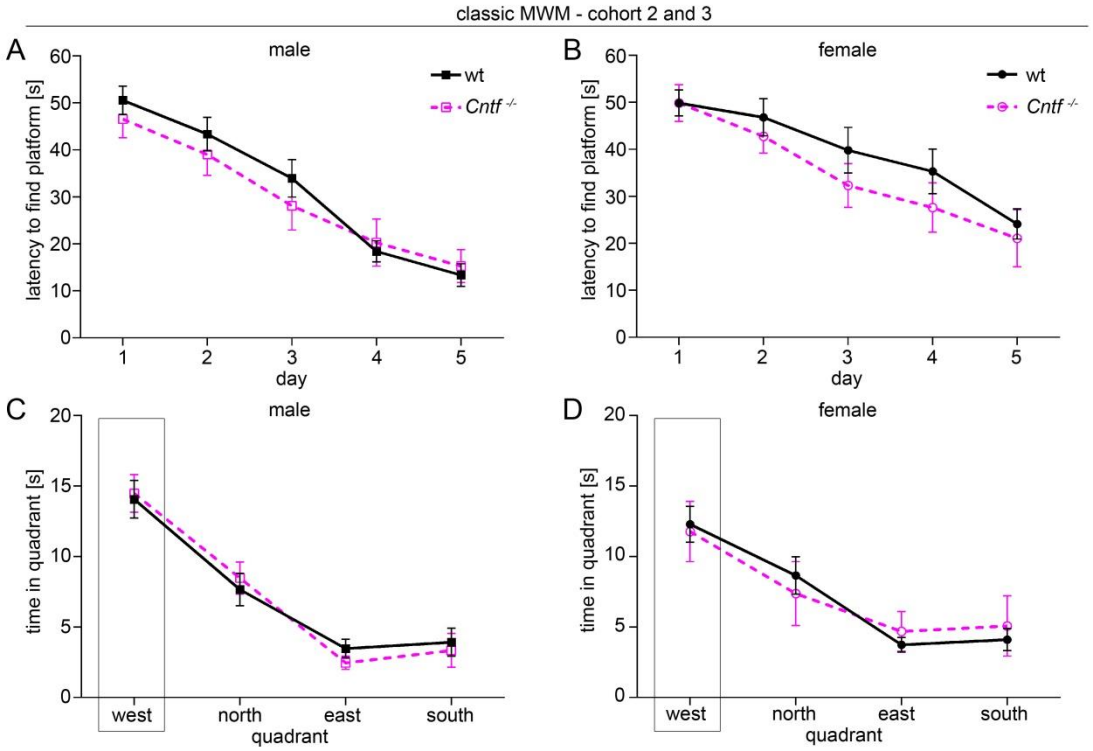

Figure 9. Wt and *Cntf* $^{-/-}$ mice in cohort 2 and 3 perform equally well in the classic Morris water maze (MWM). Mice underwent classical MWM. **(A)** Male mice of either genotype learned to find the platform faster over the course of a five-day training. **(B)** Female wt and *Cntf* $^{-/-}$ mice showed decreased latency to find the platform within five days of training. **(C)** Male mice and **(D)** female mice of both genotypes spent most time in the target quadrant on the test day, when the platform was removed. Male wt: n = 14, *Cntf* $^{-/-}$: n = 8; female wt: n = 11, *Cntf* $^{-/-}$: n = 8. Error bars are presented as ± SEM

Male mice of cohort 2 were used to establish a reminder before entering reversal MWM learning. Six runs to the platform of the classic MWM served as a reminder before the platform was moved to the opposite quadrant to start reversal learning. The latency to find the platform increased from 11.79 s in wt and 7.07 s in *Cntf* $^{-/-}$ mice on the sixth run to a mean of 45.9 s and 41 s in wt and *Cntf* $^{-/-}$ mice on the first run to the relocated platform, respectively, (Fig. 10 A). Over the subsequent 2 runs, latency decreased again in both genotypes. However, mice increasingly displayed fatigue after the 8th run and the experiment was thus stopped. Over the next 4 days, males of both genotypes remained at the same level of latency to find the platform, which they had acquired towards the end of the classic MWM (Fig. 10 B). Female mice of both genotypes decreased their latencies to find the platform over the 5 days of training (Fig. 10 C). On the test day, all animals spent most of the time in the new target quadrant (Fig. 10 D, E).

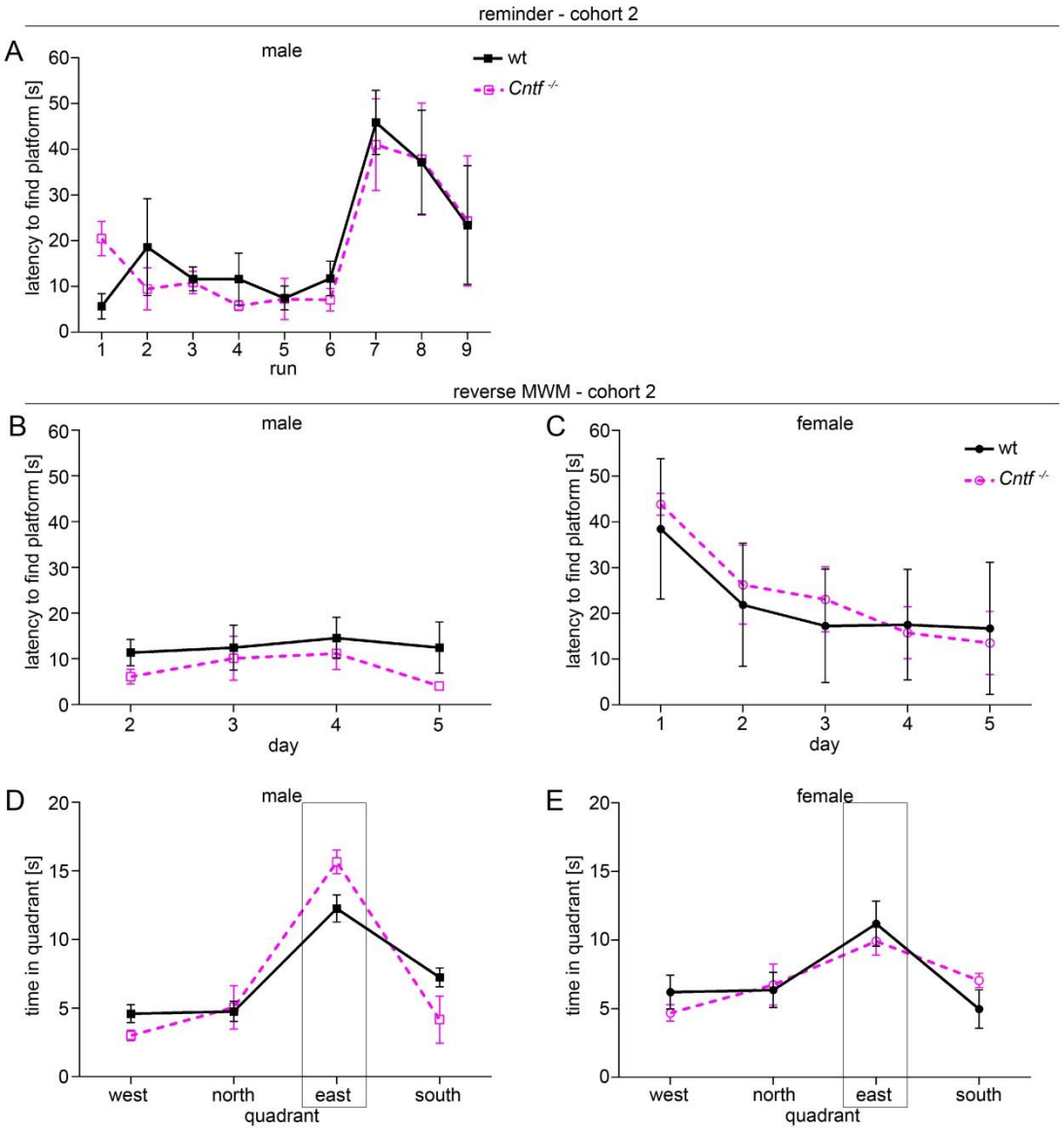

Figure 10. Wt and *Cntf* $^{-/-}$ mice in cohort 2 perform equally well in the reverse Morris water maze (MWM). Mice underwent a reminder followed by reversal MWM. **(A)** Wt and *Cntf* $^{-/-}$ male mice perform equally in the reminder test, which consists of 6 runs towards the previously learned location of the platform and 3 runs towards a relocated platform. For both groups of mice, the latency to find the relocated platform decreases within 3 runs after an initially increased latency in comparison to runs towards the former location of the platform. **(B)** Over the course of 4 further training days in the reversal MWM, both wt and *Cntf* $^{-/-}$ mice sustain the latency to find the platform. **(C)** Female mice were not subjected to a reminder test but both wt and *Cntf* $^{-/-}$ mice decrease their latencies to find the relocated platform from the first to the second training day and keep the latencies at approximately the same level of the last 4 training days. Independent of the genotype, both **(D)** male and **(E)** female mice spend most time in the new target quadrant on the test day of reversal MWM. N-numbers are too low to run statistical analysis. Squares represent male, circles female mice. Male wt: n = 8, *Cntf* $^{-/-}$: n = 3; female wt: n = 6, *Cntf* $^{-/-}$: n = 4. Rectangles in (D) and (E) mark the target quadrant on the test day. Error bars are presented as ± SEM.

Since the reminder training in the previous cohort was set for too many runs, mice in cohort 3 faced only 2 reminder runs to the classic platform location before performing 6 runs with a relocated platform. Male and female mice alike and independent of the genotype showed an increased latency to find the platform on the first run with a relocated platform (Fig. 11 A, B).

The latency decreased over the remaining 5 runs of the reminder test and continued at a decreased level of the subsequent 4 training days (Fig. 11 A-D). On the testing day, all mice spent most time in the new target quadrant (Fig. 11 E, F). Overall, *Cntf* $^{-/-}$ mice did not show a deficit in place learning neither in the classic, nor in reversal learning paradigm. In our experiments, gender did not seem to influence the spatial learning performance but due to the low n-numbers a valid conclusion cannot be made for the reversal learning at this point.

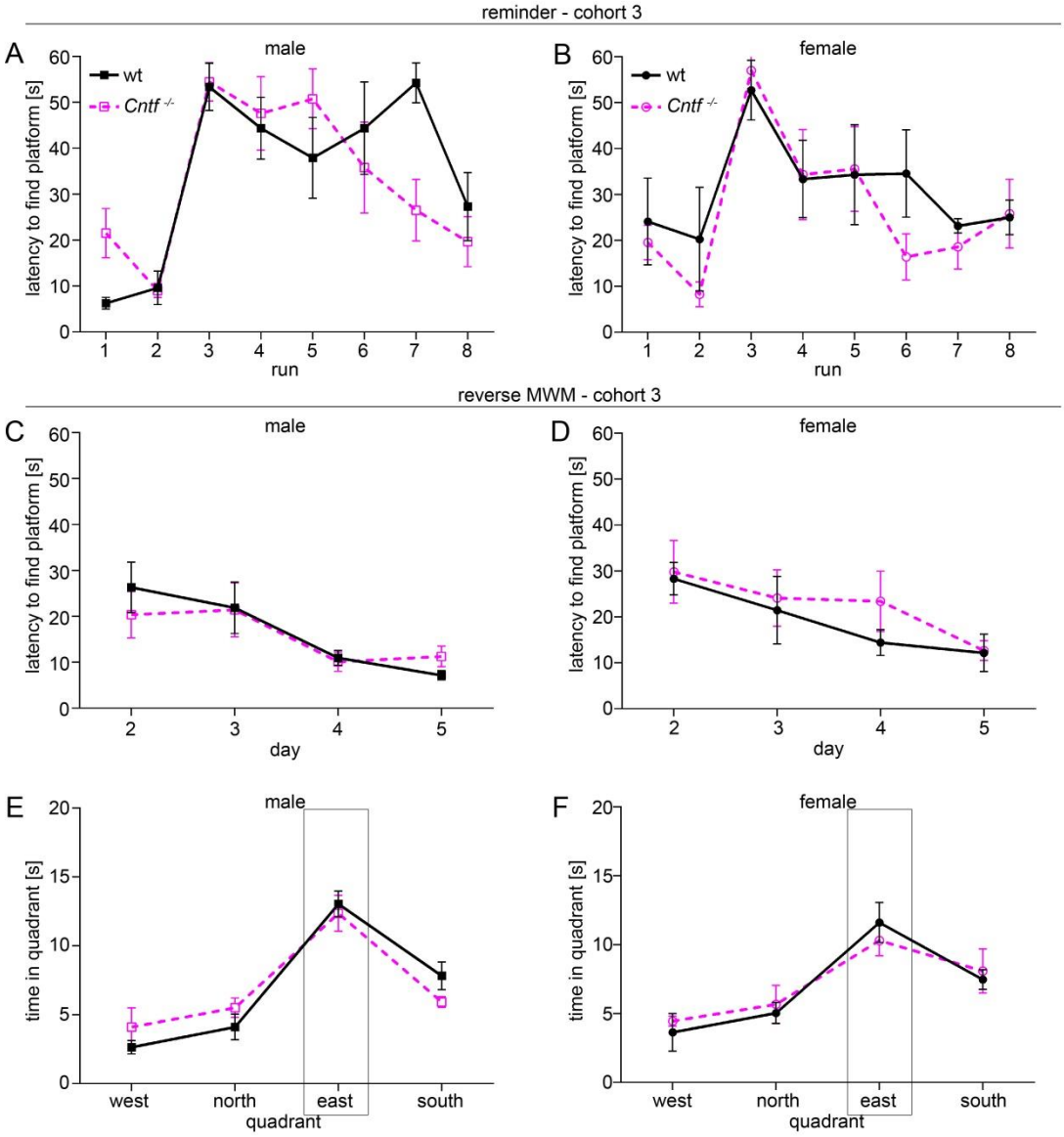

Figure 11. Wt and *Cntf* $^{-/-}$ mice of cohort 3 perform equally well in the reverse Morris water maze (MWM). Mice had to perform by a reminder training day before reversal MWM. **(A, B)** Male and female mice underwent a reminder day where two runs to the classic platform location was followed by 6 runs with a relocated platform. Both male and female, wt and *Cntf* $^{-/-}$ mice increased latencies to find the platform when the platform was first relocated. All mice decreased the latency to find the relocated platform over the course of the 6 runs. **(C)** Male wt and *Cntf* $^{-/-}$ mice slightly further decreased their latencies to find the reverse platform over 4 further training days. **(D)** Female mice of both genotypes further decreased the latency to find the platform over the remaining 4 training days. Male and female **(E, F, respectively)** mice of both genotypes spent most time on the test day in the new target quadrant, as indicated by the rectangle. N-numbers are too low to run statistical

analysis. Squares represent male, circles female mice. Male wt: n = 6, *Cntf* $^{-/-}$: n = 5; female wt: n = 5, *Cntf* $^{-/-}$: n = 4. Error bars are presented as ± SEM.

3.2.3 Cntf $^{-/-}$ mice show intact fear processing in different fear conditioning paradigms

One of the most commonly used forms to investigate fear behavior is Pavlovian fear conditioning. In brief, an animal is confronted with an initially neutral conditioned stimulus (CS), which can be a tone or a context, which is paired in its presentation with an unconditioned stimulus (US), most often an electric foot shock. If the pairing of CS and US is presented sufficiently enough, the animal will have learned that the CS predicts the US. This leads to a defense response to the CS alone, which the animal would have initially only displayed in reaction to the US. The typically displayed defense response is freezing, but also flight is an option. Pavlovian fear conditioning is a typical paradigm to investigate associative learning and memory processing (Johansen et al., 2011; LeDoux, 2014). While an acoustic cue triggers more strongly the involvement of a neuronal circuit from the auditory cortex to the amygdala, the fear circuit including the hippocampus is more involved in processing of contextual information (Phillips and LeDoux, 1992). Here, we tested three different fear conditioning paradigms.

With cohort 1 and 2, a three day paradigm was performed which involved an acoustic cue as well as contextual information (Fig. 12 A). Male mice of cohort 1 and 2 differed significantly from each other ($F(1, 13) = 7.868$, $p = 0.0149$, 2way ANOVA, male mice cohort 1 *vs.* 2; $p < 0.0001$ after shock, $p = 0.0128$ tone B, Sidak's multiple comparison) and cohorts where thus not grouped. The n-numbers in cohort 2 alone were thus too low to perform statistical analysis, but qualitative data are displayed. Freezing behavior of mice in cohort 1 did not differ between the genotypes (Fig. 12 B; $F(1, 15) = 1.608$, $p = 0.2241$, 2way ANOVA, genotype) but across phases ($F(4, 60) = 48.03$, $p < 0.0001$, 2way ANOVA, phase). Mice of both genotypes showed significantly higher freezing rates after receiving the foot shock (Fig. 12 B; wt: $p < 0.0001$, *Cntf* $^{-/-}$: $p < 0.0001$, Sidak's multiple comparison, before shock *vs.* after shock). On the following day, when the retrieval of the tone was tested in a different context, both groups of mice showed significantly higher freezing during tone presentation (Fig. 12 B; wt: $p < 0.0001$, *Cntf* $^{-/-}$: $p = 0.0011$, Sidak's multiple comparison, context B *vs.* tone B). However, on the third day, when mice were tested for retrieval of the context, freezing rates did not differ between context A and context B the previous day (Fig. 12 B; wt: $p = 0.9477$, *Cntf* $^{-/-}$: $p = 0.5649$, Sidak's multiple comparison, context B *vs*. context A). Mice in cohort 2 displayed qualitatively similar freezing dynamics (Fig. 12 C, D). *Cntf* $^{-/-}$ mice showed no

deficit in acquisition and memory retrieval of the acoustic cue, contextual information did not trigger increased freezing responses in wt or *Cntf* $^{-/-}$ mice in this paradigm.

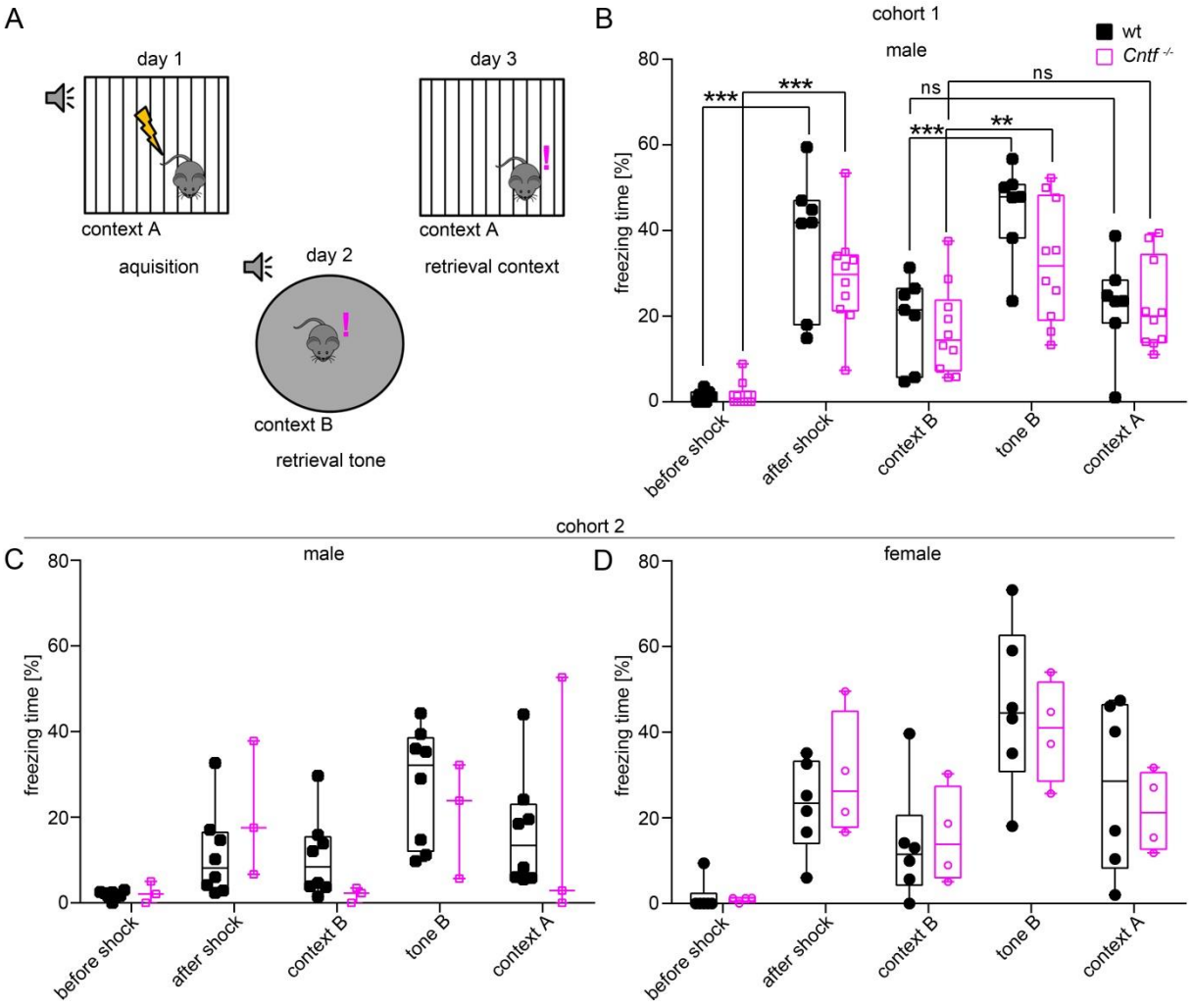

Figure 12. Wt and *Cntf* $^{-/-}$ mice in cohort 1 (B) and 2 (C, D) perform similar in a cued fear conditioning paradigm. (A) Scheme of the experimental procedure. Mice were conditioned in context A by three tone-shock pairings. Electric foot shocks were delivered via the metal grid floor. 24 h later, mice were placed in context B where after a short habituation phase the tone was presented 3 times. On the third day, mice were placed in context A without presentation of the tone. **(B)** Male wt and *Cntf* $^{-/-}$ mice of cohort 1 performed similar over the 3 day experiment. Both groups of mice froze significantly higher after receiving three electric foot shocks. On the following day, wt and *Cntf* $^{-/-}$ mice froze significantly higher upon tone presentation, compared to context B alone. Both groups of mice did not freeze more when replaced in context A on the third day, compared to freezing rates in context B. **(C, D)** The number of mice in cohort 2 was too low to analyze the difference of the effect statistically. **(C)** Male mice of either genotype froze more after the shock than before. Similar freezing levels were maintained in context B by wt mice but increased independent of the genotype upon tone presentation. Back in context A on the third day, freezing rates of wt mice were similar to freezing rates in context B, *Cntf* $^{-/-}$ mice behaved diversely. **(D)** Female mice of cohort 2, independent of the genotype, showed qualitatively comparable freezing dynamics as mice in cohort 1. Freezing rates were increased after shock perception, lower in context B alone, but increased upon tone presentation in context B. Freezing rates on the third day in context A were similar than freezing rates in context B. Squares represent male mice, circles represent female mice. Cohort 1: male wt: n = 7, *Cntf* $^{-/-}$: n = 10; cohort 2: male wt: n = 8, *Cntf* $^{-/-}$: n = 3, female wt: n = 6, *Cntf* $^{-/-}$: n = 4. ** $p < 0.01$, *** $p < 0.001$. Error bars are presented as ± SEM.

In the paradigm tested in cohort 1 and 2, cue information might have taken priority over contextual information processing. The hippocampus has been suggested to be involved in contextual modulation of fear extinction (Ji and Maren, 2007; Maren and Hobin, 2007). To include hippocampal function more strongly, we therefore tested a fear conditioning paradigm which involved extinction in the next cohort (Fig. 13 A). Statistical analysis was performed for male mice only, because the n-numbers of investigated female mice was too low. Overall, male mice of both genotypes did not behave differently from each other (Fig. 13 B, D, F; F (1, 10) = 3.350, p = 0.0971, 2way ANOVA, genotype). Both groups showed increased freezing rates after having received the foot shock, though not significantly (Fig. 13 B; wt: p = 0.0729, *Cntf* $^{-/-}$: p = 0.3448, Sidak's multiple comparison, before shock *vs*. after shock). However, wt and *Cntf* $^{-/-}$ mice displayed significantly higher freezing rates upon retrieval presentation of the tone in context B on the following day (Fig. 13 B; wt: p < 0.0001, *Cntf* $^{-/-}$: p = 0.001, Sidak's multiple comparison, context *vs*. tone in B). In the first extinction trial, *Cntf* $^{-/-}$ mice behaved differently from the wt mice: *Cntf* $^{-/-}$ mice showed higher freezing rates during the early phase of the first extinction session (Fig. 13 D; p = 0.0106, Sidak's multiple comparison, early phase E1 wt *vs*. *Cntf* $^{-/-}$). Both genotypes had reduced freezing rates in the late phase of the extinction sessions (Fig. 13 D; wt: E1 p = 0.0688, E2 p = 0.0001; *Cntf* $^{-/-}$: E1 p = 0.0002, E2 p = 0.0148, Sidak's multiple comparison, early *vs*. late). When mice where replaced in the original fear conditioning context A for fear renewal, freezing rates were increased but not significantly higher upon tone presentation (Fig. 13 F; wt: p = 0.5401, *Cntf* $^{-/-}$: p = 0.3774, Sidak's multiple comparison, context *vs*. tone A). Female wt and *Cntf* $^{-/-}$ mice showed qualitatively similar freezing dynamics (Fig. 13 C, E, G). Female and male mice of both genotypes were additionally tested in a Hot Plate paradigm at 55°C to ensure that perception of painful sensual cues delivered to the feet were unaffected (data not shown). Male wt male mice took 15.72 ± 3.127 s on average before licking their hind paw; *Cntf* $^{-/-}$ mice took 19.19 ± 2.531 s. Female wt mice took 15.65 ± 3.928 s and *Cntf* $^{-/-}$ females 14.58 ± 1.646 s. Wt as well as *Cntf* $^{-/-}$ mice in cohort 3 showed intact cued fear acquisition and fear memory retrieval. During extinction trials, freezing rates in wt and *Cntf* $^{-/-}$ male decreased from the retrieval tone presentation in B compared to the late extinction phase in E2, but not significantly (wt: p = 0.0735, *Cntf* $^{-/-}$: p = 0.3284, Sidak's multiple comparison, retrieval tone B *vs*. late extinction E2).

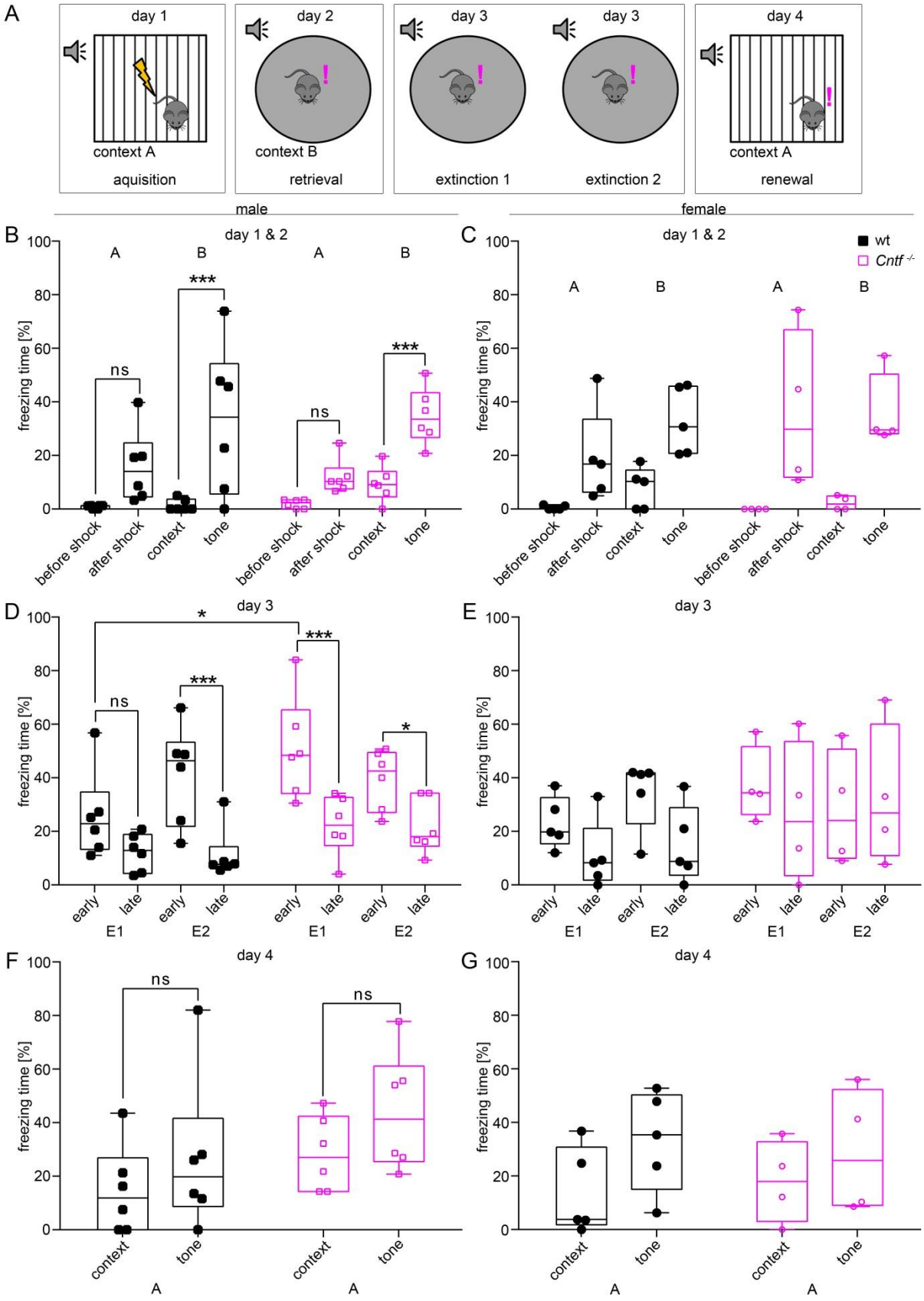

Figure 13. Wt and *Cntf* $^{-/-}$ mice of cohort 3 perform similar in a cued renewal fear conditioning paradigm. **(A)** Scheme of the experimental procedure. Mice were conditioned in context A with five pairings of an acoustic cue and an electric foot shock delivered via the metal grid floor. On the following day, mice were placed in context B, where they were presented with the tone from the previous day for retrieval. On day three, mice

underwent two extinction trials with tone presentations in context B before they were placed in the original context A and confronted with the tone again on day 4. **(B)** Male wt and *Cntf* $^{-/-}$ mice showed the same freezing dynamics during acquisition and retrieval the next day. Both groups of mice froze more after shock presentations. Freezing rates to context B alone were significantly lower than during tone presentation. **(C)** Female mice of both genotypes displayed similar freezing behavior during acquisition and retrieval than the male mice. Higher freezing rates after the shock and upon tone presentation during retrieval, compared to context B alone. **(D)** Wt and *Cntf* $^{-/-}$ mice behaved similarly during extinction. Wt and *Cntf* $^{-/-}$ mice showed within session extinction, when comparing early *vs.* late extinction phases. During the early phase of the first extinction session, *Cntf* $^{-/-}$ mice froze significantly higher than wt mice. **(E)** Female wt mice qualitatively showed within session extinction. *Cntf* $^{-/-}$ mice showed very diverse freezing rates. **(F)** In the renewal test on day 4, wt and *Cntf* $^{-/-}$ mice showed slightly increased freezing upon tone presentation compared to context A alone. **(G)** Female mice of both genotypes showed a very slight increase in overall freezing rates upon tone presentation back in context A. Only male mice were analyzed statistically. Squares represent male, circles female mice. Male wt: n = 6, *Cntf* $^{-/-}$: n = 6; female wt: n = 5, *Cntf* $^{-/-}$: n = 4. Error bars are presented as ± SEM. ns $p > 0.05$, * $p < 0.05$, *** $p < 0.001$.

To fully concentrate on hippocampal function in fear memory processing, the 4th cohort underwent a contextual AAA- fear conditioning paradigm (Fig. 14 A). Wt and *Cntf* $^{-/-}$ mice did not behave significantly different from each other (Fig. 14 B; $F(1, 15) = 2.540$, $p = 0.1318$, 2way ANOVA, genotype). Both groups of mice displayed significantly higher freezing rates after the shock (Fig. 14 B wt: $p = 0.0013$, *Cntf* $^{-/-}$: $p = 0.0042$, Sidak's multiple comparison, before shock *vs.* after shock). Likewise, wt and *Cntf* $^{-/-}$ mice froze significantly more during fear retrieval than before having received the shock (Fig. 14 B wt: $p < 0.0001$, *Cntf* $^{-/-}$: $p < 0.0001$, Sidak's multiple comparison, before shock *vs.* retrieval). After 5 extinction sessions, freezing rates were decreased in wt and *Cntf* $^{-/-}$ mice (Fig. 14 B wt: $p = 0.3089$, *Cntf* $^{-/-}$: $p = 0.0031$, Sidak's multiple comparison, retrieval *vs.* extinction). Two wt mice did not show increased freezing rates during the retrieval session but during the late extinction. Upon spontaneous recovery of memory on day 14, wt and *Cntf* $^{-/-}$ mice showed only a minor increase in freezing (Fig. 14 B wt: $p = 0.9465$, *Cntf* $^{-/-}$: $p = 0.8952$, Sidak's multiple comparison, extinction *vs.* spontaneous recovery).

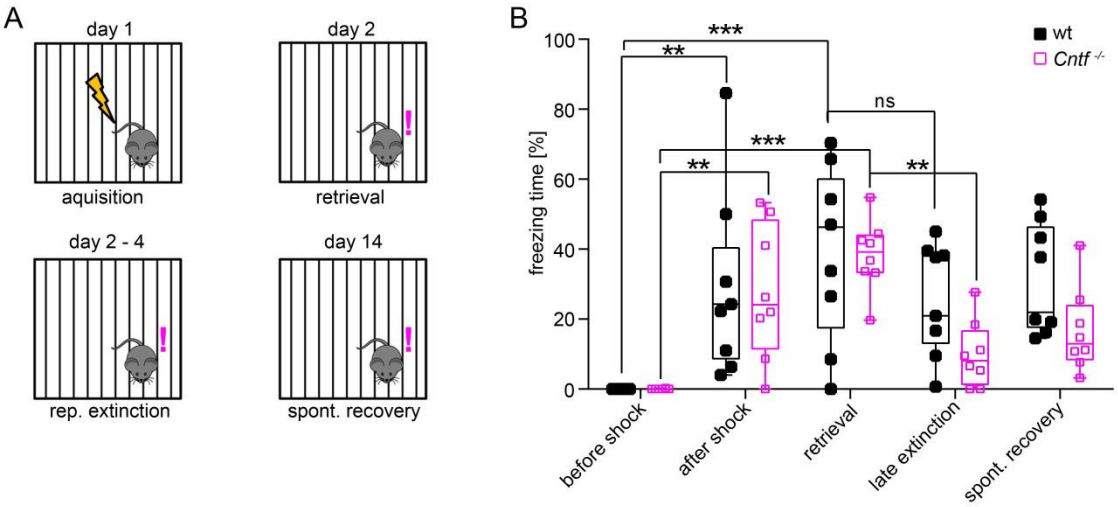

Figure 14. Wt and *Cntf* $^{-/-}$ mice of cohort 4 perform similar in a contextual AAA-fear conditioning paradigm. (A) Scheme of the experimental procedure. Mice were conditioned with Five foot shocks delivered

via the metal grid floor. Mice were placed into the same context for retrieval and a separate extinction session on the next day. On consecutive days 3 and 4, mice underwent two extinction trials per day. On day 14, mice were placed in the same context again for spontaneous recovery. **(B)** Wt and *Cntf* $^{-/-}$ mice showed similar freezing dynamics. Mice in both groups froze significantly more after shock presentation and during the retrieval session than before the shock. Both groups of mice showed a reduction in freezing from the retrieval session to the last extinction session. Wt and *Cntf* $^{-/-}$ mice showed a minimal tendency to freeze more during spontaneous recovery on day 14. Male wt: n = 8, *Cntf* $^{-/-}$: n = 8. Error bars are presented as ± SEM. ns $p > 0.05$, ** $p < 0.01$, *** $p < 0.001$.

Overall, *Cntf* $^{-/-}$ mice do not show deficits in acquisition and retrieval of either acoustic or contextual cues and show intact contextual extinction as well as extinction within sessions for acoustic cues.

Cntf $^{-/-}$ mice were also tested for anxiety-like behavior in the open field test, the elevated plus maze test and the dark/light test.

3.2.4 Cntf $^{-/-}$ *mice do not display abnormal anxiety-like or locomotor behavior in the open field test*

The open field test (OF) is commonly used to investigate locomotor behavior as well as anxiety-like behavior in mice, exploiting their dislike to wide open spaces (Carola et al., 2002). Cohort 2 and 3, which both include female mice were exposed to the OF. The groups were not paired because the cohorts differed in absolute values from each other regarding some parameters (see Table 12), but not necessarily qualitatively. Thus, due to a low n-number in all groups, results were not analyzed statistically. However, qualitative results are also displayed for both cohorts combined (Fig. 15 A-D). Male wt mice of both cohorts spent similar amounts of time in the center of the OF as the *Cntf* $^{-/-}$ mice (Fig. 15 E, I). Female mice independent of the genotype reflect that behavior (Fig. 15 G, K). The total distances travelled do not seem to differ greatly in males and females, wt and *Cntf* $^{-/-}$ of both cohorts (Fig. 15 F, J and H, L). Wt and *Cntf* $^{-/-}$ mice do not seem to differ in locomotor or anxiety-like behavior in the OF.

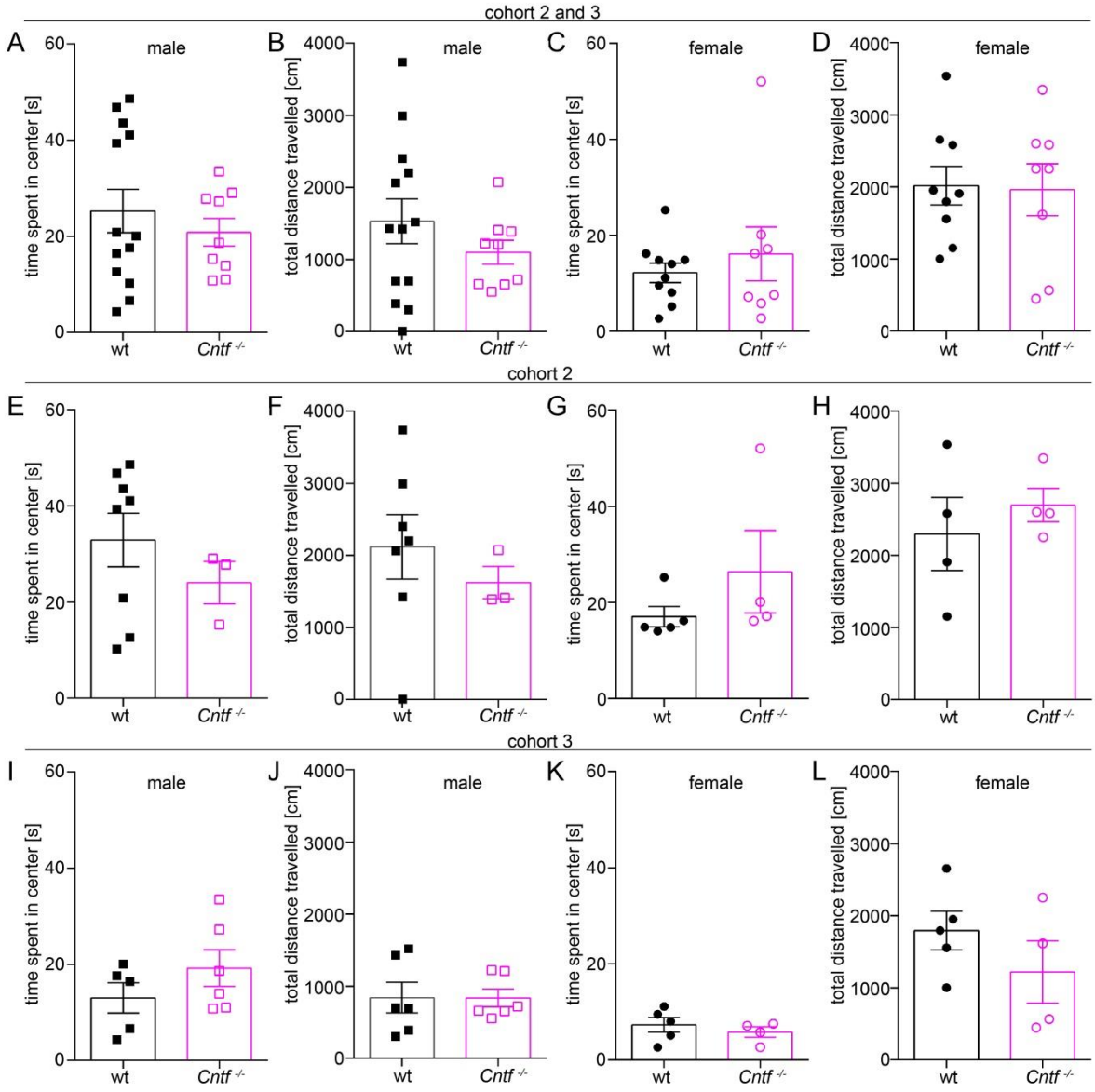

Figure 15. Wt and *Cntf* $^{-/-}$ mice of cohort 2 (E-H) and 3 (I-L) show no anxiety-like phenotype in the open field (OF) test. Data for both cohorts combined are depicted in A-D. Male wt and *Cntf* $^{-/-}$ mice of cohort 2 **(E)** and cohort 3 **(I)** did not spend a different amount of time in the center, nor did they differ in the total travel distance **(F, J)**. No difference between female wt mice compared to *Cntf* $^{-/-}$ mice in either: time spent in center **(G, K)** nor in the travel distance **(H, L)** was present in either of the cohorts. Squares represent male, circles female mice. Cohort 2: male wt: n = 8, ***Cntf*** $^{-/-}$: n = 3; female wt: n = 5, *Cntf* $^{-/-}$: n = 4; cohort 3: male wt: n = 6, k *Cntf* $^{-/-}$: n = 6; female wt: n = 5, *Cntf* $^{-/-}$: n = 5. Error bars are presented as ± SEM.

3.2.5 Cntf $^{-/-}$ *mice do not show increased anxiety-like behavior in the dark/light test*

The dark/light (DL) test is another test to investigate anxiety-like behavior. Roughly one third of the area (here the OF) is protected from light, so mice can choose to be either in the dark or light compartment (Crawley and Goodwin, 1980). Peruga *et al* reported a reduced number of entries into the light compartment as well as a 30% reduction in time spent in the light compartment of *Cntf* $^{-/-}$ mice that were backcrossed onto C57Bl/6J mice for at least 15 generations (Peruga et al., 2012). We therefore investigated Cohort 1 and 2 in the DL test.

Behavior of the male mice did not differ between the 2 cohorts (see Table 12) and were therefore grouped for statistical analysis. Neither wt male mice in cohort 1 or 2 nor wt female mice in cohort 2 spent more time in the light compartment compared to the respective *Cntf* $^{-/-}$ mice (Fig. 16 A-D; t (26) = 0.5927, p = 0.5585, unpaired t-test male mice). Male *Cntf* $^{-/-}$ mice in cohort 1 and 2 showed a reduction in the distance travelled (Fig. 16 E, t (26) = 2.795, p = 0.0096, unpaired t-test). Female mice in cohort 2 do not indicate a difference in the distance travelled (Fig 16. H). Overall, *Cntf* $^{-/-}$ mice do not show a strong effect in the DL test.

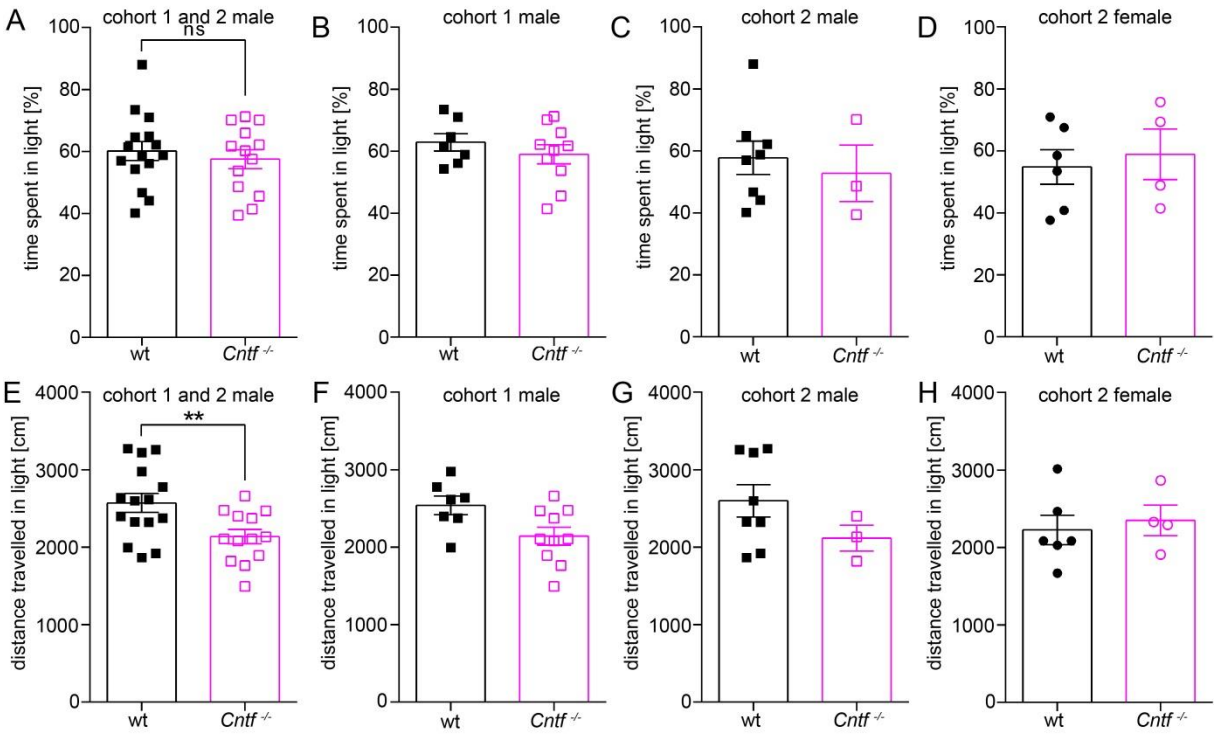

Figure 16. Wt and *Cntf* $^{-/-}$ mice of cohort 1 (B, F) and 2 (C, D, G, H) show not anxiety-like phenotype in the dark/light (DL) test. Data for male mice of cohort 1 and 2 combined are presented in A and E. **(A)** Wt mice of spent the same amount of time in the light compartment as *Cntf* $^{-/-}$ males. **(E)** *Cntf* $^{-/-}$ mice travelled significantly less compared to wt mice. **(B, C, F, G)** Time spent in light and distance travelled for male mice of cohort 1 and 2 seperately. **(D, H)** Female mice of cohort 2 indicated no differences in the time spent of distance travelled between wt and *Cntf* $^{-/-}$ mice. Squares represent male, circles female mice. Cohort 1: male wt: n = 10, *Cntf* $^{-/-}$: n = 8; cohort 2: male wt: n = 8, *Cntf* $^{-/-}$: n = 3; female wt: n = 5, *Cntf* $^{-/-}$: n = 4. Error bars are presented as ± SEM. ** $p < 0.01$.

3.2.6 Cntf $^{-/-}$ *mice do not show anxiety-like behavior in the elevated plus maze*

The elevated plus maze (EPM), like the OF test exploit the natural aversion of mice to exposed fields. In this case, mice can take cover in two arms of the cross maze, that are closed from the sides (Carola et al., 2002). Cohort 2 and 3 were exposed to the EPM. Mice in the two cohorts differed regarding some parameters (see Table 12) and were not grouped but qualitative results of both cohorts together are displayed (Fig. 17 A-D). *Cntf* $^{-/-}$ male and female mice of both cohorts did not spend more or less time on the open arms than their

respective wt controls (Fig. 17 E, I and G, K). The total distance travelled does not obviously differ between groups (Fig. 17 F, J and H, L). The numbers of entries for all anxiety-related paradigms are listed in table 11.

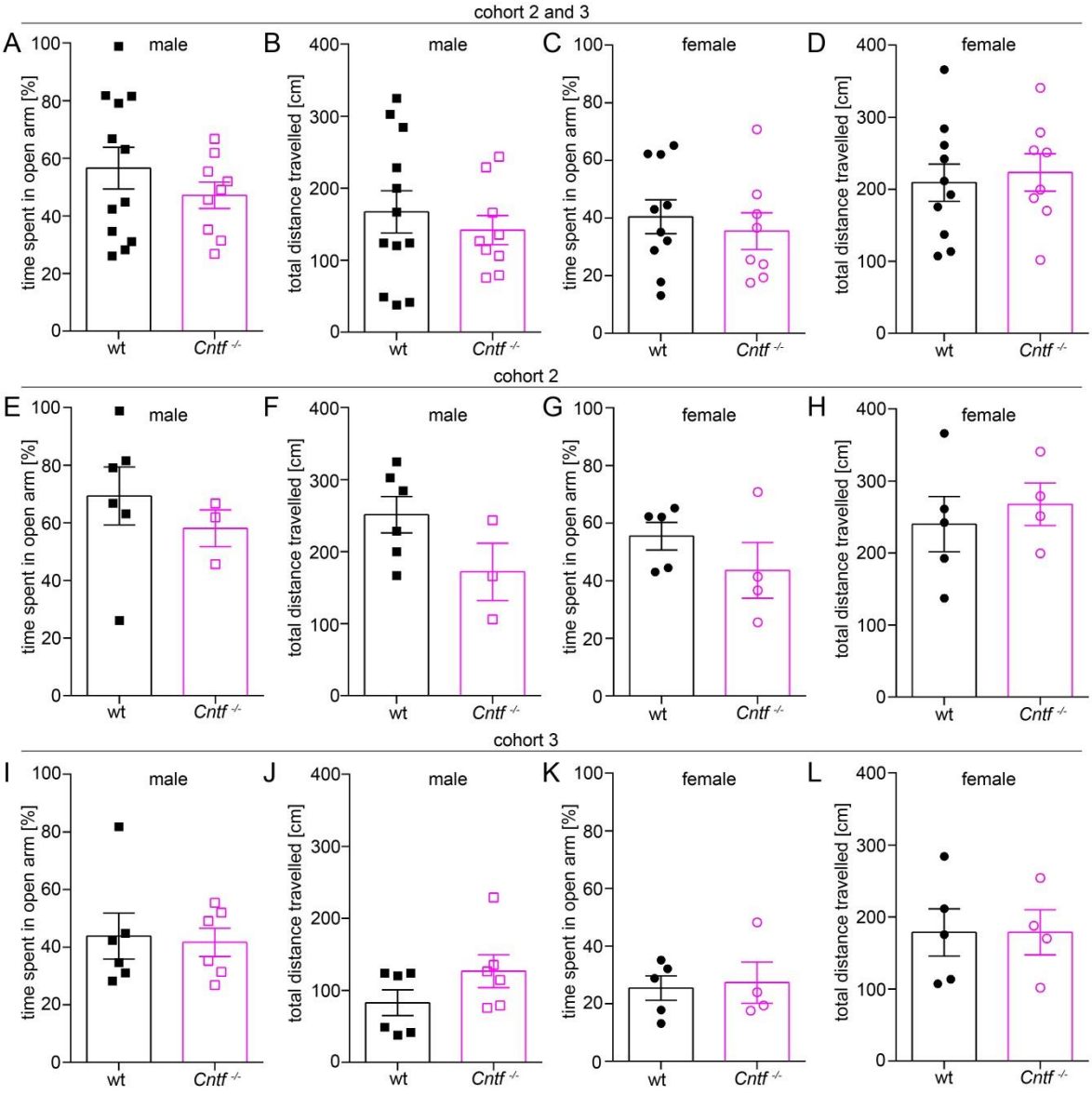

Figure 17. Wt and *Cntf* $^{-/-}$ mice of cohort 2 (E-H) and 3 (I-L) show no anxiety-related phenotype in the elevated plus maze (EPM). Combined data of cohort 2 and 3 are shown in A-D. **(E)** Male *Cntf* $^{-/-}$ mice in cohort 2 showed a tendency to spend less time on the open arms and to **(F)** travel less in total. Male mice in cohort 3, where n-number in *Cntf* $^{-/-}$ mice were higher, **(I)** spent the same amount of time on the open arms and **(J)** *Cntf* $^{-/-}$ mice tended to travel more in total. **(G)** Apart from a slight tendency to spend less time in the open arm in cohort 2, female *Cntf* $^{-/-}$ mice of either cohort did not seem to behave differently from wt mice regarding **(G, K)** the time spent or **(H, L)** distance travelled. Except for cohort 1, n-numbers are too low to run statistical analysis. Squares represent male, circles female mice. Cohort 1, male wt: n = 10, *Cntf* $^{-/-}$: n = 8; cohort 2, male wt: n = 8, *Cntf* $^{-/-}$: n = 3; female wt: n = 6, *Cntf* $^{-/-}$: n = 4. Error bars are presented as ± SEM.

Taken together, *Cntf* $^{-/-}$ mice do not seem to have an obvious behavioral phenotype. We therefore decided to continue analysis in the model system where the LTP deficit in *Cntf* $^{-/-}$ mice was found: the organotypic cultures.

3.3 pStat3 levels of *Cntf* $^{-/-}$ organotypic cultures are affected

3.3.1 Cntf is present in Gfap-positive astrocytes in organotypic cultures

The technique of culturing organotypic hippocampal cultures was established in collaboration with the lab of Prof. Dr. Martin Korte (TU Braunschweig). In order to verify that the model-system of organotypic cultures reflected the observed distribution of Cntf adult mice, immunofluorescent stainings were performed on 4-week old wt and *Cntf* $^{-/-}$ organotypic cultures. Cntf immunoreactivity was strong in wt organotypic cultures (Fig. 18 A). Most abundant staining was present along the fissure as well as around the edges of the slice. Specific Cntf immunoreactivity was absent in *Cntf* $^{-/-}$ cultures (Fig. 18 B).

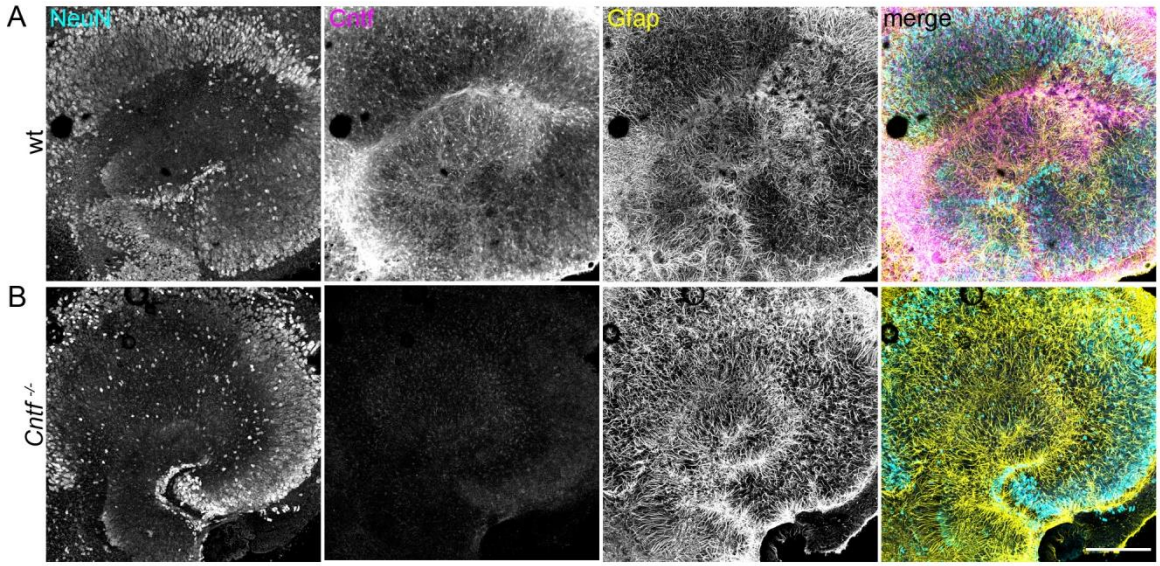

Figure 18. Cntf immunoreactivity is highly abundant in wt but absent in *Cntf* $^{-/-}$ organotypic cultures. Immunofluorescent stainings in mature organotypic cultures. **(A)** Immunoreactivity for Cntf is most abundant along the fissure and along the edges of the slice. **(B)** Specific staining for Cntf is absent in *Cntf* $^{-/-}$ organotpyic cultures. Scale bar: 500 µm.

High-resolution confocal microscopy shows Cntf IR to be present in the fibers of Gfap-positive astrocytes (Fig. 19 A, B). These astrocytes were nestled between NeuN positive neurons (Fig. 19 C, D). These stainings confirm that Cntf is present in certain Gfap-positive astrocytes, as already observed *in vivo*.

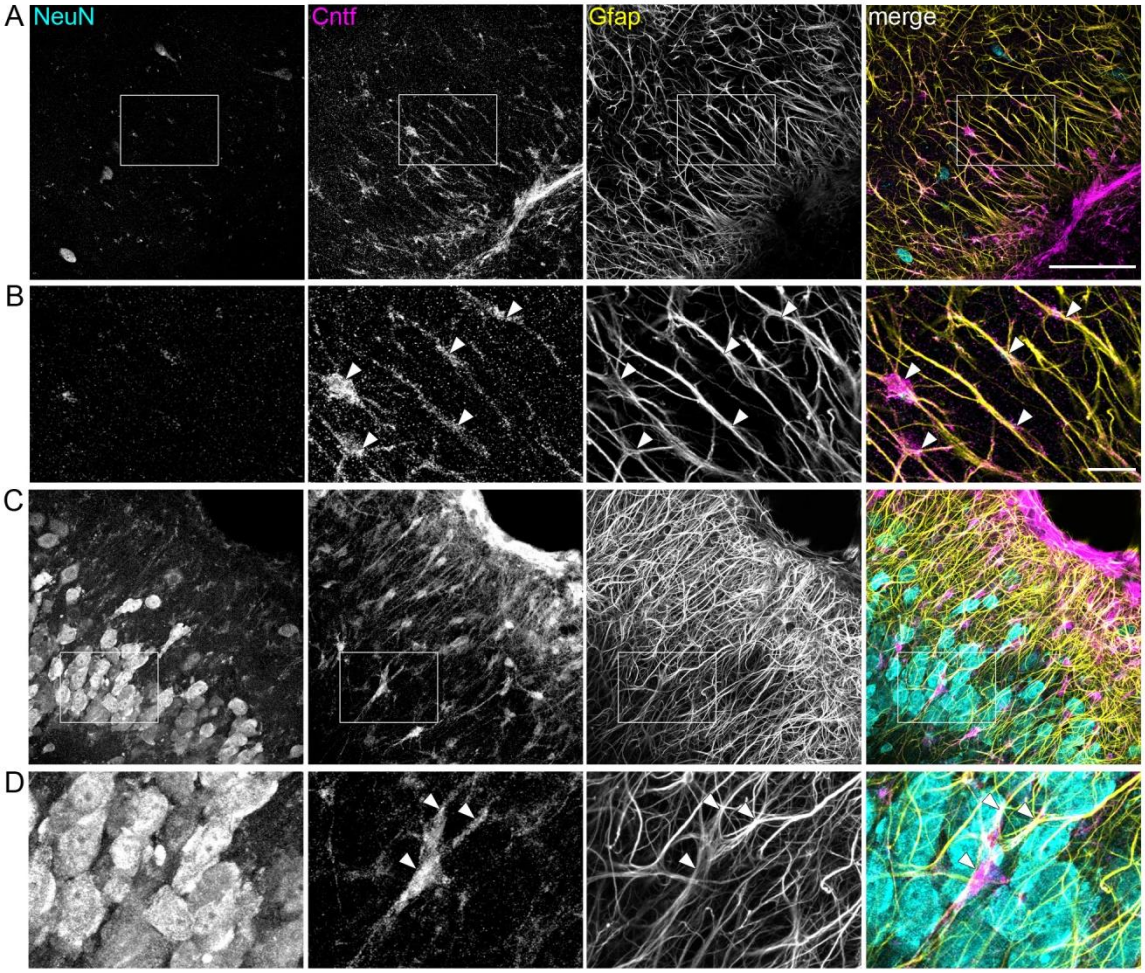

Figure 19. Cntf immunoreactivity is present in cells that are also positive for Gfap. Immunofluorescencestainings in mature wt organotypic cultures. **(A)** Overview of a region above the fissure. **(B)** Arrows highlight where Cntf immunoreactivity merges on Gfap-positive fibers of astrocytes. **(C)** Overview of region close to the edge of the slice. **(D)** Arrows highlight an overlap of Cntf and Gfap immunoreactivity in an astrocyte located between NeuN-positive but Cntf-negative neurons. Scale bar in A: 100 µm; scale bar in B: 10 µm.

3.3.2 pStat3 levels are reduced under baseline conditions in Cntf $^{-/-}$ organotypic cultures

The observed LTP deficit in *Cntf* $^{-/-}$ organotypic cultures were likewise measured in acute slices of neuronal-specific Stat3 knockout mice (unpublished data by Prof. Dr. Martin Korte, Braunschweig). The phosphorylation of Stat3 upon activation of the Jak2 kinase and other kinases by Cntf has been described before (Darnell et al., 1994; Zhong et al., 1994; Heim et al., 1995). We therefore wanted to investigate, whether Cntf/Stat3 interaction, possibly mediated via Jak2, was present and affected in *Cntf* $^{-/-}$ organotypic cultures. We first performed a proof-of-principle experiment, where 2-week old organotypic cultures of wt and *Cntf* $^{-/-}$ mice were stimulated with Cntf.

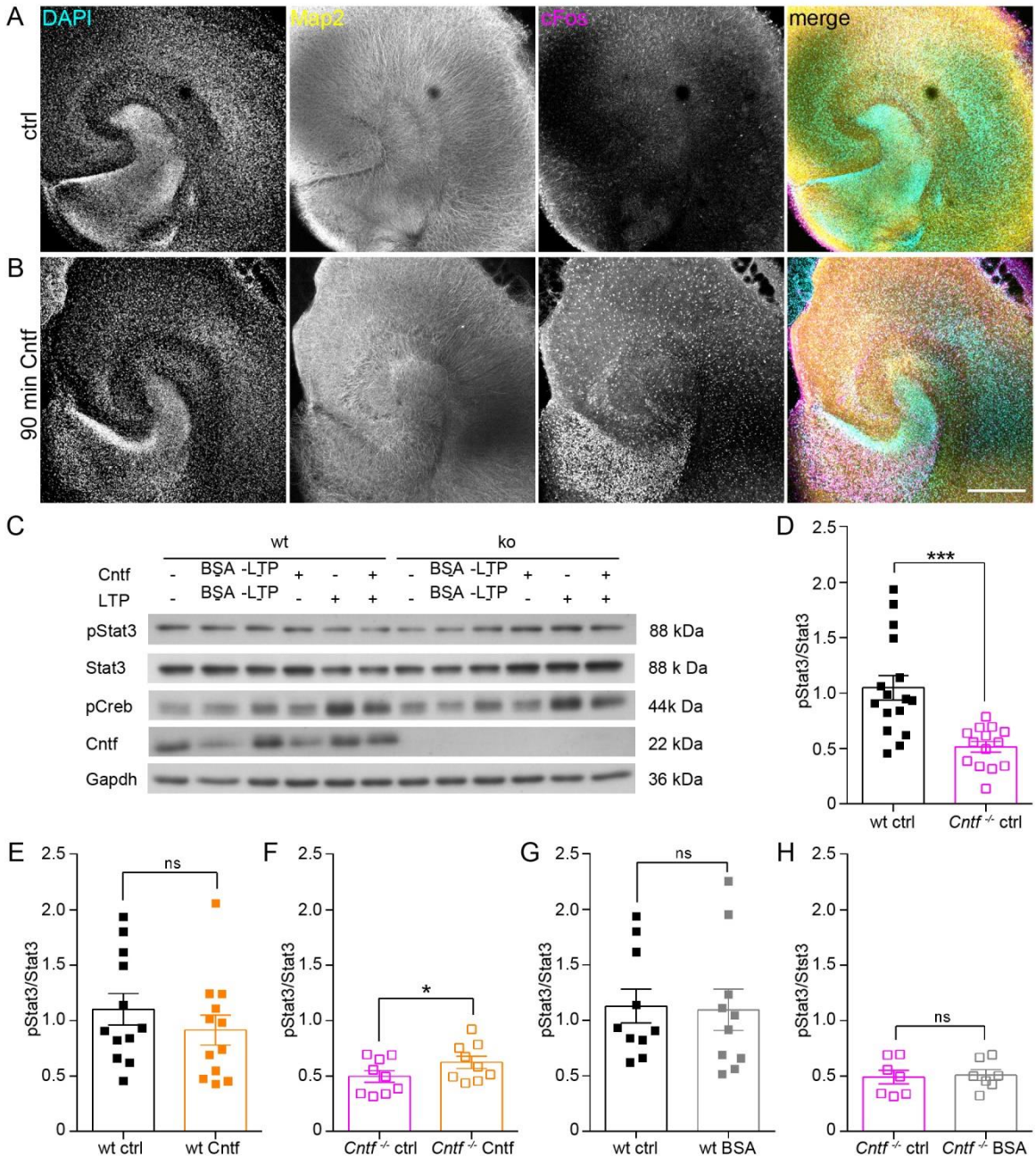

Figure 20. pStat3 is reduced in *Cntf* $^{-/-}$ organotypic cultures and elevated upon Cntf stimulation. (A, B) Stimulation of wt organotypic cultures. The number of cFos-positive cells increases **(**in B**)** 90 min after Cntf stimulation compared to culture without Cntf treatment **(**in A**). (C)** Representative western blot of 2 week old organotypic cultures probed for pStat3, Stat3, pCreb, Cntf and Gapdh after control- and Cntf or LTP stimulation. **(D-H)** Quantitative western blot analysis. (H) Under control conditions, *Cntf* $^{-/-}$ cultures have significantly lower levels of pStat3. **(E)** pStat3 levels do not change in wt cultures upon Cntf stimulation. **(F)** If *Cntf* $^{-/-}$ cultures are stimulated with Cntf, levels of pStat3 increase significantly. Control stimulations with BSA do not change levels of pStat3 in **(G)** wt or **(H)** *Cntf* $^{-/-}$ cultures. pStat3 is normalized to Stat3 levels. One data point represents one culture. Scale bar: 300 µm. Error bars are presented as ± SEM. ns $p > 0.05$, * $p < 0.05$, *** $p < 0.001$.

After 90 min, the sections were fixed with PFA and immunofluorescence stainings were performed to detect cFos. cFos is an immediate early gene product and commonly used as activity-dependent marker (Sheng and Greenberg, 1990). Typically, cFos abundance peaks

60-90 min upon induction of neuronal activity (Holtmaat and Caroni, 2016). The number of cFos-positive cells was strongly increased after Cntf stimulation compared to the control situation (Fig. 20 A, B) proofing a general reactivity upon Cntf stimulation. Next, 2-week old organotypic cultures of wt and *Cntf* $^{-/-}$ were exposed to different stimulations, lysed and analyzed on western blot level (representative western blot Fig. 20 C). Quantitative analysis revealed a reduced level of pStat3 in *Cntf* $^{-/-}$ organotypic cultures under baseline conditions (Fig. 20 D, $t(28) = 4.157$, $p = 0.0003$, unpaired t-test). Upon Cntf stimulation, the levels of pStat3 do not differ in wt organotypic cultures (Fig. 20 E, $p = 0.0522$, Mann Whitney). In *Cntf* $^{-/-}$ organotypic cultures however, stimulation with Cntf lead to a significant increase in pStat3 levels (Fig. 20 F, $t(8) = 3.095$, $p = 0.0148$, paired t-test). No changes in pStat3 levels were observed when organotypic cultures were treated with BSA control (Fig. 20 G, H, $t(9) = 0.3976$, $p = 0.7002$, paired t-test wt; $p = 0.9015$, Mann Whitney *Cntf* $^{-/-}$). These results are a first indication that Cntf mediated phosphorylation of Stat3 might be present in hippocampal organotypic cultures.

3.3.3 pStat3 levels are not influenced by LTP stimulation in organotypic cultures

The next question was, whether pStat3 levels could be influenced by LTP stimulation. First, a proof-of-principle experiment was performed. To test whether the organotypic cultures were responsive to LTP stimulation, 4-week old organotypic wt cultures were chemically stimulated with LTP solution, fixed with PFA and immunofluorescence staining on cFos was performed. The number of cFos-positive cells strongly increased upon LTP stimulation in comparison to the control stimulation condition (Fig. 21 A, B). The experiment proofed a general responsiveness of the organotypic cultures to LTP stimulation (Fig. 21 C). Quantitative analysis of pCreb levels, an activity-dependent transcription factor involved in the induction of LTP (Impey et al., 1996; Silva et al., 1998), increased upon LTP stimulation in both, wt and *Cntf* $^{-/-}$ organotypic cultures (Fig. 21 C, D; $t(10) = 3.480$, $p = 0.0059$, paired t-test wt, $t(4) = 5.544$, $p = 0.0052$, paired t-test *Cntf* $^{-/-}$). This confirmed again the responsiveness of the organotypic cultures to LTP stimulation. The levels of pStat3 did not increase in wt or *Cntf* $^{-/-}$ organotypic cultures in response to LTP stimulation alone or in combination with Cntf (Fig. 21 E, F).

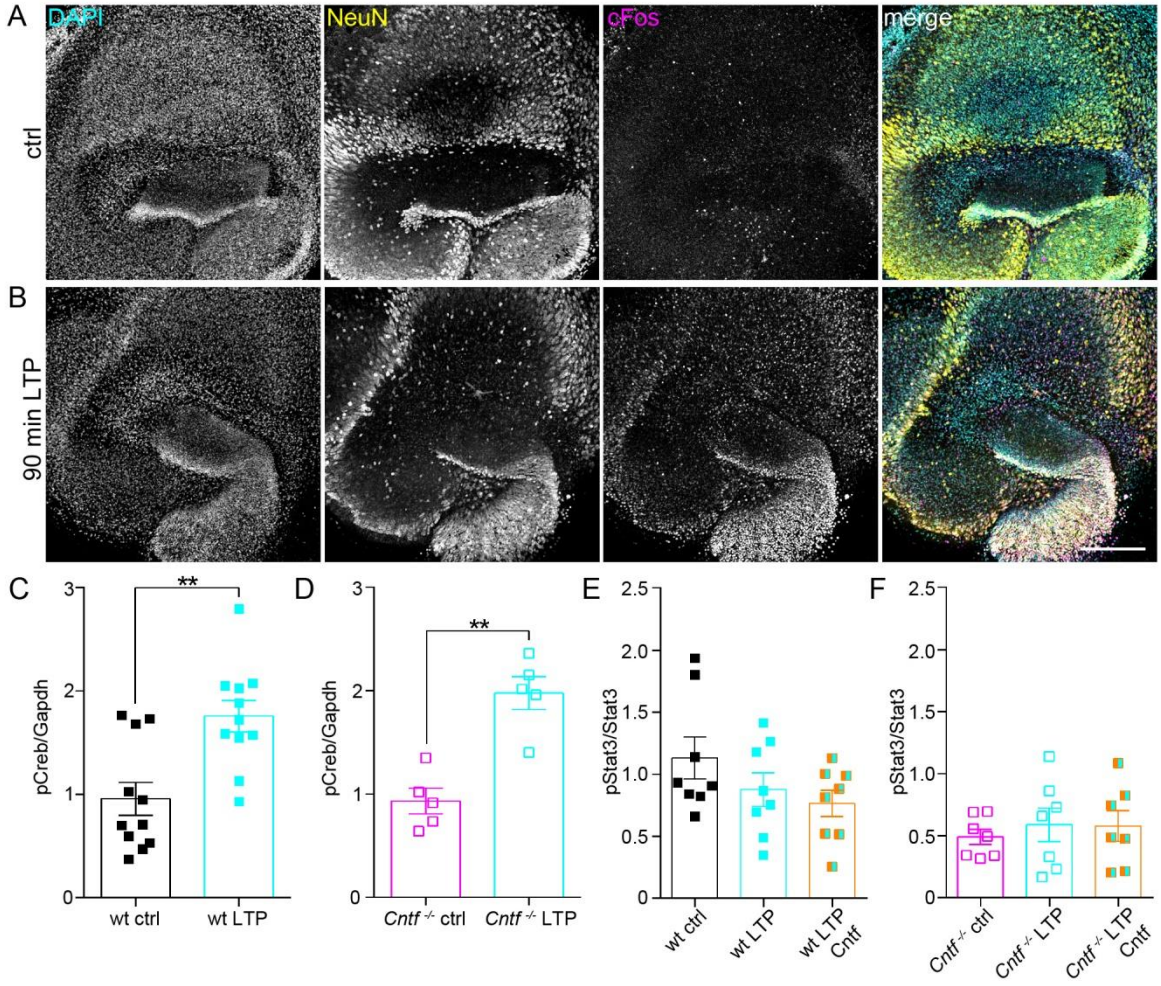

Figure 21. pStat3 levels do not increase upon LTP stimulation in wt and *Cntf* $^{-/-}$ organotypic cultures. **(A, B)** Stimulation of wt cultures with LTP solution. The number of cFos-positive cells increases (in B) 90 min after LTP stimulation compared to control conditions **(**in A**)**. **(C-F)** Quantitative western blot analysis. Levels of pCreb relative to Gapdh increase after LTP stimulation in wt **(**in C**)** and *Cntf* $^{-/-}$ cultures **(**in D**)**. **(E, F)** Stimulation with LTP alone or LTP in combination with Cntf slightly decreases pStat3 levels relative to Stat3 in **(E)** wt and does not induce changes in **(F)** *Cntf* $^{-/-}$ cultures. One data point represents one culture. Scale bar: 300 µm. Error bars are presented as ± SEM. ** $p < 0.01$.

Stimulation of the organotypic cultures by chemical LTP induction did not lead to an increase in pStat3 in wt or *Cntf* $^{-/-}$ cultures. However, either phosphorylation of Stat3 is not influenced by our chemical LTP stimulation protocol or possible synaptic effects could have been masked by a whole-slice lysis and thus be lost on the western blot level. Stimulation with Cntf on the other hand had led to an increase in pStat3 levels in *Cntf* $^{-/-}$ organotypic cultures. To gain a better understanding about Cntf/pStat3 dynamics at the level of the spine, we continued *in vitro*.

3.4 *In vitro* analysis of pStat3 at the level of the dendritic spine

3.4.1 In vitro cultures respond to Cntf stimulation with increased levels of pStat3

First, hippocampal neurons were cultured for 21 DIV, fixed with PFA and immunofluorescence stainings were performed. Cultured hippocampal neurons looked healthy and after 21 DIV had developed a high number of vGluT-positive synapses (Fig. 22 A). Neurons were co-cultured with astrocytes and often grew in close contact or on top of them (Fig. 22 B).

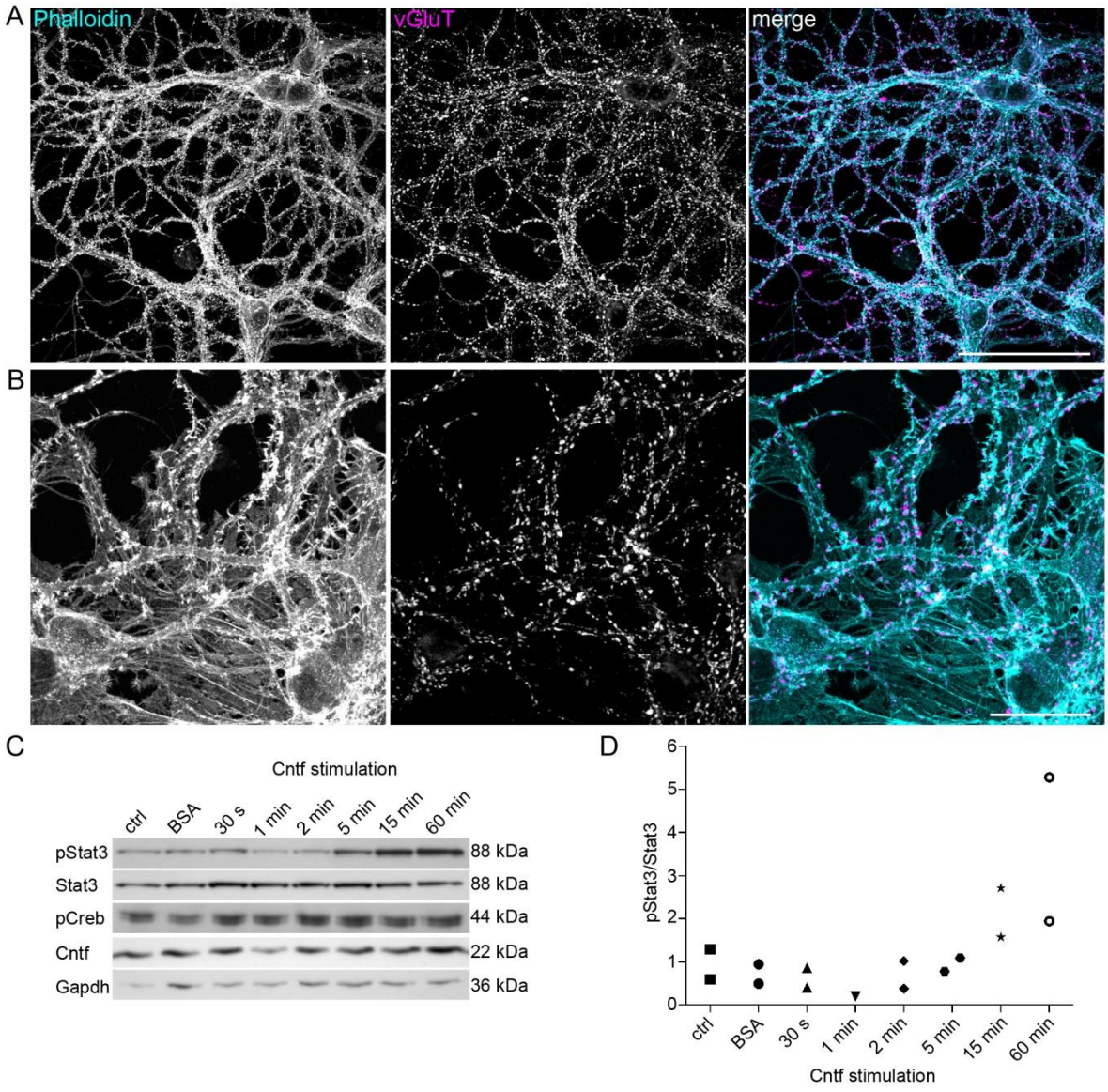

Figure 22. Cultured hippocampal neurons increase pStat3 levels upon Cntf stimulation. (A) Immunofluorescence stainings show a high number of vGluT-positive presynapses in 3-week-old cultured wt hippocampal neurons. **(B)** Example of how neurons grow on top of astrocytes in 3-week-old cultured wt hippocampal neurons. **(C)** Representative western blot of pStat3, Stat3, pCreb, Cntf and Gapdh in 3 week old hippocampal wt neurons after Cntf stimulation. **(D)** Western blot analysis indicate that hippocampal cultures respond with an increased level of pStat3 to Cntf stimulation. Scale bar in A: 50 µm, scale bar in B: 20 µm.

In order to investigate whether the Cntf/Stat3 signaling is also active in cultured hippocampal neurons, cultures were stimulated with Cntf. The cells were then lysed and analyzed by western blot techniques. Western blots indicated that pStat3 levels increased upon Cntf stimulation in cultured hippocampal neurons in a time-dependent manner (Fig. 22 C, D). It seemed that the cultured hippocampal neurons were therefore acceptable as a model system to investigate whether Cntf activates Stat3 at synapses. For quantitative analysis, the n-number needs to be increased to validate these results.

3.4.2 pStat3 is primarily located in the presynapse

In order to investigate whether dynamics between Cntf and pStat3 were located in the postsynaptic spine structure, an adequate staining had to be established. Spines were henceforth labelled with fluorescent Phalloidin, a high-affinity filamentous actin (F-actin) probe, to identify the postsynapse (Cooper, 1987; Chazotte, 2010; Sidenstein et al., 2016). As counterstain, vesicular glutamate transporter (vGluT) (Ni et al., 1994; Fujiyama et al., 2001; Herzog et al., 2001) was labeled to identify the corresponding presynapse (Fig. 23 A, B). First, the localization of pStat3 at the spine was investigated under control conditions. Analysis of pStat3 colocalization revealed that this was highest with vGluT with a Pearson's R value of 0.5991 ± 0.061 for wt and 0.5592 ± 0.067 for *Cntf* $^{-/-}$ cultures (Fig. 23 C). Colocalization between pStat3 and Phalloidin reached Pearson's R values of 0.3180 ± 0.0419 for wt and 0.2846 ± 0.0877 for *Cntf* $^{-/-}$ cultures (Fig. 23 D). Colocalization between pStat3 and Phalloidin was significantly lower than colocalization between pStat3 and vGluT ($F(3, 48) = 72.22$, $p < 0.0001$, 1way ANOVA; $p < 0.0001$ wt pStat3/Phal *vs*. wt pStat3/vGluT and *Cntf* $^{-/-}$ pStat3/Phal *vs*. *Cntf* $^{-/-}$ pStat3/vGluT, Tukey's multiple comparison). Colocalization between Phalloidin and vGluT were calculated to validate their suitability to distinguish pre – from postsynaptic structures (Fig. 23 E). Pearson's R values reached 0.2544 ± 0.054 for wt and 0.2003 ± 0.0776 for *Cntf* $^{-/-}$ cultures. This indicates a non-random overlap between the pStat3 immunoreactivity and the presynaptic marker vGluT. Next, the pStat3 intensity in pre- and postsynapses was investigated. Areas of pre- and postsynaptic pairs were labelled in the individual channels as regions of interest (ROI). These ROIs where used as mask to compute the anti-pStat3 signal in corresponding confocal 12-bit images (Fig. 23 F). Independent of the genotype, pStat3 IR signals were significantly higher in the presynaptic, vGluat-positive structure than in Phalloidin-positive postsynaptic structures (Fig. 23 G, $p < 0.0001$ across conditions, Kruskal-Wallis; wt: $p < 0.0001$ pre *vs*. post, *Cntf* $^{-/-}$: $p < 0.0001$ pre v.s post, Dunn's multiple comparison).

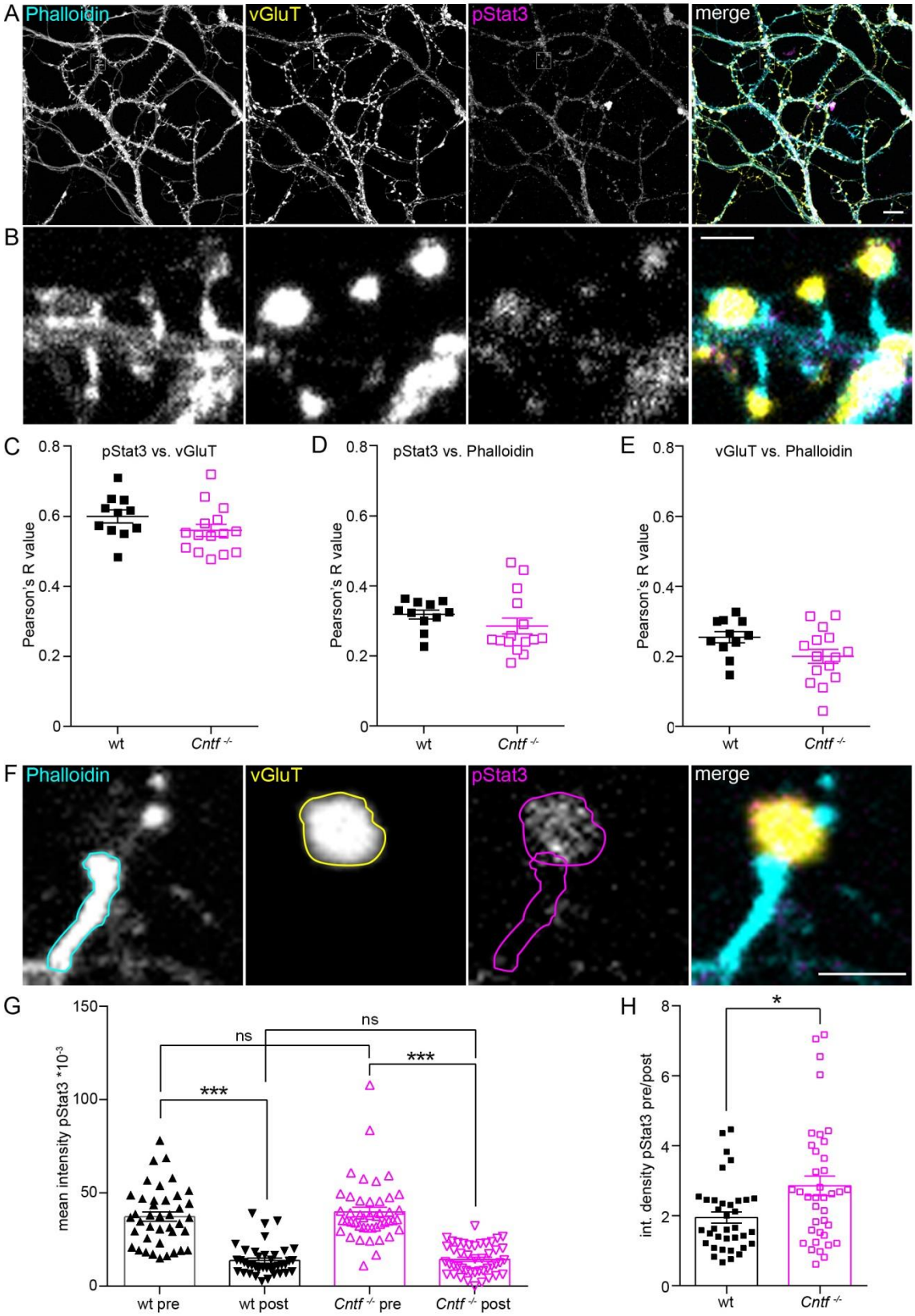

Figure 23. Presynaptic localization of pStat3 in cultured wt hippocampal neurons. (A, B) Labeling of synapses with Phalloidin, vGluT and pStat3. **(C-E)** Pearson's R value of colocalization between Phalloidin, vGluT and pStat3. One data point represents the mean of three analyzed regions exemplary shown in **(B)** per cell. **(C)** Colocalization between vGluT and pStat3 in wt and *Cntf* $^{-/-}$ cultures, **(D)** between Phalloidin and pStat3 and **(E)** between Phalloidin and vGluT. **(F)** Example of manual tracing to compare pre- and postsynaptic pStat3 in spines. **(G)** Quantification of pre- and post-synaptic pSTAT3 mean intensity in wt and *Cntf* $^{-/-}$ cultures. In both,

wt and *Cntf* $^{-/-}$ cultures, the mean pStat3 intensity is higher in the presynapse. One data point represents one pre- or postsynapse, respectively. wt pre: n = 40, wt post: n = 41, *Cntf* $^{-/-}$ pre: n = 45, *Cntf* $^{-/-}$ post: n = 45. **(H)** The ratio of pre-over post-synaptic amount of pStat3 (measured in integrated density) is higher in *Cntf* $^{-/-}$ cultures, than in wt cultures. One data point represents the ratio within one pair of pre-and postsynapse. wt: n = 36, *Cntf* $^{-/-}$: n = 38. Scale bar in A: 10 µm, in B and F: 1 µm. Error bars are presented as ± SEM. ns $p > 0.05$, * $p < 0.05$, *** $p < 0.001$.

The pStat3 intensity in wt presynapses did not differ significantly from the pStat3 intensity in *Cntf* $^{-/-}$ presynapses (Fig. 23 G, $p > 0.9999$ wt pre *vs.* *Cntf* $^{-/-}$ pre, Dunn's multiple comparison). There was also no difference in pStat3 intensity between the postsynapses of wt and *Cntf* $^{-/-}$ cultures (Fig. 23 G, $p > 0.9999$ wt post *vs.* *Cntf* $^{-/-}$ post, Dunn's multiple comparison).

Taken together, these results indicate that pStat3 is primarily located in the presynapse as indicated by the high signal overlap of pStat3 IR and vGluT IR in high-resolution microscopy images. The pre- and postsynaptic structures at one synapse supposedly come from different neurons or axons of the same neuron and can form a functional unit when in contact. For the next analysis, pairs of pre- and postsynapse were defined as a working unit. The ratio of the integrated density of pStat3, which takes intensity as well as area into account, was calculated for each pair. In *Cntf* $^{-/-}$ cultures, the ratio of integrated density of pStat3 between pre- and postsynapse is slightly but significantly higher compared to those of wt cultures (Fig. 23 H, $p= 0.0103$, Mann Whitney). The integrated density of pStat3 thus is shifted more to the presynapse in *Cntf* $^{-/-}$ cultures.

3.4.3 pStat3 abundance is highest in wt synapses which are in contact to astrocytes

During the previous experiments we realized that pStat3 immunoreactivity seemed to be more abundant in astrocytes (Fig. 24 C, D). We therefore wondered whether there was more pStat3 in presynapses that were in contact with astrocytes than in those that were not in contact with astrocytes (Fig. 24 A-D).

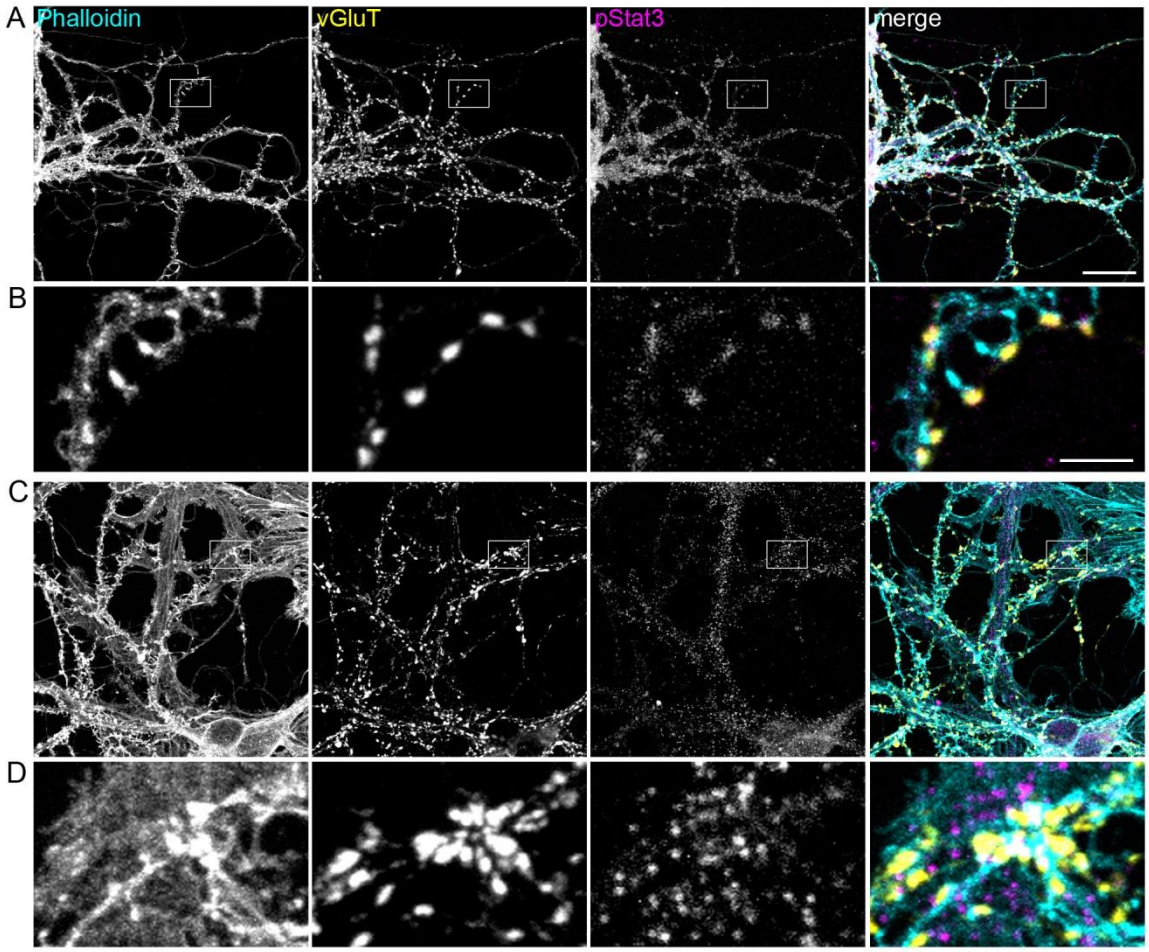

Figure 24. Immunofluorescence staining of presynapses in contact and without contact to astrocytes in cultured hippocampal neurons. (A-D) Examples of presynapses that are not in contact with astrocytes **(**in A, B**)** versus presynapses that are in contact with astrocytes **(**in C, D**)**. Presynapses are visualized with vGluT and postsynapes are visualized with Phalloidin-488. Scale bar in A: 10 µm and B: 2 µm.

Since previous results revealed that pStat3 was prominently located in the presynapse, the area and the integrated density of pStat3 in the presynapse were analyzed. Analysis of the synapse area revealed that presynapses in wt cultures were larger than those of *Cntf* $^{-/-}$ cultures (Fig. 25, A; p = 0.0436 wt presyn. *vs*. *Cntf* $^{-/-}$ presyn, Dunn's multiple comparison). This difference in presynapse area was more pronounced when in contact with astrocytes (Fig. 25, A; p < 0.0001 wt astro *vs*. *Cntf* $^{-/-}$ astro, Dunn's multiple comparison). Presynapses in wt cultures were larger when in contact with astrocytes compared to presynapses that were not contacting astrocytes (Fig. 25, A; p = 0.0009 wt presyn. *vs*. wt astro, Dunn's multiple comparison). This was not the case for presynapses in *Cntf* $^{-/-}$ cultures (Fig. 25, A; p > 0.9999 *Cntf* $^{-/-}$ presyn. *vs*. *Cntf* $^{-/-}$ astro, Dunn's multiple comparison). Regarding the integrated density of pStat3, wt and *Cntf* $^{-/-}$ cultures, this was higher in presynapses that were in contact with astrocytes (Fig. 25 B; p < 0.0001 wt presyn. *vs*. wt astro, p = 0.0018 *Cntf* $^{-/-}$ presyn. *vs*. *Cntf* $^{-/-}$ astro, Dunn's multiple comparison). Comparing presynapses that were not in contact

with astrocytes, integrated density of presynaptic pStat3 in *Cntf* $^{-/-}$ cultures did not differ from those in wt cultures (Fig. 24 B, p > 0.9999 wt presyn. *vs.* *Cntf* $^{-/-}$ presyn, Dunn's multiple comparison). However, analysis of the presynapses that were in contact with astrocytes revealed, that there was significantly more pStat3 in presynapses of wt compared to *Cntf* $^{-/-}$ cultures (Fig 25 B, p < 0.0001, wt astro *vs.* *Cntf* $^{-/-}$ astro, Dunn's multiple comparison). Dot-plots of the integrated density of pStat3 plotted against the presynapse area, the two parameters which are combined into the integrated density value, are depicted qualitatively in Fig. 25 (C, D and E, F; R square = 0.8432 wt presyn., R square = 0.8034 *Cntf* $^{-/-}$ presyn., R square = 0.7682 wt astro, R square = 0.8076 *Cntf* $^{-/-}$ astro, linear regression).

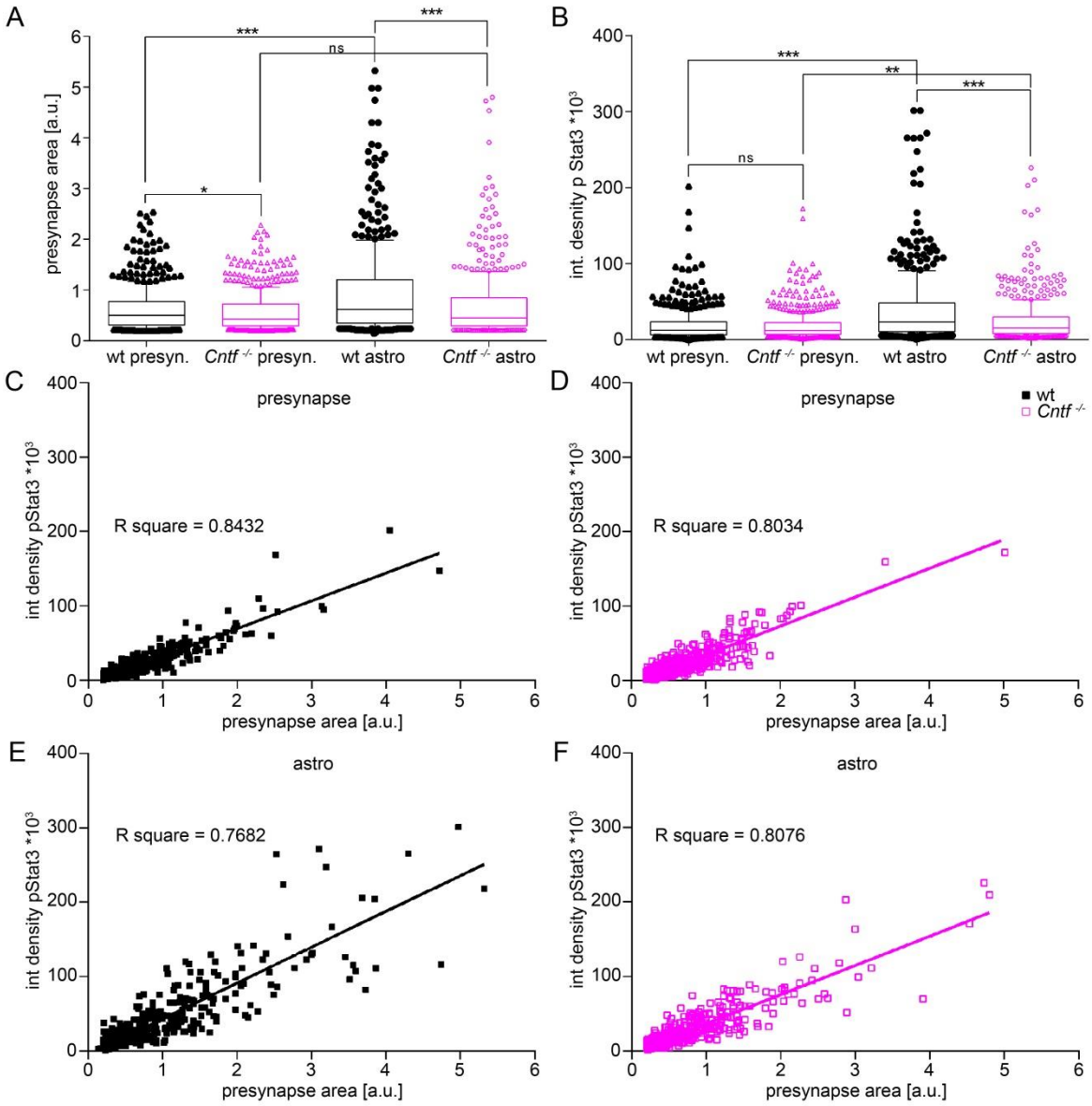

Figure 25. Presynapses in wt cultures are larger and have an increased amount of pStat3 than *Cntf* $^{-/-}$ cultures in presynapses contacting astrocytes. (A) Presynapse area in wt and *Cntf* $^{-/-}$ cultures. Presynapses of wt cultures are larger compared to *Cntf* $^{-/-}$ cultures which is even more pronounced in presynapses that contact astrocytes. Area of the presynapse increases in wt, but not in *Cntf* $^{-/-}$ cultures when in contact to astrocytes. **(B)**

The integrated density of pStat3 in presynapses that are not contact with astrocytes is comparable between wt and *Cntf* $^{-/-}$ cultures. In presynapses contacting astrocytes integrated density values are higher in wt than in *Cntf* $^{-/-}$ cultures. The amount of pStat3 in wt and *Cntf* $^{-/-}$ presynapses contacting astrocytes is higher than in those without contact to astrocytes. (A, B) One data point represents one vGluT-positive presynapse. Data are represented in the boxblot/single points in a ratio of 90/10%, respectively. **(C, D)** Dotblots showing the size of a vGluT-positive presynapses in relation to the mean intensity of pStat3 signals in wt **(C)** and **(D)** *Cntf* $^{-/-}$ presynapses that are not in contact with astrocytes. **(E, F)** Dotblots showing the size of a vGluT-positive presynapse in relation to the integrated density of pStat3 in wt **(E)** and **(F)** *Cntf* $^{-/-}$ presynapses that are in contact with astrocytes. (C-F) One data point represents 1 vGluT positive presynapse. Wt presyn.: n = 487, *Cntf* $^{-/-}$: presyn. n = 683, wt astro: n = 469, *Cntf* $^{-/-}$: astro n = 556. ns $p > 0.05$, * $p < 0.05$, ** $p < 0.01$, *** $p < 0.0001$.

In vitro analysis revealed that pStat3 is more abundant in the pre- than in the postsynapse and even more abundant in presynapses that are in contact with astrocytes. Presynapses of wt cultures were larger than those of *Cntf* $^{-/-}$ cultures which was also more pronounced in presynapses that are in contact with astrocytes. Here is where *Cntf* $^{-/-}$ cultures showed less pStat3 abundance than wt control cultures.

4 Discussion

Cntf is a pleiotropic factor involved in the survival and maintenance of motoneurons in the central nervous system (Sendtner et al., 1990; Sendtner et al., 1991; Friedman et al., 1992). However, Cntf is also present in the hippocampus (Stockli et al., 1991; Ip et al., 1993a) and although evidence has been provided that it could be involved in neurogenesis (Emsley and Hagg, 2003; Muller et al., 2009), its exact role in the hippocampus remains unclear.

In this thesis, we provide evidence that (1) Cntf localizes to subtypes of astrocytes in the hippocampus. We show that, (2) although a drastic LTP deficit was measured in the Schaffer-collateral-CA1 synapse of hippocampal slices and organotypic cultures, *Cntf* $^{-/-}$ mice appear to have no phenotype in hippocampus-dependent and anxiety-related mouse behavior paradigms. Furthermore, (3) in organotypic slice cultures, an *ex vivo* model to investigate circuit signaling in synaptic plasticity, baseline pStat3 levels – which is a recognized downstream factor of Cntf signaling – are strongly reduced when Cntf is deficient. (4) In cultured hippocampal neurons, a model system to investigate synaptic signaling at individual synapses *in vitro*, pStat3 immmunoreacivity seems to be predominantly located to the presynapse and (5) Cntf-deficient hippocampal neurons reveal a decreased amount of presynaptic pStat3 in synapses that are particularly in contact with astrocytes, compared to wt controls. However, the evidence for the specificity of the pStat3 antibody in these stainings needs to be further validated in order to draw unambiguous conclusions. In summary, this work suggests that Cntf, which most likely originates from astrocytes, might affect synaptic plasticity, at least on a cellular level, via Cntf mediated phosphorylation of Stat3.

4.1 Localization of Cntf in the mouse hippocampus *in vivo*

Early studies in the rat have reported that Cntf bioactivity is highly enriched in the sciatic nerve as well as in other motor and sensory nerves (Williams et al., 1984). Cntf-coding mRNA levels are not detectable by conventional northern blot analyes in newborn rats (Stockli et al., 1989) and peak postnatally in the adult nerve around week 4 (Stockli et al., 1991). In line with this finding and on the basis of lacking phenotypes in the nervous system of developing *Cntf* $^{-/-}$ mice, it has been suggested that Cntf is not involved in embryonic development of the central or peripheral nervous system (Stockli et al., 1991). Within the central nervous system of the adult rat, Cntf-coding mRNA levels were highest in the optic nerve, olfactory bulb and spinal cord (Stockli et al., 1991; Ip et al., 1993d). However, low quantities of Cntf-coding mRNA were also detected in the hippocampus (Stockli et al., 1991; Ip et al., 1993d). These studies were performed on northern blot level and confirmed the

presence of Cntf-coding mRNA in the respective regions. *In situ* hybridizations revealed that the high amounts of mRNA in the sciatic nerve most likely originated from Schwann cells (Friedman et al., 1992). Within the adult brain, Cntf-coding mRNA was only present at the ventral surface of the midbrain adjacent to the glia limitans (Ip et al., 1993d). *In vitro* experiments suggest that Cntf-coding mRNA detected in specific brain regions *in vivo* might originate from glial cells since Cntf-coding mRNA was detected in glia cultures from cortex, cerebellum as well as hippocampus (Rudge et al., 1992; Carroll et al., 1993). Other evidences for a glial source of Cntf in the adult rat CNS were provided by lesion experiments where it was observed that reactive astrocytes in the hippocampus surrounding the lesion site express high levels of Cntf-coding mRNA (Ip et al., 1993a; Guthrie et al., 1997). The levels of Cntf-coding mRNA found in various hippocampal regions in our LMD-qPCR experiments, might also originate from glial cells surrounding the neuronal somata. This would be in line with the immunofluorescence stainings of Cntf protein, which showed a prominent localization in individual Gfap-positive astrocytes. Previous Cntf stainings in the optic nerve also show a localization of Cntf in Gfap-positive astrocytes (Stockli et al., 1991; Dobrea et al., 1992). On the other hand, Henderson *et al* detected Cntf signals in nuclei of hippocampal CA1 neurons *in vivo* (Henderson et al., 1994). However, our immunofluorescent Cntf stainings in wildtype and *Cntf*$^{-/-}$ mice cannot provide sufficient evidence for a substantial Cntf abundance in hippocampal neurons or localization in neuronal nuclei.

The highest Cntf-coding mRNA levels as well as the strongest anti-Cntf IR was present in cells along the lateral ventricles. This region was used as a control region for both sets of experiments because stainings of Cntf and its receptor as well as their functional involvement in forebrain neurogenesis at this site has been shown before (Ip et al., 1993d; Shimazaki et al., 2001; Emsley and Hagg, 2003; Gregg and Weiss, 2005; Alpar et al., 2018; Jia et al., 2018). The second highest presence of Cntf-coding mRNA, as well as anti-Cntf IR was observed in the region below the dentate gyrus (DG), which most likely represents meningeal areas. A high IR for Cntf within Gfap-positive cells was also observed around the fimbria below the CA3 area. Cntf localization along the lateral ventricles and close to as well as within the DG locates Cntf-positive cells to areas showing adult neurogenesis in the mouse brain (McKay, 1997; Gage et al., 1998; Gage, 2000; Kempermann and Gage, 2000; Deng et al., 2010). In fact, *Cntf* $^{-/-}$ animals display a reduced number of adult-born immature neurons in the dentate gyrus (Muller et al., 2009). Our results do not address the question which cell types are functionally responsible for the Cntf effect on immature, newborn neurons. Even though a

quite high amount of Cntf-coding mRNA was identified in the DG, strong anti-Cntf IR could not be attributed to specific cells located within the DG.

In early *in vitro* studies, Cntf was found to induce type-2 astrocyte differentiation (Hughes et al., 1988; Lillien et al., 1988; Lillien and Raff, 1990a, b; Lillien et al., 1990) highlighting its role in stem cell differentiation. Neurosphere studies confirmed a strong astrogenic effect of Cntf, resulting in 98% of Gfap-positive astrocytes after Cntf treatment (Johe et al., 1996; Chang et al., 2003).

Recent experiments indicate that Cntf influences adult neurogenesis not only by astrogenic properties. Ding and He investigated the effect of Cntf on spontaneous differentiation of neural stem cells (NSCs) (Ding et al., 2013a). They found that Cntf-neutralizing antibodies can inhibit the spontaneous differentiation of neural progenitor cells into mature neural cells (Ding et al., 2013a). They also confirmed previous findings that this Cntf effect is signaled by counteracting the effect of Fgf-2, which keeps NCS in an immature state and therefore suppresses neurogenesis of adult hippocampal progenitors (Chen et al., 2007; He et al., 2012; Ding et al., 2013a; Ding et al., 2013d). Intriguingly, hippocampal astrocytes but not astrocytes from spinal cord were able to promote neuronal differentiation of NCS (Song et al., 2002). This was the case irrespective of whether NSCs were in direct or no contact with the astrocytes, suggesting that the astrocytic effect was asserted by a soluble factor. Cntf has also been shown to assert its effect on neurogenesis as a soluble factor (Emsley and Hagg, 2003). CntfRα expression on the other hand has been reported on DG granule neurons, and only very scarcely on Gfap-positive cells in the DG (Emsley and Hagg, 2003). Taken together these findings suggest that in hippocampal adult neurogenesis, Cntf might have an astrocytic origin but asserts its function on NSCs and neurons.

In conclusion, Cntf seems to be an important factor for NCS and neurogenesis and thus our findings that highest levels of Cntf-coding mRNA in the hippocampus are present in the DG and the meninges beneath the DG, as well in the SVZ are in line with the literature (Song et al., 2002; Emsley and Hagg, 2003; Ding et al., 2013d). Notably, IR for Cntf was only observed in the meninges below the DG, not in Gfap-positive astrocytes within the DG.

4.2 *Cntf* $^{-/-}$ mice appear to have no concludent phenotype in hippocampus-dependent and anxiety-related paradigms

Around 3% of the human population is CNTF deficient (Takahashi et al., 1994). There are several reports emphasizing a potential modulatory role for CNTF in motoneuron disease

(Giess et al., 1998; Giess et al., 2002a; Giess et al., 2002e) but it appears that CNTF-deficiency per se does not correspond to any other neurological disorder (Takahashi et al., 1994; Thome et al., 1996a, c; Gelernter et al., 1997; Munzberg et al., 1998; Grunblatt et al., 2006). In line with these findings in human patients, a discrete but clearly detectable motor phenotype has been intendified in rodents (Masu et al., 1993), whereas little is known about further behavioral phenotypes related to potential cellular and synaptic dysfunctions of cortical or hippocampal neurons in *Cntf* $^{-/-}$ mice. Since the LTP deficit in *Cntf* $^{-/-}$ mice was measured in CA1 (unpublished data by Prof. Dr. Martin Korte, TU Braunschweig) we wanted to investigate the behavior of *Cntf* $^{-/-}$ mice in hippocampus-dependent tasks. Furthermore, Peruga *et al* reported an anxiety-like phenotype in *Cntf* $^{-/-}$ mice (Peruga et al., 2012) but no further studies mention similar results. To elucidate this situation, we submitted *Cntf* $^{-/-}$ mice to three anxiety-related tests.

4.2.1 Hippocampus-dependent learning behavior of Cntf $^{-/-}$ *mice seems largely inconspicuous*

The hippocampus is part of the limbic system and is an important structure for memory formation (Hirsh, 1974; Zola-Morgan et al., 1986; Squire and Zola, 1996; Izquierdo and Medina, 1997; Burgess et al., 2002; Eichenbaum, 2004). While the dorsal hippocampus plays a prominent role in the formation of declarative and spatial memory, the ventral hippocampus has been shown to play an important role in the fear circuit (O'Keefe and Dostrovsky, 1971; Kjelstrup et al., 2002; Bannerman et al., 2004; Sahay and Hen, 2007). As the DG is an important structure for processing of certain aspects of hippocampal memory, such as pattern separation (Kesner, 2013), and since Cntf seems to be involved in LTP and DG neurogenesis, the novel object recognition (NOR) task was used to investigate how Cntf-deficiency affects object learning and novel object discrimination.

4.2.1.1 Performance of Cntf $^{-/-}$ *mice in the novel object recognition task*

The DG is involved in pattern separation and defects in the DG presumably affect object discrimination in the NOR task (de Lima et al., 2006; Broadbent et al., 2010; Sahay et al., 2011; Kesner, 2013; Rolls, 2013; Knierim and Neunuebel, 2016). Due to its strong innervation of GABAergic interneurons in the CA3 region via the mossy fiber projection, the DG is also important for memory precision (Acsady et al., 1998; Galimberti et al., 2006; Ruediger et al., 2011). While the DG seems to be more involved in pattern separation, the CA3 is thought to be more essential for pattern completion (Gilbert and Kesner, 2006; Johnston et al., 2016; Knierim and Neunuebel, 2016). Although the exact roles of the DG and CA3 in pattern separation and completion are still controversially discussed (Winters et al.,

2008), neurogenesis in the DG seems to have an impact on performance in pattern separation (Kesner, 2013; Johnston et al., 2016). . While hippocampal involvement in the NOR task in rodents is still debated (Winters et al., 2008), experiments in humans and monkey shows a clear involvement of the hippocampus in NOR (McKee and Squire, 1993; Pascalis and Bachevalier, 1999; Zola et al., 2000; Nemanic et al., 2004; Pascalis et al., 2004).

We investigated three cohorts in the NOR. The first cohort, which consisted of male mice only, had to be excluded because wt mice did not learn to discriminate between two different objects. The second cohort included female mice, which also had to be removed from analysis because female wt mice did not learn the paradigm as well. Interestingly, this was also the case in previous experiments, where neither female wt nor *Cntf* $^{-/-}$ mice spent more time at the novel object (R von Collenberg, 2015). Out of the remaining 18 wt and 11 *Cntf* $^{-/-}$ mice male mice, 88.8% of the wt mice were learners whereas only 72.7% of the *Cntf* $^{-/-}$ mice learned. One could argue that there is a difference of 16.1%, but at a biological level there are 3 out of 11 *Cntf* $^{-/-}$ mice and also 2 out of 18 wt mice which did not learn the paradigm at all. At the same time, 8 *Cntf* $^{-/-}$ mice did spend more time at the novel object, which does not justify the conclusion that *Cntf* $^{-/-}$ mice show a severe phenotype in the NOR. Moreover, in previous experiments *Cntf* $^{-/-}$ mice learned at a rate comparable to wt mice (R von Collenberg, 2015). In any case, the role of the hippocampus in object recognition is controversial (Winters et al., 2008) which might be due to differences in experimental approaches to the NOR (Antunes and Biala, 2012). The involvement and the importance of the hippocampus seems to differ and depend on the level of temporal, spatial and contextual information included in the test (de Lima et al., 2006; Reger et al., 2009; Goulart et al., 2010; Oliveira et al., 2010). Thus, it might prove valuable to change the experimental setup accordingly and retest the performance of *Cntf* $^{-/-}$ mice in a recently introduced pattern separation task (van Hagen et al., 2015). This object pattern separation task allows screening for DG and CA3 related deficits (van Hagen et al., 2015) and might be useful to better address and elucidate potential Cntf-mediated deficits in the hippocampus.

4.2.1.2 Performance in the Morris water maze

The discovery of place cells in the hippocampal CA1 area provided first evidence that the hippocampus is involved in place mapping and spatial memory processing (O'Keefe and Dostrovsky, 1971). Several studies have likewise shown the importance of the hippocampus in spatial memory and navigation in humans (Maguire et al., 1996b; Maguire et al., 1996a; Abrahams et al., 1997; Abrahams et al., 1999; Spiers et al., 2001a; Burgess et al., 2002;

Bartsch et al., 2010). Lesion experiments confirmed that the hippocampus plays a role in spatial navigation, a cognitive function that can be analyzed with the help of the Morris water maze (MWM) test (Morris et al., 1982; Morris, 1984). Virtual mazes are the correlate of the MWM in humans and have been used in several studies to further confirm and investigate the spatial function of the human hippocampus (Maguire et al., 1998b; Maguire et al., 1998a; Spiers et al., 2001b; Burgess et al., 2002; King et al., 2002). In a translational study using a virtual water maze it was shown that focal lesions of human hippocampal CA1 neurons in transient global amnesia impair place memory (Bartsch et al., 2010). In addition, it has been shown that spatial learning in the rodent hippocampus is NMDA-dependent, suggesting forms of associative LTP to be involved in spatial memory formation (Morris et al., 1986; Sakimura et al., 1995; Wilson and Tonegawa, 1997).

The LTP deficit in organotypic cultures and acute slices of *Cntf* $^{-/-}$ mice suggests a hippocampal role for Cntf in the CA1 region. We therefore chose to investigate *Cntf* $^{-/-}$ mice in the MWM. However, the MWM had to be established at our behavioral facility and thus several cohorts underwent partially varying paradigms. Since the point mutation in the *CNTF* gene in humans occurs in men and women (Takahashi et al., 1994), we decided to study male and female mice. The number of animals that can be tested simultaneously was limited. Therefore, we planned for two cohorts, each consisting of wt and *Cntf* $^{-/-}$ male and female mice which were supposed to be grouped for feasible statistical analysis. Subsequent statistical analyses showed that behavior between mice of both genotypes and genders did not differ for the classic MWM and were therefore grouped. Male and female mice in both samples were able to learn the location of the platform in the classic MWM. We then further exploited the possibilities of the MWM by relocating the platform to the opposite quadrant, to investigate whether *Cntf* $^{-/-}$ mice were able to relearn a location or whether they would persist on the previously learned location. Before the platform was relocated, reminder runs to the classic platform were performed. Six runs in cohort 2 and two runs in cohort 3, followed by three and six runs with the relocated platform, respectively. Although qualitatively the results were similar, an arithmetic grouping of the two cohorts for the reverse MWM was not feasible – also given that the reminder paradigms were performed in a slightly different manner. Neither paradigm revealed behavioral differences or differences in spatial navigation in male or female *Cntf* $^{-/-}$ mice in the reversal MWM. This finding is surprising, since the LTP deficit in *Cntf* $^{-/-}$ mice was measured as reduced excitatory postsynaptic potentials (EPSPs), suggesting a deficit in CA1, an area in the hippocampus which is known to be involved in spatial navigation and place learning (O'Keefe and Dostrovsky, 1971), both are routinely

investigated with the help of the MWM (Morris et al., 1982; Morris, 1984). It is possible that either these deficits are compensated *in vivo* or do not affect the hippocampal function sufficiently to reveal an apparent behavioral phenotype.

4.2.1.3 Performance in fear (threat) conditioning paradigms

Spatial memory performance is predominantly encoded in the dorsal hippocampus, while the ventral hippocampus is more involved in fear and anxiety related learning (Kjelstrup et al., 2002; Bannerman et al., 2004). Fear is an adaptive state of apprehension that begins rapidly but also subsides quickly once the threat has disappeared (Davis et al., 2010). One of the projection sites of the ventral hippocampus is the amygdala, a region which is strongly involved in the processing of fear and fear memory (Pape and Pare, 2010). Parts of these projections are formed by the CA1 area of the hippocampus (van Groen and Wyss, 1990; Pitkanen et al., 2000). Therefore, we wanted to test whether Cntf deficiency has impacts on fear learning and whether the measured LTP deficit in CA1 area affects fear memory processing. The amygdala is strongly involved in cued fear conditioning (Phillips and LeDoux, 1992), i.e., when the unconditioned stimulus (US), usually a foot shock, is predicted by a conditioned stimulus (CS), usually an acoustic tone. After sufficient and timely precise CS-US presentation, the animal learns that the CS predicts the US and displays a defense reaction in response to the CS. The most commonly displayed defense reaction is freezing (Maren, 2011; Tovote et al., 2015). This form of Pavlovian conditioning is widely and successfully applied to study associative learning and memory processing in rodents, as well as in humans (Pavlov, 1927; Phelps and LeDoux, 2005; Johansen et al., 2011; LeDoux, 2014). The first two cohorts underwent a cued conditioning paradigm, in which three CS-US pairings were presented. The CS was a tone, US an electric foot shock. On the second day, mice were presented with the CS but within a different context to test for intact cue retrieval. On the third day, mice were returned to the context, where the conditioning had taken place. *Cntf* $^{-/-}$ and wt mice showed intact fear acquisition as well as intact fear retrieval in response to the cue but not to the context.

Since the involvement of the cue might have led to a predomination of amygdala over hippocampal processing, we subjected the third cohort to a similar paradigm but included extinction phases. Extinction, a learning-dependent process, has previously been demonstrated to depend on an intact hippocampus (Phillips and LeDoux, 1992; Ji and Maren, 2007; Maren and Hobin, 2007). In our paradigm, *Cntf* $^{-/-}$ mice displayed intact fear acquisition and fear retrieval in response to cue presentation, confirming the finding in the first

experiment. Wt and *Cntf* $^{-/-}$ mice also showed within extinction sessions. To achieve successful extinction between sessions, probably more extinction session are needed.

Concentrating on hippocampal contribution to contextual learning (Phillips and LeDoux, 1992; Anagnostaras et al., 2001), which has also been demonstrated in humans (Kalisch et al., 2006), we focused on an AAA-paradigm in the last cohort. Confirming findings in the previous experiment, *Cntf* $^{-/-}$ mice showed intact fear acquisition. Contextual fear retrieval was also intact and *Cntf* $^{-/-}$ mice displayed successful contextual extinction. Thus, in all three paradigms, *Cntf* $^{-/-}$ mice behaved like wt mice. The cohorts that were not analyzed statistically due to low n-numbers mostly displayed comparable freezing dynamics.

4.2.2 Performance in anxiety-related tests

In contrast to fear, anxiety can be triggered without the actual physical presence of a threat and can prolong even after the threat is gone (Davis et al., 2010). These circumstances leave the state of anxiety vulnerable to taking on features of psychological disorders, which is estimated for a yearly 14% prevalence in Europe and similar ranges worldwide (Kessler et al., 2007; Wittchen et al., 2011). Peruga *et al* reported in 2012, that *Cntf* $^{-/-}$ mice displayed an anxiety-like phenotype, spending 30% less in the lit area in a dark/light (DL) transition test (Peruga et al., 2012). In conclusion to this finding, we subjected part of our cohorts to anxiety-related tests like the DL, open field (OF) and elevated plus maze (EPM). In our hands, *Cntf* $^{-/-}$ mice did not show an anxiety-like phenotype in the DL test, such as previously reported (Peruga et al., 2012). Male mice in one cohort travelled less in the light compartment but results of the OF test suggest normal locomotor behavior in male *Cntf* $^{-/-}$ mice. Female mice did not indicate a clear difference in travel distance in the DL nor the OF. They did not display a difference to wt animals with regard to time spent in the lit compartment or the center of the OF. Results in the EPM do not reveal obvious differences between wt and *Cntf* $^{-/-}$ mice, regardless of the gender.

Here, the behavioral analyses of *Cntf* $^{-/-}$ mice reveal no apparent phenotype, neither in hippocampus-dependent nor in anxiety-related paradigms. With respect to hippocampus-dependent learning tasks such as the classic MWM and the NOR, as well as the anxiety-related DL test in the contextual fear conditioning paradigm, the corresponding male mice were subjected to statistical analyses. At given n-numbers no significant differences were observed. However, for the EPM and the OF, the two investigated cohorts could not be grouped. Therefore, it is not feasible to draw a conclusion based on statistical analysis. In previous behavioral experiments with *Cntf* $^{-/-}$ mice from the same animal facility and

conducted in the same behavioral facility, cohorts with higher n-numbers were investigated in EPM and OF paradigms. Notably, neither male (n = 8) nor female *Cntf* $^{-/-}$ mice (n = 8) showed any behavioral differences or an apparent anxiety-like phenotype in comparison to their wildtypic littermates (male wt n=7, female wt n=8). This indicates an effect size of less than 1.4, at n-numbers of 8, using the one-tail-t-test, at a first error of 0.05% and a second error of 20% (power of 80%), for the above mentioned behavioral tasks. According to this estimation, it cannot be excluded that effect sizes of less than 1.4 can become biologically relevant for Cntf-deficient mice.

Since Cntf is a member of the Il-6 cytokine family which all bind to different combinations of the same receptor subunits (Davis et al., 1991; Ip et al., 1991; Ip et al., 1992; Ip and Yancopoulos, 1992; Patterson, 1992; Pasquin et al., 2015), a compensatory mechanism might be a possible explanation for the discrepancy between *in vitro*, *ex vivo* and behavioral results in this study. Leukemia inhibitory factor (Lif) is known to maintain embryonic stem cells pluripotency by inhibiting differentiation (Smith et al., 1988; Williams et al., 1988; Ogawa et al., 2004; Kawahara et al., 2009) and is a promising candidate to ameliorate in-vitro-fertilization in humans (Stewart et al., 1992; Aghajanova, 2004). It can also trigger similar cellular responses in neuronal cells as Cntf and Il-6 (Rao et al., 1990; Rose and Bruce, 1991; Hall and Rao, 1992; Ip et al., 1992; Gregg and Weiss, 2005). Interleukin 6 (Il-6) is a pleiotropic cytokine and, for example, plays an important role in regulating the immune response (Muraguchi et al., 1988; Kamimura et al., 2003; Hofer and Campbell, 2016; Rothaug et al., 2016). Il-6 is capable of crossing the blood-brain-barrier and has been associated with a number of inflammatory diseases in the human brain (Banks et al., 1994; Hofer and Campbell, 2016). While its classical signaling via the Il-6 receptor (Il-6R) and the glycoprotein of 130 kDa (gp130) mostly triggers downstream pathways in microglia, so called trans-signaling via a soluble form of the Il-6R enables interaction with a number of other cell types including neurons and astrocytes (Taga et al., 1989a; Taga et al., 1989d; Hibi et al., 1990; Mullberg et al., 1994; Rose-John and Heinrich, 1994; Rothaug et al., 2016). The fact that Il-6 can cross the blood-brain-barrier and can interact with neurons and astrocytes, makes it a possible candidate for compensational effects in *Cntf* $^{-/-}$ mice. Indications that functions of members of the Il-6 cytokine family are additive, at least on the level of motoneuron maintenance, were provided by a study in *Cntf/Lif/Ct-1* triple knockout mice. These mice displayed a higher decrease in grip strength than *Cntf* $^{-/-}$ mice alone but also highlighted, that these cytokines seem to play distinct roles in motoneuron maintenance (Masu et al., 1993; Sendtner et al., 1996; Holtmann et al., 2005). It would be interesting to check (1) the mRNA

and/or protein levels of these factors in *Cntf* $^{-/-}$ mice and (2) whether downstream of pStat3 signaling defects in the context of synaptic plasticity are detectable when Cntf is absent. Finally, the *Cntf/Lif/Ct-1* triple knockout mouse could also be subjected to the aforementioned behavioral analyses challenging the compensation hypothesis. After all, the high prevalence of CNTF-deficient, but viable, fertile and overall healthy humans (Takahashi et al., 1994) most likely indicates a strong compensation of CNTF function *in vivo*.

4.3 Cntf and pStat3 in organotypic cultures

While the behavioral analysis of *Cntf* $^{-/-}$ mice did not reveal apparent deficits in learning-related paradigms, the electrophysiological measurements in organotypic cultures do indicate an important role of Cntf in long-term potentiation (LTP). LTP is believed to be a cellular correlate of learning which is characterized by coincident activation of the pre- and postsynapse that results in a prolonged increase in synaptic strength (Bliss and Lomo, 1973; Bliss and Collingridge, 1993; Nicoll and Malenka, 1995; Nicoll, 2017). Recent data even show a causal link between synaptic processes during LTP and LTD and memory (Nabavi et al., 2014). The Schaffer-collateral projections from hippocampal CA3 to CA1 represent a classic site of LTP investigation (Collingridge et al., 1983; Harris and Teyler, 1984; Nicoll, 2017) and acute slices of the hippocampus have been used early on to investigate LTP (Schwartzkroin and Wester, 1975; Alger and Teyler, 1976). The technique of organotypic cultures from young animals, which allows culturing and examination over several weeks in contrast to a few hours using acute slices, was introduced by Gähwiler and later modified by Stoppini (Gahwiler, 1981c, a, b; Stoppini et al., 1991). Stoppini *et al* reported that the tetanic stimulation of the CA3 Schaffer-collateral was followed by a long lasting increase in size of synaptic response in CA1 which featured all properties of LTP (Bliss and Gardner-Medwin, 1973; Stoppini et al., 1991). Notably, these long lasting responses were not detected in cultures of 3-5 days, suggesting that a developmental aspect is important to express certain plasticity also *ex vivo* (Harris and Teyler, 1984; Stoppini et al., 1991).

The LTP deficits in *Cntf* $^{-/-}$ mice were measured both in acute slices from 8 week old mice and in organotypic cultures (unpublished data by Prof. Dr. Martin Korte, TU Braunschweig). The measured decrease in EPSPs was rescued by an acute application of Cntf, in addition to a 24h pre-incubation with Cntf, suggesting a functional role for Cntf in this form of LTP. As LTP-deficits were also found in organotypic cultures of Stat3-deficient mice (unpublished data by Prof. Dr. Martin Korte, TU Braunschweig) and since Cntf exerts its actions on motoneurons via Stat3 signaling (Selvaraj et al., 2012), we focused on Stat3 phosphorylation.

4.3.1 Phosphorylation of Stat3

Phosphorylation of Stat3 can occur at two sites. Phosphorylation at Tyr-705 is Jak dependent and can lead to transcriptional activation of Stat3 (Wen et al., 1995). Phosphorylation at Ser-272, which is dependent on the Ser/Thr kinase Akt, can lead to several other cellular responses (Wen et al., 1995; Chung et al., 1997; Jain et al., 1998; Lim and Cao, 1999; Decker and Kovarik, 2000). Furthermore, Stat3 is activated by Src via Egf and Pdgf receptors (Levy and Darnell, 2002; Levy and Lee, 2002), and in line with these findings, several members of the Stat family, including Stat3, are involved in cancer (Bromberg, 2002; Levy and Darnell, 2002; Levy and Lee, 2002) where they can favor tumorgenesis through their connection to growth factor signaling and compromising of immune surveillance (Bromberg, 2002). Both phosphorylation sites of Stat3 have been shown to be important for activity-dependent nuclear transition of Stat3 in hippocampal neurons (Murase and McKay, 2014). Work by Nicolas *et al* demonstrated that the Jak/Stat3 pathway is involved in hippocampal plasticity, but only in the context of long-term depression (LTD), not LTP (Nicolas et al., 2012). Interestingly, Cntf is known to act via the Jak/Stat pathway (Darnell et al., 1994; Zhong et al., 1994; Heim et al., 1995; Selvaraj et al., 2012), strengthening the working hypothesis of this study to investigate the role of Cntf in hippocampal plasticity.

In a first step, we started to investigate pStat3 levels in 2-week old organotypic cultures. Under baseline conditions, pStat3 levels were significantly reduced compared to wt organotypic cultures indicating that Cntf is a regulator of pStat3 levels in hippocampal organotypic cultures. *Vice versa*, stimulation with Cntf resulted in increased pStat3 levels in *Cntf* $^{-/-}$ organotypic cultures suggesting that Cntf is both necessary and sufficient for the regulation of pStat3 levels in this experimental setup.

4.3.2 Stat3 – regulation and implications in neuronal survival

Intriguingly, pStat3 signals are still detectable in *Cntf*$^{-/-}$ cultures raising the open question how these pStat3 levels are regulated and which players contribute to their regulation. A plausible explanation could be that these remaining pStat3 levels could originate from other signaling pathways than Cntf/Jak. In addition, the suppressor of cytokine signaling (Socs) family which is an important inhibitor of the Jak/Stat pathway could play an important role (Croker et al., 2008; Babon et al., 2012; Linossi et al., 2013). In fact, there are strong similarities between Socs3 and Stat3 knockout mice suggesting a direct interaction (Costa-Pereira et al., 2002; Lang et al., 2003). More recent work by Babon (Babon et al., 2012) confirmed that Socs3 binds to the gp130 receptor (Nicholson et al., 2000), as well as the Jak receptor. However,

Socs3 appears to be only a non-competitive inhibitor of Jak2 and is unlikely to block its activity (Babon et al., 2012). Interestingly, Socs3 is expressed downstream of Stat3 and by local translocation of pStat3 to the nucleus and by exerting its transcription factor activity, Stat3 is capable to indirectly regulate its own level of phosphorylation within the Jak/Stat3 pathway (Levy and Darnell, 2002). Thus, it would be interesting to examine how Socs activity and pStat3 inhibition is regulated in the *Cntf* $^{-/-}$ mouse. This may help to explain the detected pStat3 levels in *Cntf* $^{-/-}$ organotypic cultures and it is tempting to speculate that this regulating mechanism might also result in a compensated phenotype *in vivo*.

Furthermore, the experiments on organotypic cultures did not answer the question whether acute Cntf/pStat3 signaling is a mediator of synaptic plasticity in LTP itself or whether LTP-deficits in Cntf-deficient mice is caused by more general neural circuit deficits. It has been shown, for example, that Stat3 might play a role in neuronal survival: during development, at first hippocampal neurons depend on neurotrophic factors for their survival (Murase et al., 2011). Later on, this dependency is switched to pStat3, which blocks p53 expression and its pro-apoptotic target gene *Bax*. This switch is controlled by proteasomal degradation of pStat3 during early phases of development (Murase et al., 2012; Murase, 2013). Moreover, over-excitation in mature hippocampal cultures leads to enhanced vulnerability in neurons, which can result in apoptosis and is caused by a reduced phosphorylation of Stat3 at Ser^{727} due to impaired Erk1/2 signaling (Murase et al., 2012). A role for Stat3 signaling in neuronal survival has also been demonstrated in other neurons as well (Schweizer et al., 2002; Dziennis et al., 2007; Jung et al., 2009), but whether the Jak dependent Tyr705 site is involved in hippocampal survival remains unclear.

4.3.3 Organotypic cultures and Cntf

One distinct feature of organotypic cultures is that there is a massive upregulation in astrogliosis already after 3 DIV (Gerlach et al., 2016) reflecting a situation similar to a lesion *in vivo*. Consequently, a simultaneous increase of Gfap-positive astrocytes and Cntf within these cells was observed in both cases (Ip et al., 1993a; Guthrie et al., 1997; Gerlach et al., 2016). Thus, it is tempting to speculate that this massive increase of Cntf in organotypic cultures somehow helps to maintain the functional integrity of the slice which could contribute to functional LTP in wt organotypic cultures as opposed to *Cntf* $^{-/-}$ cultures. At the same time, Gerlach *et al* observed reduced neurogenesis in this particular condition (Gerlach et al., 2016) and an application of Cntf further potentiated the observed decrease (Gerlach et al., 2016). This raises the question whether under inflammatory conditions, such as in the

organotypic culture, Cntf is primarily involved in regulating a switch from neurogenesis to astrogenesis to ensure the functional integrity of the tissue.

However, an increase in pCreb after LTP stimulation in wt and *Cntf* $^{-/-}$ cultures in our experiments indicated that basic signaling cascades are intact albeit the postulated inflammatory acute condition and that the role of Cntf in LTP seems to be very specific. Also, pStat3 levels were not influenced by LTP stimulation, at least on western blot levels of whole slice samples. The role of Cntf/pStat3 signaling in hippocampal LTP might be specifically restricted to the Schaffer-collateral and thus be masked in western blots of whole slice samples. Alternatively, Cntf/Stat3 signaling might not be directly involved in LTP signaling, but might facilitate LTP by providing intact and functional spine structures due to influencing microtubule dynamics (Selvaraj et al., 2012).

4.4 Cntf/pStat3 at the level of the spine *in vitro*

During LTP stimulation, the postsynapse can undergo structural plasticity (Engert and Bonhoeffer, 1999; Maletic-Savatic et al., 1999; Yuste and Bonhoeffer, 2001; Matsuzaki et al., 2004; Herring and Nicoll, 2016). The rapid increase of AMPAR during LTP is a direct result of CaMKII activation via Ca^{2+} influx through the NMDAR (Lisman et al., 2012). Dynamics in AMPA-and NMDA receptors are accompanied by structural changes of the spine (Herring and Nicoll, 2016). These changes are most likely based on actin dynamics (Fischer et al., 1998; Kim and Lisman, 1999; Nimchinsky et al., 2002; Honkura et al., 2008; Bosch and Hayashi, 2012; Fortin et al., 2012) since inhibition of actin dynamics abolishes NMDAR-dependent spine enlargement (Matsuzaki et al., 2004; Harvey et al., 2008). The remodeling of the actin cytoskeleton in turn is most likely mediated by Rho GTPases which are downstream targets of the CaMKII (Nakayama et al., 2000; Murakoshi et al., 2011).

4.4.1 Microtubule dynamics in synaptic plasticity

However, increasing evidence suggests that also microtubule dynamics are involved in spine plasticity. Microtubules can enter dendritic spines sporadically under baseline conditions (Hu et al., 2008; Jaworski et al., 2009) and have also been observed to enter spines in an activity-dependent manner (Hu et al., 2011; Merriam et al., 2011). This is assisted by actin remodeling at the base of the spine (Schatzle et al., 2018). Under NMDA-stimulated conditions, the number of spine entries per spine per hour was only increased to 1.5 in contrast to 1 under control conditions (Schatzle et al., 2018) suggesting microtubule entry into spines to be a rare event. It would be thrilling to investigate whether microtubule spine invasion is a more

frequent event in the presynapse, particularly upon induced activity, since our results point to a prominent pStat3 staining in this specific compartment.

A role of Cntf in microtubule dynamics has been reported in the *pmn* mouse model for motoneuron disease (Selvaraj et al., 2012). Here, Cntf mediated its effects via the Jak/Stat pathway, resulting first in a phosphorylation of Stat3. While Stat3 can dimerize and translocate to the nucleus (Shuai, 1994; Shuai et al., 1994), it can also interact locally with stathmin and interfere with its microtubule destabilizing activity (Ng et al., 2006). Phosphorylation of Stat3 in the *pmn* mouse model by CNTF application thus led to phosphorylation of stathmin, which results in the release of α/β tubulin heterodimers. This in turn can lead to axonal stabilization and mediate the rescue of the *pmn* phenotype (Sendtner et al., 1992e; Selvaraj et al., 2012). Based on these findings we addressed the major open question, whether Cntf also influences microtubule dynamics in hippocampal spines in a similar manner which could result in LTP deficits in *Cntf* $^{-/-}$ mice. To test this hypothesis we turned to cultured hippocampal neurons *in vitro*.

4.4.2 pStat3 and the presynapse

First, we observed that cultured hippocampal wt neurons are able to respond to Cntf stimulation with an increase of pStat3 validating the feasibility of this *in vitro* system. To our surprise, we found evidence that both in wt and *Cntf* $^{-/-}$ cultures, pStat3 appears to be primarily localized to the presynapse. This was first indicated by colocalization analysis of pStat3 and pre-and postsynaptic markers. Highest overlap of IR was found between pStat3 and vGluT, a presynaptic vesicular transporter of glutamate (Ni et al., 1994; Fujiyama et al., 2001; Herzog et al., 2001). Colocalization of pStat3 and Phalloidin, a marker for accumulated F-actin in the postsynapse (Cooper, 1987; Chazotte, 2010; Sidenstein et al., 2016), was significantly lower. Immunofluorescent stainings confirmed a predominant localization of pStat3 in the presynapse. Nevertheless, pStat3 IR was also found in the postsynapse. This relative distribution was independent of the analyzed genotype. However, these *in vitro* results must not be over interpreted since a robust validation and verification of the specificity of the applied antibody on an immunofluorescent level, for example by using cell cultures or slice preparations from conditional Stat3 knockout animals remains open. Western blot results reveal very clean bands without background pointing to a low probability of unspecific binding. Furthermore, the corresponding company Cell Signaling states on its provider platform that this antibody “does not cross-react with phospho-EGFR or the corresponding phospho-tyrosines of other Stat proteins.” (https://www.cellsignal.de/products/primary-

antibodies/phospho-stat3-tyr705-d3a7-xp-rabbit-mab/9145, last visited on 18th September 2019). Finally, *in vitro* immunofluorescence stainings of HeLa cells, also presented on the provider platform, indicate utility of this antibody in *in vitro* stainings. Cell Signaling list 1166 citations, out of which 119 have performed immunohistochemistry and 21 have performed immunofluorescence *in vivo* stainings, which have successfully published using this pStat3 (D3A7) antibody. The pStat3 (D3A7) antibody appears to be of high quality and specificity. However, a lentiviral-mediated knockdown of Stat3 or the analysis of *Stat3* knockout hippocampal neurons may further confirm the specificity of the used antibody validating the observed and described distribution of pStat3 immunoreactivity in pre- and postsynapse. In this context it might be worthwhile investigating the subcellular distribution of Cntf receptor CntfRα which acts upstream of Stat3.

4.4.3 Pre-and postsynapse in LTP

The roles and contributions of pre- and postsynapse to LTP and LTP induction are controversial and widely discussed, resulting in an exhausting amount of literature. For sure, the presynapse can release increased amounts of transmitter (quantal content) and the postsynapse in turn, can increase in transmitter sensitivity (quantal amplitude) (Muller et al., 1988; Bekkers and Stevens, 1990; Malinow and Tsien, 1990; Foster and McNaughton, 1991; Kullmann and Nicoll, 1992; Larkman et al., 1992; Manabe et al., 1992; Voronin, 1993; Liao et al., 1995). While most research is concerned with the role of the postsynapse in LTP, a review by Lauri *et al* from 2007 pointed out, that at least two forms of LTP, namely short-term potentiation and early LTP, both at the CA1 synapses in the hippocampus, involve presynaptic mechanisms (Lauri et al., 2007). LTP at the mossy fiber synapse from the DG to CA3 is NMDAR-independent and exclusively expressed presynaptically (Nicoll and Schmitz, 2005), while LTP at the Schaffer collateral however is NMDAR dependent (Collingridge et al., 1983). Here, NMDAR independent and presynaptic LTP involvement in CA1 has only been observed under specific conditions (Grover and Teyler, 1990; Zakharenko et al., 2001). However, presynaptic transmitter release is involved in all forms of LTP (Watkins and Jane, 2006; Herring and Nicoll, 2016; Nicoll, 2017) and therefore it can be assumed that that presynaptic Stat3 regulation by Cntf affects presynaptic transmitter release functions specifying the direction of signal transmission.

Presynaptic transmitters are packed in synaptic vesicles which in turn are transported anterogradely along microtubules by members of the kinesin transporter family (Del Castillo and Katz, 1954; Okada et al., 1995; Chia et al., 2013; Rizzoli, 2014; Wilhelm et al., 2014;

Kevenaar et al., 2016; Guedes-Dias et al., 2019). It therefore seems plausible that microtubule dynamics are involved in LTP at both, the pre-and the postsynapse and thus an influence of Cntf via pStat3 and stathmin on microtubule dynamics seems likely. Notably, presynapses were smaller in *Cntf* $^{-/-}$ than in wt cultures which could be related to a reduced number of transported vesicles due to disruptions in axonal microtubule dynamics. After all, altered axonal transport of mitochondria was rescued by Cntf application in the *pmn* mouse model (Selvaraj et al., 2012). To investigate how Cntf/pStat3 dynamics are involved in pre-or postsynaptic changes in the cytoskeleton it might be worth wile to turn to live cell imaging. Virus delivered or endogenous expression of GFP-tagged EB3 – a protein in the dynamic plus end of the microtubule (Akhmanova and Steinmetz, 2008) – could be used to investigate microtubule dynamics (Stepanova et al., 2003; Jaworski et al., 2009) and actin dynamics could be investigated using a GFP-tagged cytoplasmic actin construct which incorporates into actin-containing structures, as reported previously (Fischer et al., 1998; Sivadasan et al., 2016; Dombert et al., 2017).

4.4.4 pStat3, presynapses and astrocytes

When presynapses appeared in positioned on astrocytes, even higher amounts of pStat3 were found in these subcellular structures. Again, presynaptic structures in wt cultures were significantly larger and had significantly higher immunoreactivity for pStat3 than those in *Cntf* $^{-/-}$ cultures. Considering the amount of evidence pointing to an astrocytic source of Cntf, as discussed above, astrocytes might provide an endogenous source of Cntf in wt cultures. This could explain the increased levels of pStat3 but needs to be addressed by further experiments. There is still the plausible explanation that these detected *in vitro* findings arise from an astrocytic property that is not related to Cntf. The analysis of astrocyte-specific conditional *Cntf* $^{-/-}$ mice may provide answers.

Astrocytes have undergone an image change of merely taking a supportive role for neurons and synapses to a more active, even modulating role in synaptic communication (Haydon, 2001; Volterra and Meldolesi, 2005; Eroglu and Barres, 2010). Even synaptogenesis is reduced when the astrocyte-neuron communication is inhibited (Christopherson et al., 2005; Kucukdereli et al., 2011). The concept of the tripartite synapse has recently received more and more attention (Araque et al., 1999; Perea and Araque, 2002; Perea et al., 2009; Santello et al., 2012; Perez-Alvarez and Araque, 2013; Linne and Jalonen, 2014; Allen and Eroglu, 2017; Adamsky and Goshen, 2018; Durkee and Araque, 2019). Astrocytes are not electrically excitable themselves but can release neuroactive substances like ATP and D-serine in a Ca^{2+}

dependent manner and express a variety of functional neurotransmitter receptors (Porter and McCarthy, 1996, 1997; Araque et al., 2014; Adamsky and Goshen, 2018). D-serine can bind to the glycine binding site of the NMDAR, which is important for LTP induction (Johnson and Ascher, 1987; Bashir et al., 1990). It has been shown that via the release of D-serine, astrocytes played a role in hippocampal LTP (Yang et al., 2003). More recently, however, it is doubted whether D-serine really has its origin in astrocytes or whether astrocytes release L-serine, which is then taken up by the neurons and turned into D-serine (Wolosker et al., 2016; Mothet et al., 2019). Transplantation experiments with neuronal precursor cells (NPCs) from Il-1 deficient mice which later matured into astrocytes, provided further evidence, that astrocytes play an important role in hippocampal LTP (Ben Menachem-Zidon et al., 2011). Wt mice with transplanted Il-1 knockout derived NPCs showed deficits in hippocampal dependent learning tasks while at the same time, behavior of Il-1 knockout mice with hippocampal transplants of wt NPCs was rescued. A study by Blanco-Suarez *et al* showed, that astrocytic released Chordin-like 1 can increase the number of AMPAR subunit GluA2 and is involved in synapse maturation (Blanco-Suarez et al., 2018). Work by Farhy-Tselnicker *et al* demonstrated, that astrocytic release of Glypican 4 leads to an increase in AMPAR clustering in the postsynapse via activating pathways in the presynapse (Farhy-Tselnicker et al., 2017). This study shows how astrocytes can modulate pre- and postsynapse as a functional unit. Intriguingly, pairing of pre-and postsynapse and subsequent analysis of pStat3 amounts revealed a difference between *Cntf* $^{-/-}$ and wt cultures. The ratio of pre- over postsynaptic pStat3 was higher in *Cntf* $^{-/-}$ cultures, suggesting a presynaptic shift in pStat3 levels. However, it must be kept in mind that we are not investigating a fixed amount of pStat3 molecules that can move between pre- and postsynapse but that these are two distinct cells and cellular compartments with distinct states of activity. Therefore, this analysis must be interpreted carefully and might only allow conclusions when pre- and postsynapse are considered as one functional unit influenced by the close positioned astrocyte.

Overall more and more evidence cumulates on how soluble factors secreted by astrocytes actively modulate synaptic function. Adamsky *et al* even suggest the potential of astrocytes to induce *de novo* NMDAR dependent LTP in hippocampal CA1 (Adamsky et al., 2018). It is therefore plausible that astrocytic Cntf can modulate pre- or postsynaptic function of LTP. Our results point to an involvement in regulation of pStat3, which we predominantly observed in the presynapse. The LTP deficits in *Cntf* $^{-/-}$ mice on the other hand, were measured on the post-synaptic site. In addition, paired-pulse experiments indicated that the Cntf-effect on LTP is more likely to be of postsynaptic origin (unpublished data by Prof. Dr. Korte, TU

Braunschweig). It is possible that, similar to the work by Farhy-Tselnicker *et al*, astrocytic secreted factors, such as Cntf, can first influence processes on the presynaptic site which in turn lead to consequences on the post-synaptic site (Farhy-Tselnicker et al., 2017). Again, subcellular analysis of Cntf receptor subunits and actin cytoskeleton, as well as microtubule dynamics may help to unravel the underlying cellular mechanism of Cntf-mediated LTP in hippocampal neuronal structures.

4.4.5 The role of stathmin in microtubule dynamics and neurogenesis

It is evident that the role of stathmin needs to be analyzed when the question is experimentally addressed how Cntf might influence microtubule dynamics (Sobel et al., 1989; Gavet et al., 1998). Stathmin binds the α/β tubulin heterodimers of which microtubules are comprised which leading to microtubule catastrophe *in vitro* (Belmont and Mitchison, 1996; Di Paolo et al., 1997). As mentioned before, phosphorylation of stathmin by Cntf/pStat3 signaling results in increased axonal microtubule stability and this effect is thus able to rescue the *pmn* phenotype *in vivo* and *in vitro* (Sendtner et al., 1992e; Selvaraj et al., 2012). Further work provided evidence that the *tubulin-specific chaperone E (Tbc*e) gene is affected in the *pmn* mouse (Bommel et al., 2002). The protein encoded by *Tbce* is important for the formation of α/β-tubulin heterodimers and thus this work further confirms that microtubule dynamics are involved in the *pmn* phenotype (Bommel et al., 2002). Works by Uchida and Shumyatski demonstrated that stathmin plays an important role in hippocampal learning and memory in a time-dependent manner (Uchida and Shumyatsky, 2015). In a first phase, dephosphorylation of stathmin resulted in increased microtubule instability while the second phase was characterized by a hyperphosphorylation of stathmin and hyperstable microtubules (Uchida et al., 2014). Consequently, GluA2 AMPAR subunits were transported anterogradely by the Kif5 transporter along these hyperstable microtubules. Working with microtubule stabilizing or destabilizing drugs in either early or late phase consequently increased or decreased learning in hippocampus specific behavioral paradigms (Uchida et al., 2014). These works demonstrate that stathmin/microtubule interactions are involved in hippocampal memory formation. Whether Cntf/pStat3 signaling is upstream of these processes would be highly interesting and needs to be addressed experimentally, i.e.by investigating in a first step the dynamic and acute effects of Cntf/pStat3 on the phosphorylation levels of stathmin *in vitro*.

Another possibility of how Cntf could influence hippocampal performance on a network level via pStat3/stathmin and microtubule dynamics is via its involvement in neurogenesis. Stathmin has four phosphorylation sites of which mostly Ser ^{16} and Ser ^{63} are involved in the

microtubule binding capacity (Di Paolo et al., 1997; Larsson et al., 1997; Manna et al., 2009). Phosphorylation at Ser ^{25} and Ser ^{38} are primarily targets for Cyclin-dependent protein kinases and are involved in mitotic cell division (Larsson et al., 1995; Marklund et al., 1996; Larsson et al., 1997; Rubin and Atweh, 2004). Interestingly, stathmin is strongly expressed in the hippocampal DG and is involved in adult hippocampal neurogenesis (Boekhoorn et al., 2014; Martel et al., 2016). Similar to *Cntf* $^{-/-}$ mice, stathmin knockout mice displayed a reduced number and a reduced complexity of Doublecortin-positive immature neurons (Muller et al., 2009; Boekhoorn et al., 2014; Martel et al., 2016). Hippocampus-dependent learning like contextual fear conditioning was also reduced in mice expressing an unphosphorylatable and therefore constitutively active form of stathmin (Martel et al., 2016). A potential explanation for the LTP deficit in *Cntf* $^{-/-}$ mice in organotypic cultures could therefore also be mediated indirectly via altered neurogenesis, possibly mediated via Cntf/pStat3/stathmin and microtubule dynamics. However, as mentioned earlier, other results show that application of Cntf actually decreased neurogenesis in the organotypic cultures (Gerlach et al., 2016) due to the lesion-related astrogliosis and acute prioritization of resources.

In the end, there are at least two possible starting points from which Cntf could exert its effect on LTP via pStat3/stathmin and microtubule dynamics in the hippocampus. Whether it is directly involved in synaptic plasticity at CA1 dendrites, possibly in the manner of a trisynaptic synapse, or whether the cause for the LTP deficit originates from the DG and its role in neurogenesis – involvements of stathmin and microtubule dynamics have been demonstrated and therefore render the possibility of functional Cntf signaling at central synapses. However, the importance of Cntf-induced or mediated signaling in this context appears indisputable.

4.5 Conclusion

In conclusion, Cntf appears to be involved in hippocampal Stat3 signaling. First, preliminary data point to a Cntf-dependent regulation of presynaptic levels of pStat3. Altered Cntf/Stat3 signaling, possibly resulting in a downstream effect on microtubule dynamics, might be responsible for the observed LTP deficit in acute slices and organotypic cultures of *Cntf* $^{-/-}$ mice. This deficit seems to be compensated *in vivo* by other factors which act upstream of pStat3, since behavior in hippocampal-dependent learning tasks is largely inconspicuous. Overall, this thesis highlights aspects of a new role for Cntf in hippocampal Stat3 signaling.

The most intriguing question is certainly why Cntf-deficient mice develop a strong deficit in LTP but reveal no obvious phenotype on a behavioral level *in vivo*. The high predisposition of

CNTF null mutants – roughly 3% of the human population – who do not display major neurological or psychiatric phenotypes strongly indicates that there are effective compensatory mechanisms for the deficiency of CNTF both in humans and rodents *in vivo*.

5 References

Abrahams S, Pickering A, Polkey CE, Morris RG (1997) Spatial memory deficits in patients with unilateral damage to the right hippocampal formation. Neuropsychologia 35:11-24.

Abrahams S, Morris RG, Polkey CE, Jarosz JM, Cox TC, Graves M, Pickering A (1999) Hippocampal involvement in spatial and working memory: a structural MRI analysis of patients with unilateral mesial temporal lobe sclerosis. Brain Cogn 41:39-65.

Acsady L, Kamondi A, Sik A, Freund T, Buzsaki G (1998) GABAergic cells are the major postsynaptic targets of mossy fibers in the rat hippocampus. J Neurosci 18:3386-3403.

ACTS (1995) A phase I study of recombinant human ciliary neurotrophic factor (rHCNTF) in patients with amyotrophic lateral sclerosis. The ALS CNTF Treatment Study (ACTS) Phase I-II Study Group. Clin Neuropharmacol 18:515-532.

ACTS (1996) A double-blind placebo-controlled clinical trial of subcutaneous recombinant human ciliary neurotrophic factor (rHCNTF) in amyotrophic lateral sclerosis. ALS CNTF Treatment Study Group. Neurology 46:1244-1249.

Adamsky A, Goshen I (2018) Astrocytes in Memory Function: Pioneering Findings and Future Directions. Neuroscience 370:14-26.

Adamsky A, Kol A, Kreisel T, Doron A, Ozeri-Engelhard N, Melcer T, Refaeli R, Horn H, Regev L, Groysman M, London M, Goshen I (2018) Astrocytic Activation Generates De Novo Neuronal Potentiation and Memory Enhancement. Cell.

Adler R, Landa KB, Manthorpe M, Varon S (1979) Cholinergic neuronotrophic factors: intraocular distribution of trophic activity for ciliary neurons. Science 204:1434-1436.

Aghajanova L (2004) Leukemia inhibitory factor and human embryo implantation. Ann N Y Acad Sci 1034:176-183.

Akhmanova A, Steinmetz MO (2008) Tracking the ends: a dynamic protein network controls the fate of microtubule tips. Nature reviews Molecular cell biology 9:309-322.

Alger BE, Teyler TJ (1976) Long-term and short-term plasticity in the CA1, CA3, and dentate regions of the rat hippocampal slice. Brain Res 110:463-480.

Allen NJ, Eroglu C (2017) Cell Biology of Astrocyte-Synapse Interactions. Neuron 96:697-708.

Allison DW, Gelfand VI, Spector I, Craig AM (1998) Role of actin in anchoring postsynaptic receptors in cultured hippocampal neurons: differential attachment of NMDA versus AMPA receptors. J Neurosci 18:2423-2436.

Alonzi T, Middleton G, Wyatt S, Buchman V, Betz UA, Muller W, Musiani P, Poli V, Davies AM (2001) Role of STAT3 and PI 3-kinase/Akt in mediating the survival actions of cytokines on sensory neurons. Mol Cell Neurosci 18:270-282.

Alpar A et al. (2018) Hypothalamic CNTF volume transmission shapes cortical noradrenergic excitability upon acute stress. EMBO J 37.

Anagnostaras SG, Gale GD, Fanselow MS (2001) Hippocampus and contextual fear conditioning: recent controversies and advances. Hippocampus 11:8-17.

Anand P, Terenghi G, Birch R, Wellmer A, Cedarbaum JM, Lindsay RM, Williams-Chestnut RE, Sinicropi DV (1997) Endogenous NGF and CNTF levels in human peripheral nerve injury. Neuroreport 8:1935-1938.

Antunes M, Biala G (2012) The novel object recognition memory: neurobiology, test procedure, and its modifications. Cognitive processing 13:93-110.

Arakawa Y, Sendtner M, Thoenen H (1990) Survival effect of ciliary neurotrophic factor (CNTF) on chick embryonic motoneurons in culture: comparison with other neurotrophic factors and cytokines. J Neurosci 10:3507-3515.

Araque A, Parpura V, Sanzgiri RP, Haydon PG (1999) Tripartite synapses: glia, the unacknowledged partner. Trends Neurosci 22:208-215.

Araque A, Carmignoto G, Haydon PG, Oliet SH, Robitaille R, Volterra A (2014) Gliotransmitters travel in time and space. Neuron 81:728-739.

Ascher P, Nowak L (1988) The role of divalent cations in the N-methyl-D-aspartate responses of mouse central neurones in culture. J Physiol 399:247-266.

Atwood HL, Karunanithi S (2002) Diversification of synaptic strength: presynaptic elements. Nat Rev Neurosci 3:497-516.

Babon JJ, Kershaw NJ, Murphy JM, Varghese LN, Laktyushin A, Young SN, Lucet IS, Norton RS, Nicola NA (2012) Suppression of cytokine signaling by SOCS3: characterization of the mode of inhibition and the basis of its specificity. Immunity 36:239-250.

Banks WA, Kastin AJ, Gutierrez EG (1994) Penetration of interleukin-6 across the murine blood-brain barrier. Neurosci Lett 179:53-56.

Bannerman DM, Rawlins JN, McHugh SB, Deacon RM, Yee BK, Bast T, Zhang WN, Pothuizen HH, Feldon J (2004) Regional dissociations within the hippocampus--memory and anxiety. Neurosci Biobehav Rev 28:273-283.
Barbin G, Manthorpe M, Varon S (1984) Purification of the chick eye ciliary neuronotrophic factor. J Neurochem 43:1468-1478.
Barde YA (1994) Neurotrophins: a family of proteins supporting the survival of neurons. Prog Clin Biol Res 390:45-56.
Barde YA, Edgar D, Thoenen H (1982) Purification of a new neurotrophic factor from mammalian brain. EMBO J 1:549-553.
Bartsch T, Schonfeld R, Muller FJ, Alfke K, Leplow B, Aldenhoff J, Deuschl G, Koch JM (2010) Focal lesions of human hippocampal CA1 neurons in transient global amnesia impair place memory. Science 328:1412-1415.
Bashir ZI, Tam B, Collingridge GL (1990) Activation of the glycine site in the NMDA receptor is necessary for the induction of LTP. Neurosci Lett 108:261-266.
Bazan JF (1991) Neuropoietic cytokines in the hematopoietic fold. Neuron 7:197-208.
Bekkers JM, Stevens CF (1990) Presynaptic mechanism for long-term potentiation in the hippocampus. Nature 346:724-729.
Belmont LD, Mitchison TJ (1996) Identification of a protein that interacts with tubulin dimers and increases the catastrophe rate of microtubules. Cell 84:623-631.
Ben Menachem-Zidon O, Avital A, Ben-Menahem Y, Goshen I, Kreisel T, Shmueli EM, Segal M, Ben Hur T, Yirmiya R (2011) Astrocytes support hippocampal-dependent memory and long-term potentiation via interleukin-1 signaling. Brain, behavior, and immunity 25:1008-1016.
Birch DG, Bennett LD, Duncan JL, Weleber RG, Pennesi ME (2016) Long-term Follow-up of Patients With Retinitis Pigmentosa Receiving Intraocular Ciliary Neurotrophic Factor Implants. American journal of ophthalmology 170:10-14.
Birch DG, Weleber RG, Duncan JL, Jaffe GJ, Tao W, Ciliary Neurotrophic Factor Retinitis Pigmentosa Study G (2013) Randomized trial of ciliary neurotrophic factor delivered by encapsulated cell intraocular implants for retinitis pigmentosa. American journal of ophthalmology 156:283-292 e281.
Blanco-Suarez E, Liu TF, Kopelevich A, Allen NJ (2018) Astrocyte-Secreted Chordin-like 1 Drives Synapse Maturation and Limits Plasticity by Increasing Synaptic GluA2 AMPA Receptors. Neuron 100:1116-1132 e1113.
Bliss TV, Gardner-Medwin AR (1973) Long-lasting potentiation of synaptic transmission in the dentate area of the unanaestetized rabbit following stimulation of the perforant path. J Physiol 232:357-374.
Bliss TV, Lomo T (1973) Long-lasting potentiation of synaptic transmission in the dentate area of the anaesthetized rabbit following stimulation of the perforant path. J Physiol 232:331-356.
Bliss TV, Collingridge GL (1993) A synaptic model of memory: long-term potentiation in the hippocampus. Nature 361:31-39.
Boekhoorn K, van Dis V, Goedknegt E, Sobel A, Lucassen PJ, Hoogenraad CC (2014) The microtubule destabilizing protein stathmin controls the transition from dividing neuronal precursors to postmitotic neurons during adult hippocampal neurogenesis. Dev Neurobiol 74:1226-1242.
Bommel H, Xie G, Rossoll W, Wiese S, Jablonka S, Boehm T, Sendtner M (2002) Missense mutation in the tubulin-specific chaperone E (Tbce) gene in the mouse mutant progressive motor neuronopathy, a model of human motoneuron disease. The Journal of cell biology 159:563-569.
Bosch M, Hayashi Y (2012) Structural plasticity of dendritic spines. Curr Opin Neurobiol 22:383-388.
Bosch M, Castro J, Saneyoshi T, Matsuno H, Sur M, Hayashi Y (2014) Structural and molecular remodeling of dendritic spine substructures during long-term potentiation. Neuron 82:444-459.
Broadbent NJ, Gaskin S, Squire LR, Clark RE (2010) Object recognition memory and the rodent hippocampus. Learn Mem 17:5-11.
Bromberg J (2002) Stat proteins and oncogenesis. The Journal of clinical investigation 109:1139-1142.
Burgess N, Maguire EA, O'Keefe J (2002) The human hippocampus and spatial and episodic memory. Neuron 35:625-641.
Camporeale A, Demaria M, Monteleone E, Giorgi C, Wieckowski MR, Pinton P, Poli V (2014) STAT3 Activities and Energy Metabolism: Dangerous Liaisons. Cancers 6:1579-1596.
Carola V, D'Olimpio F, Brunamonti E, Mangia F, Renzi P (2002) Evaluation of the elevated plus-maze and open-field tests for the assessment of anxiety-related behaviour in inbred mice. Behavioural brain research 134:49-57.
Carroll P, Sendtner M, Meyer M, Thoenen H (1993) Rat ciliary neurotrophic factor (CNTF): gene structure and regulation of mRNA levels in glial cell cultures. Glia 9:176-187.
Cavus I, Teyler T (1996) Two forms of long-term potentiation in area CA1 activate different signal transduction cascades. Journal of neurophysiology 76:3038-3047.

Chang MY, Son H, Lee YS, Lee SH (2003) Neurons and astrocytes secrete factors that cause stem cells to differentiate into neurons and astrocytes, respectively. Mol Cell Neurosci 23:414-426.
Chao MV (2003) Neurotrophins and their receptors: a convergence point for many signalling pathways. Nat Rev Neurosci 4:299-309.
Chazotte B (2010) Labeling cytoskeletal F-actin with rhodamine phalloidin or fluorescein phalloidin for imaging. Cold Spring Harb Protoc 2010:pdb prot4947.
Chen H, Tung YC, Li B, Iqbal K, Grundke-Iqbal I (2007) Trophic factors counteract elevated FGF-2-induced inhibition of adult neurogenesis. Neurobiol Aging 28:1148-1162.
Chia PH, Li P, Shen K (2013) Cell biology in neuroscience: cellular and molecular mechanisms underlying presynapse formation. J Cell Biol 203:11-22.
Chiba T, Yamada M, Sasabe J, Terashita K, Shimoda M, Matsuoka M, Aiso S (2009) Amyloid-beta causes memory impairment by disturbing the JAK2/STAT3 axis in hippocampal neurons. Molecular psychiatry 14:206-222.
Christopherson KS, Ullian EM, Stokes CC, Mullowney CE, Hell JW, Agah A, Lawler J, Mosher DF, Bornstein P, Barres BA (2005) Thrombospondins are astrocyte-secreted proteins that promote CNS synaptogenesis. Cell 120:421-433.
Chung J, Uchida E, Grammer TC, Blenis J (1997) STAT3 serine phosphorylation by ERK-dependent and -independent pathways negatively modulates its tyrosine phosphorylation. Mol Cell Biol 17:6508-6516.
Collingridge GL, Kehl SJ, McLennan H (1983) Excitatory amino acids in synaptic transmission in the Schaffer collateral-commissural pathway of the rat hippocampus. J Physiol 334:33-46.
Cooper JA (1987) Effects of cytochalasin and phalloidin on actin. J Cell Biol 105:1473-1478.
Costa-Pereira AP, Tininini S, Strobl B, Alonzi T, Schlaak JF, Is'harc H, Gesualdo I, Newman SJ, Kerr IM, Poli V (2002) Mutational switch of an IL-6 response to an interferon-gamma-like response. Proc Natl Acad Sci U S A 99:8043-8047.
Crawley J, Goodwin FK (1980) Preliminary report of a simple animal behavior model for the anxiolytic effects of benzodiazepines. Pharmacol Biochem Behav 13:167-170.
Croker BA, Kiu H, Nicholson SE (2008) SOCS regulation of the JAK/STAT signalling pathway. Seminars in cell & developmental biology 19:414-422.
Curmi PA, Andersen SS, Lachkar S, Gavet O, Karsenti E, Knossow M, Sobel A (1997) The stathmin/tubulin interaction in vitro. J Biol Chem 272:25029-25036.
Darnell JE, Jr., Kerr IM, Stark GR (1994) Jak-STAT pathways and transcriptional activation in response to IFNs and other extracellular signaling proteins. Science 264:1415-1421.
Davis M, Walker DL, Miles L, Grillon C (2010) Phasic vs sustained fear in rats and humans: role of the extended amygdala in fear vs anxiety. Neuropsychopharmacology 35:105-135.
Davis S, Aldrich TH, Valenzuela DM, Wong VV, Furth ME, Squinto SP, Yancopoulos GD (1991) The receptor for ciliary neurotrophic factor. Science 253:59-63.
Davis S, Aldrich TH, Ip NY, Stahl N, Scherer S, Farruggella T, DiStefano PS, Curtis R, Panayotatos N, Gascan H, et al. (1993) Released form of CNTF receptor alpha component as a soluble mediator of CNTF responses. Science 259:1736-1739.
de Lima MN, Luft T, Roesler R, Schroder N (2006) Temporary inactivation reveals an essential role of the dorsal hippocampus in consolidation of object recognition memory. Neurosci Lett 405:142-146.
DeChiara TM, Vejsada R, Poueymirou WT, Acheson A, Suri C, Conover JC, Friedman B, McClain J, Pan L, Stahl N, Ip NY, Yancopoulos GD (1995) Mice lacking the CNTF receptor, unlike mice lacking CNTF, exhibit profound motor neuron deficits at birth. Cell 83:313-322.
Decker T, Kovarik P (2000) Serine phosphorylation of STATs. Oncogene 19:2628-2637.
Deckert J et al. (2017) GLRB allelic variation associated with agoraphobic cognitions, increased startle response and fear network activation: a potential neurogenetic pathway to panic disorder. Molecular psychiatry 22:1431-1439.
Del Castillo J, Katz B (1954) Quantal components of the end-plate potential. J Physiol 124:560-573.
Deng W, Aimone JB, Gage FH (2010) New neurons and new memories: how does adult hippocampal neurogenesis affect learning and memory? Nat Rev Neurosci 11:339-350.
Denninger JK, Smith BM, Kirby ED (2018) Novel Object Recognition and Object Location Behavioral Testing in Mice on a Budget. Journal of visualized experiments : JoVE.
Di Paolo G, Antonsson B, Kassel D, Riederer BM, Grenningloh G (1997) Phosphorylation regulates the microtubule-destabilizing activity of stathmin and its interaction with tubulin. FEBS letters 416:149-152.
Ding J, He Z, Ruan J, Liu Y, Gong C, Sun S, Chen H (2013a) Influence of endogenous ciliary neurotrophic factor on neural differentiation of adult rat hippocampal progenitors. Neural Regen Res 8:301-312.
Ding J, He Z, Ruan J, Ma Z, Liu Y, Gong C, Iqbal K, Sun S, Chen H (2013d) Role of ciliary neurotrophic factor in the proliferation and differentiation of neural stem cells. Journal of Alzheimer's disease : JAD 37:587-592.

Dittrich F, Thoenen H, Sendtner M (1994) Ciliary Neurotrophic Factor - Pharmacokinetics and Acute-Phase Response in Rat. Ann Neurol 35:151-163.
Dittrich F, Ochs G, GrosseWilde A, Berweiler U, Yan Q, Miller JA, Toyka KV, Sendtner M (1996) Pharmacokinetics of intrathecally applied BDNF and effects on spinal motoneurons. Experimental Neurology 141:225-239.
Dobrea GM, Unnerstall JR, Rao MS (1992) The expression of CNTF message and immunoreactivity in the central and peripheral nervous system of the rat. Brain Res Dev Brain Res 66:209-219.
Dobrunz LE, Stevens CF (1997) Heterogeneity of release probability, facilitation, and depletion at central synapses. Neuron 18:995-1008.
Dombert B, Balk S, Luningschror P, Moradi M, Sivadasan R, Saal-Bauernschubert L, Jablonka S (2017) BDNF/trkB Induction of Calcium Transients through Cav2.2 Calcium Channels in Motoneurons Corresponds to F-actin Assembly and Growth Cone Formation on beta2-Chain Laminin (221). Frontiers in molecular neuroscience 10:346.
Durkee CA, Araque A (2019) Diversity and Specificity of Astrocyte-neuron Communication. Neuroscience 396:73-78.
Dziennis S, Jia T, Ronnekleiv OK, Hurn PD, Alkayed NJ (2007) Role of signal transducer and activator of transcription-3 in estradiol-mediated neuroprotection. J Neurosci 27:7268-7274.
Eichenbaum H (2004) Hippocampus: cognitive processes and neural representations that underlie declarative memory. Neuron 44:109-120.
Emsley JG, Hagg T (2003) Endogenous and exogenous ciliary neurotrophic factor enhances forebrain neurogenesis in adult mice. Exp Neurol 183:298-310.
Engert F, Bonhoeffer T (1999) Dendritic spine changes associated with hippocampal long-term synaptic plasticity. Nature 399:66-70.
Ennaceur A (2010) One-trial object recognition in rats and mice: methodological and theoretical issues. Behav Brain Res 215:244-254.
Ennaceur A, Delacour J (1988) A new one-trial test for neurobiological studies of memory in rats. 1: Behavioral data. Behav Brain Res 31:47-59.
Ernsberger U, Sendtner M, Rohrer H (1989) Proliferation and differentiation of embryonic chick sympathetic neurons: effects of ciliary neurotrophic factor. Neuron 2:1275-1284.
Eroglu C, Barres BA (2010) Regulation of synaptic connectivity by glia. Nature 468:223-231.
Esteves da Silva M, Adrian M, Schatzle P, Lipka J, Watanabe T, Cho S, Futai K, Wierenga CJ, Kapitein LC, Hoogenraad CC (2015) Positioning of AMPA Receptor-Containing Endosomes Regulates Synapse Architecture. Cell Rep 13:933-943.
Ettinger MP, Littlejohn TW, Schwartz SL, Weiss SR, McIlwain HH, Heymsfield SB, Bray GA, Roberts WG, Heyman ER, Stambler N, Heshka S, Vicary C, Guler HP (2003) Recombinant variant of ciliary neurotrophic factor for weight loss in obese adults: a randomized, dose-ranging study. JAMA 289:1826-1832.
Fagerberg L et al. (2014) Analysis of the human tissue-specific expression by genome-wide integration of transcriptomics and antibody-based proteomics. Mol Cell Proteomics 13:397-406.
Farhy-Tselnicker I, van Casteren ACM, Lee A, Chang VT, Aricescu AR, Allen NJ (2017) Astrocyte-Secreted Glypican 4 Regulates Release of Neuronal Pentraxin 1 from Axons to Induce Functional Synapse Formation. Neuron 96:428-445 e413.
Fischer M, Kaech S, Knutti D, Matus A (1998) Rapid actin-based plasticity in dendritic spines. Neuron 20:847-854.
Fortin DA, Srivastava T, Soderling TR (2012) Structural modulation of dendritic spines during synaptic plasticity. Neuroscientist 18:326-341.
Foster TC, McNaughton BL (1991) Long-term enhancement of CA1 synaptic transmission is due to increased quantal size, not quantal content. Hippocampus 1:79-91.
Friedman B, Scherer SS, Rudge JS, Helgren M, Morrisey D, McClain J, Wang DY, Wiegand SJ, Furth ME, Lindsay RM, et al. (1992) Regulation of ciliary neurotrophic factor expression in myelin-related Schwann cells in vivo. Neuron 9:295-305.
Fujiyama F, Furuta T, Kaneko T (2001) Immunocytochemical localization of candidates for vesicular glutamate transporters in the rat cerebral cortex. The Journal of comparative neurology 435:379-387.
Gage FH (2000) Mammalian neural stem cells. Science 287:1433-1438.
Gage FH, Kempermann G, Palmer TD, Peterson DA, Ray J (1998) Multipotent progenitor cells in the adult dentate gyrus. J Neurobiol 36:249-266.
Gahwiler BH (1981a) Nerve cells in organotypic cultures. JAMA 245:1858-1859.
Gahwiler BH (1981b) Morphological differentiation of nerve cells in thin organotypic cultures derived from rat hippocampus and cerebellum. Proc R Soc Lond B Biol Sci 211:287-290.
Gahwiler BH (1981c) Organotypic monolayer cultures of nervous tissue. J Neurosci Methods 4:329-342.

Galimberti I, Gogolla N, Alberi S, Santos AF, Muller D, Caroni P (2006) Long-term rearrangements of hippocampal mossy fiber terminal connectivity in the adult regulated by experience. Neuron 50:749-763.
Gavet O, Ozon S, Manceau V, Lawler S, Curmi P, Sobel A (1998) The stathmin phosphoprotein family: intracellular localization and effects on the microtubule network. J Cell Sci 111 (Pt 22):3333-3346.
Gelernter J, Van Dyck C, van Kammen DP, Malison R, Price LH, Cubells JF, Berman R, Charney DS, Heninger G (1997) Ciliary neurotrophic factor null allele frequencies in schizophrenia, affective disorders, and Alzheimer's disease. Am J Med Genet 74:497-500.
Gerlach J, Donkels C, Munzner G, Haas CA (2016) Persistent Gliosis Interferes with Neurogenesis in Organotypic Hippocampal Slice Cultures. Frontiers in cellular neuroscience 10:131.
Ghasemi M, Alizadeh E, Saei Arezoumand K, Fallahi Motlagh B, Zarghami N (2018) Ciliary neurotrophic factor (CNTF) delivery to retina: an overview of current research advancements. Artif Cells Nanomed Biotechnol 46:1694-1707.
Giess R, Goetz R, Schrank B, Ochs G, Sendtner M, Toyka K (1998) Potential implications of a ciliary neurotrophic factor gene mutation in a German population of patients with motor neuron disease. Muscle & nerve 21:236-238.
Giess R, Holtmann B, Braga M, Grimm T, Muller-Myhsok B, Toyka KV, Sendtner M (2002a) Early onset of severe familial amyotrophic lateral sclerosis with a SOD-1 mutation: potential impact of CNTF as a candidate modifier gene. Am J Hum Genet 70:1277-1286.
Giess R, Maurer M, Linker R, Gold R, Warmuth-Metz M, Toyka KV, Sendtner M, Rieckmann P (2002e) Association of a null mutation in the CNTF gene with early onset of multiple sclerosis. Arch Neurol 59:407-409.
Gilbert PE, Kesner RP (2006) The role of the dorsal CA3 hippocampal subregion in spatial working memory and pattern separation. Behav Brain Res 169:142-149.
Giovannini M, Romo AJ, Evans GA (1993) Chromosomal localization of the human ciliary neurotrophic factor gene (CNTF) to 11q12 by fluorescence in situ hybridization. Cytogenet Cell Genet 63:62-63.
Gotz R, Schartl M (1994) The conservation of neurotrophic factors during vertebrate evolution. Comparative biochemistry and physiology Pharmacology, toxicology and endocrinology 108:1-10.
Gough DJ, Corlett A, Schlessinger K, Wegrzyn J, Larner AC, Levy DE (2009) Mitochondrial STAT3 Supports Ras-Dependent Oncogenic Transformation. Science 324:1713-1716.
Goulart BK, de Lima MN, de Farias CB, Reolon GK, Almeida VR, Quevedo J, Kapczinski F, Schroder N, Roesler R (2010) Ketamine impairs recognition memory consolidation and prevents learning-induced increase in hippocampal brain-derived neurotrophic factor levels. Neuroscience 167:969-973.
Gregg C, Weiss S (2005) CNTF/LIF/gp130 receptor complex signaling maintains a VZ precursor differentiation gradient in the developing ventral forebrain. Development 132:565-578.
Grover LM, Teyler TJ (1990) Two components of long-term potentiation induced by different patterns of afferent activation. Nature 347:477-479.
Grover LM, Teyler TJ (1992) N-methyl-D-aspartate receptor-independent long-term potentiation in area CA1 of rat hippocampus: input-specific induction and preclusion in a non-tetanized pathway. Neuroscience 49:7-11.
Grunblatt E, Hupp E, Bambula M, Zehetmayer S, Jungwirth S, Tragl KH, Fischer P, Riederer P (2006) Association study of BDNF and CNTF polymorphism to depression in non-demented subjects of the "VITA" study. J Affect Disord 96:111-116.
Guedes-Dias P, Nirschl JJ, Abreu N, Tokito MK, Janke C, Magiera MM, Holzbaur ELF (2019) Kinesin-3 Responds to Local Microtubule Dynamics to Target Synaptic Cargo Delivery to the Presynapse. Curr Biol 29:268-282 e268.
Guthrie KM, Woods AG, Nguyen T, Gall CM (1997) Astroglial ciliary neurotrophic factor mRNA expression is increased in fields of axonal sprouting in deafferented hippocampus. J Comp Neurol 386:137-148.
Hall AK, Rao MS (1992) Cytokines and neurokines: related ligands and related receptors. Trends Neurosci 15:35-37.
Hallbook F, Ibanez CF, Persson H (1991) Evolutionary studies of the nerve growth factor family reveal a novel member abundantly expressed in Xenopus ovary. Neuron 6:845-858.
Hanley JG (2014) Actin-dependent mechanisms in AMPA receptor trafficking. Frontiers in cellular neuroscience 8:381.
Harris EW, Ganong AH, Cotman CW (1984) Long-term potentiation in the hippocampus involves activation of N-methyl-D-aspartate receptors. Brain Res 323:132-137.
Harris KM, Teyler TJ (1984) Developmental onset of long-term potentiation in area CA1 of the rat hippocampus. J Physiol 346:27-48.
Harris KM, Sultan P (1995) Variation in the number, location and size of synaptic vesicles provides an anatomical basis for the nonuniform probability of release at hippocampal CA1 synapses. Neuropharmacology 34:1387-1395.

Harvey CD, Svoboda K (2007) Locally dynamic synaptic learning rules in pyramidal neuron dendrites. Nature 450:1195-1200.
Harvey CD, Yasuda R, Zhong H, Svoboda K (2008) The spread of Ras activity triggered by activation of a single dendritic spine. Science 321:136-140.
Haydon PG (2001) GLIA: listening and talking to the synapse. Nat Rev Neurosci 2:185-193.
He Z, Ding J, Zhang J, Liu Y, Gong C, Sun S, Chen H (2012) Fibroblast growth factor-2 counteracts the effect of ciliary neurotrophic factor on spontaneous differentiation in adult hippocampal progenitor cells. J Huazhong Univ Sci Technolog Med Sci 32:867-871.
Heim MH, Kerr IM, Stark GR, Darnell JE, Jr. (1995) Contribution of STAT SH2 groups to specific interferon signaling by the Jak-STAT pathway. Science 267:1347-1349.
Helfand SL, Smith GA, Wessells NK (1976) Survival and development in culture of dissociated parasympathetic neurons from ciliary ganglia. Dev Biol 50:541-547.
Henderson JT, Seniuk NA, Roder JC (1994) Localization of CNTF immunoreactivity to neurons and astroglia in the CNS. Brain Res Mol Brain Res 22:151-165.
Herring BE, Nicoll RA (2016) Long-Term Potentiation: From CaMKII to AMPA Receptor Trafficking. Annu Rev Physiol 78:351-365.
Herzog E, Bellenchi GC, Gras C, Bernard V, Ravassard P, Bedet C, Gasnier B, Giros B, El Mestikawy S (2001) The existence of a second vesicular glutamate transporter specifies subpopulations of glutamatergic neurons. J Neurosci 21:RC181.
Hibi M, Nakajima K, Hirano T (1996) IL-6 cytokine family and signal transduction: a model of the cytokine system. J Mol Med (Berl) 74:1-12.
Hibi M, Murakami M, Saito M, Hirano T, Taga T, Kishimoto T (1990) Molecular cloning and expression of an IL-6 signal transducer, gp130. Cell 63:1149-1157.
Hirsh R (1974) The hippocampus and contextual retrieval of information from memory: a theory. Behav Biol 12:421-444.
Hofer MJ, Campbell IL (2016) Immunoinflammatory diseases of the central nervous system - the tale of two cytokines. Br J Pharmacol 173:716-728.
Holtmaat A, Caroni P (2016) Functional and structural underpinnings of neuronal assembly formation in learning. Nat Neurosci 19:1553-1562.
Holtmann B, Wiese S, Samsam M, Grohmann K, Pennica D, Martini R, Sendtner M (2005) Triple knock-out of CNTF, LIF, and CT-1 defines cooperative and distinct roles of these neurotrophic factors for motoneuron maintenance and function. J Neurosci 25:1778-1787.
Honkura N, Matsuzaki M, Noguchi J, Ellis-Davies GC, Kasai H (2008) The subspine organization of actin fibers regulates the structure and plasticity of dendritic spines. Neuron 57:719-729.
Hu X, Viesselmann C, Nam S, Merriam E, Dent EW (2008) Activity-dependent dynamic microtubule invasion of dendritic spines. The Journal of neuroscience : the official journal of the Society for Neuroscience 28:13094-13105.
Hu X, Ballo L, Pietila L, Viesselmann C, Ballweg J, Lumbard D, Stevenson M, Merriam E, Dent EW (2011) BDNF-induced increase of PSD-95 in dendritic spines requires dynamic microtubule invasions. The Journal of neuroscience : the official journal of the Society for Neuroscience 31:15597-15603.
Huang EJ, Reichardt LF (2001) Neurotrophins: roles in neuronal development and function. Annual review of neuroscience 24:677-736.
Huganir RL, Nicoll RA (2013) AMPARs and synaptic plasticity: the last 25 years. Neuron 80:704-717.
Hughes SM, Lillien LE, Raff MC, Rohrer H, Sendtner M (1988) Ciliary neurotrophic factor induces type-2 astrocyte differentiation in culture. Nature 335:70-73.
Ibanez CF, Andressoo JO (2017) Biology of GDNF and its receptors - Relevance for disorders of the central nervous system. Neurobiology of disease 97:80-89.
Impey S, Mark M, Villacres EC, Poser S, Chavkin C, Storm DR (1996) Induction of CRE-mediated gene expression by stimuli that generate long-lasting LTP in area CA1 of the hippocampus. Neuron 16:973-982.
Ip NY, Yancopoulos GD (1992) Ciliary neurotrophic factor and its receptor complex. Prog Growth Factor Res 4:139-155.
Ip NY, Wiegand SJ, Morse J, Rudge JS (1993a) Injury-induced regulation of ciliary neurotrophic factor mRNA in the adult rat brain. Eur J Neurosci 5:25-33.
Ip NY, Li YP, van de Stadt I, Panayotatos N, Alderson RF, Lindsay RM (1991) Ciliary neurotrophic factor enhances neuronal survival in embryonic rat hippocampal cultures. J Neurosci 11:3124-3134.
Ip NY, McClain J, Barrezueta NX, Aldrich TH, Pan L, Li Y, Wiegand SJ, Friedman B, Davis S, Yancopoulos GD (1993d) The alpha component of the CNTF receptor is required for signaling and defines potential CNTF targets in the adult and during development. Neuron 10:89-102.

Ip NY, Nye SH, Boulton TG, Davis S, Taga T, Li Y, Birren SJ, Yasukawa K, Kishimoto T, Anderson DJ, et al. (1992) CNTF and LIF act on neuronal cells via shared signaling pathways that involve the IL-6 signal transducing receptor component gp130. Cell 69:1121-1132.
Isaac JT, Nicoll RA, Malenka RC (1995) Evidence for silent synapses: implications for the expression of LTP. Neuron 15:427-434.
Izquierdo I, Medina JH (1997) Memory formation: the sequence of biochemical events in the hippocampus and its connection to activity in other brain structures. Neurobiol Learn Mem 68:285-316.
Jain N, Zhang T, Fong SL, Lim CP, Cao X (1998) Repression of Stat3 activity by activation of mitogen-activated protein kinase (MAPK). Oncogene 17:3157-3167.
Jaworski J, Kapitein LC, Gouveia SM, Dortland BR, Wulf PS, Grigoriev I, Camera P, Spangler SA, Di Stefano P, Demmers J, Krugers H, Defilippi P, Akhmanova A, Hoogenraad CC (2009) Dynamic microtubules regulate dendritic spine morphology and synaptic plasticity. Neuron 61:85-100.
Jessen KR, Mirsky R (1992) Schwann cells: early lineage, regulation of proliferation and control of myelin formation. Curr Opin Neurobiol 2:575-581.
Ji J, Maren S (2007) Hippocampal involvement in contextual modulation of fear extinction. Hippocampus 17:749-758.
Jia C, Keasey MP, Lovins C, Hagg T (2018) Inhibition of astrocyte FAK-JNK signaling promotes subventricular zone neurogenesis through CNTF. Glia 66:2456-2469.
Jo SA, Wang E, Benowitz LI (1999) Ciliary neurotrophic factor is an axogenesis factor for retinal ganglion cells. Neuroscience 89:579-591.
Johansen JP, Cain CK, Ostroff LE, LeDoux JE (2011) Molecular mechanisms of fear learning and memory. Cell 147:509-524.
Johe KK, Hazel TG, Muller T, Dugich-Djordjevic MM, McKay RD (1996) Single factors direct the differentiation of stem cells from the fetal and adult central nervous system. Genes Dev 10:3129-3140.
Johnson JW, Ascher P (1987) Glycine potentiates the NMDA response in cultured mouse brain neurons. Nature 325:529-531.
Johnston ST, Shtrahman M, Parylak S, Goncalves JT, Gage FH (2016) Paradox of pattern separation and adult neurogenesis: A dual role for new neurons balancing memory resolution and robustness. Neurobiology of learning and memory 129:60-68.
Jourdain L, Curmi P, Sobel A, Pantaloni D, Carlier MF (1997) Stathmin: a tubulin-sequestering protein which forms a ternary T2S complex with two tubulin molecules. Biochemistry 36:10817-10821.
Jung JE, Kim GS, Narasimhan P, Song YS, Chan PH (2009) Regulation of Mn-superoxide dismutase activity and neuroprotection by STAT3 in mice after cerebral ischemia. J Neurosci 29:7003-7014.
Kalisch R, Korenfeld E, Stephan KE, Weiskopf N, Seymour B, Dolan RJ (2006) Context-dependent human extinction memory is mediated by a ventromedial prefrontal and hippocampal network. J Neurosci 26:9503-9511.
Kamimura D, Ishihara K, Hirano T (2003) IL-6 signal transduction and its physiological roles: the signal orchestration model. Rev Physiol Biochem Pharmacol 149:1-38.
Kapitein LC, Yau KW, Hoogenraad CC (2010) Microtubule dynamics in dendritic spines. Methods in cell biology 97:111-132.
Kapitein LC, Yau KW, Gouveia SM, van der Zwan WA, Wulf PS, Keijzer N, Demmers J, Jaworski J, Akhmanova A, Hoogenraad CC (2011) NMDA receptor activation suppresses microtubule growth and spine entry. J Neurosci 31:8194-8209.
Kaupmann K, Sendtner M, Stockli KA, Jockusch H (1991) The Gene for Ciliary Neurotrophic Factor (CNTF) Maps to Murine Chromosome 19 and its Expression is Not Affected in the Hereditary Motoneuron Disease 'Wobbler' of the Mouse. Eur J Neurosci 3:1182-1186.
Kawahara Y, Manabe T, Matsumoto M, Kajiume T, Matsumoto M, Yuge L (2009) LIF-free embryonic stem cell culture in simulated microgravity. PLoS One 4:e6343.
Kelly PT, McGuinness TL, Greengard P (1984) Evidence that the major postsynaptic density protein is a component of a Ca2+/calmodulin-dependent protein kinase. Proc Natl Acad Sci U S A 81:945-949.
Kempermann G, Gage FH (2000) Neurogenesis in the adult hippocampus. Novartis Found Symp 231:220-235; discussion 235-241, 302-226.
Kennedy MB (1993) The postsynaptic density. Curr Opin Neurobiol 3:732-737.
Kennedy MB, Bennett MK, Erondu NE (1983) Biochemical and immunochemical evidence that the "major postsynaptic density protein" is a subunit of a calmodulin-dependent protein kinase. Proc Natl Acad Sci U S A 80:7357-7361.
Kesner RP (2013) An analysis of the dentate gyrus function. Behavioural brain research 254:1-7.
Kessler RC et al. (2007) Lifetime prevalence and age-of-onset distributions of mental disorders in the World Health Organization's World Mental Health Survey Initiative. World Psychiatry 6:168-176.
Kevenaar JT, Bianchi S, van Spronsen M, Olieric N, Lipka J, Frias CP, Mikhaylova M, Harterink M, Keijzer N, Wulf PS, Hilbert M, Kapitein LC, de Graaff E, Ahkmanova A, Steinmetz MO, Hoogenraad CC (2016)

Kinesin-Binding Protein Controls Microtubule Dynamics and Cargo Trafficking by Regulating Kinesin Motor Activity. Curr Biol 26:849-861.
Kim CH, Lisman JE (1999) A role of actin filament in synaptic transmission and long-term potentiation. J Neurosci 19:4314-4324.
King JA, Burgess N, Hartley T, Vargha-Khadem F, O'Keefe J (2002) Human hippocampus and viewpoint dependence in spatial memory. Hippocampus 12:811-820.
Kjelstrup KG, Tuvnes FA, Steffenach HA, Murison R, Moser EI, Moser MB (2002) Reduced fear expression after lesions of the ventral hippocampus. Proc Natl Acad Sci U S A 99:10825-10830.
Knierim JJ, Neunuebel JP (2016) Tracking the flow of hippocampal computation: Pattern separation, pattern completion, and attractor dynamics. Neurobiol Learn Mem 129:38-49.
Kucukdereli H, Allen NJ, Lee AT, Feng A, Ozlu MI, Conatser LM, Chakraborty C, Workman G, Weaver M, Sage EH, Barres BA, Eroglu C (2011) Control of excitatory CNS synaptogenesis by astrocyte-secreted proteins Hevin and SPARC. Proc Natl Acad Sci U S A 108:E440-449.
Kullmann DM, Nicoll RA (1992) Long-term potentiation is associated with increases in quantal content and quantal amplitude. Nature 357:240-244.
Lambert PD, Anderson KD, Sleeman MW, Wong V, Tan J, Hijarunguru A, Corcoran TL, Murray JD, Thabet KE, Yancopoulos GD, Wiegand SJ (2001) Ciliary neurotrophic factor activates leptin-like pathways and reduces body fat, without cachexia or rebound weight gain, even in leptin-resistant obesity. Proc Natl Acad Sci U S A 98:4652-4657.
Lang R, Pauleau AL, Parganas E, Takahashi Y, Mages J, Ihle JN, Rutschman R, Murray PJ (2003) SOCS3 regulates the plasticity of gp130 signaling. Nat Immunol 4:546-550.
Larkman A, Hannay T, Stratford K, Jack J (1992) Presynaptic release probability influences the locus of long-term potentiation. Nature 360:70-73.
Larsen JV, Hansen M, Moller B, Madsen P, Scheller J, Nielsen M, Petersen CM (2010) Sortilin facilitates signaling of ciliary neurotrophic factor and related helical type 1 cytokines targeting the gp130/leukemia inhibitory factor receptor beta heterodimer. Mol Cell Biol 30:4175-4187.
Larsson N, Melander H, Marklund U, Osterman O, Gullberg M (1995) G2/M transition requires multisite phosphorylation of oncoprotein 18 by two distinct protein kinase systems. J Biol Chem 270:14175-14183.
Larsson N, Marklund U, Gradin HM, Brattsand G, Gullberg M (1997) Control of microtubule dynamics by oncoprotein 18: dissection of the regulatory role of multisite phosphorylation during mitosis. Mol Cell Biol 17:5530-5539.
Lauri SE, Palmer M, Segerstrale M, Vesikansa A, Taira T, Collingridge GL (2007) Presynaptic mechanisms involved in the expression of STP and LTP at CA1 synapses in the hippocampus. Neuropharmacology 52:1-11.
Lavail MM, Unoki K, Yasumura D, Matthes MT, Yancopoulos GD, Steinberg RH (1992) Multiple Growth-Factors, Cytokines, and Neurotrophins Rescue Photoreceptors from the Damaging Effects of Constant Light. P Natl Acad Sci USA 89:11249-11253.
LeDoux JE (2014) Coming to terms with fear. Proc Natl Acad Sci U S A 111:2871-2878.
Leibrock J, Lottspeich F, Hohn A, Hofer M, Hengerer B, Masiakowski P, Thoenen H, Barde YA (1989) Molecular cloning and expression of brain-derived neurotrophic factor. Nature 341:149-152.
Levi-Montalcini R, Meyer H, Hamburger V (1954) In vitro experiments on the effects of mouse sarcomas 180 and 37 on the spinal and sympathetic ganglia of the chick embryo. Cancer research 14:49-57.
Levy DE, Lee CK (2002) What does Stat3 do? The Journal of clinical investigation 109:1143-1148.
Levy DE, Darnell JE, Jr. (2002) Stats: transcriptional control and biological impact. Nature reviews Molecular cell biology 3:651-662.
Liao D, Hessler NA, Malinow R (1995) Activation of postsynaptically silent synapses during pairing-induced LTP in CA1 region of hippocampal slice. Nature 375:400-404.
Lillien LE, Raff MC (1990a) Differentiation signals in the CNS: type-2 astrocyte development in vitro as a model system. Neuron 5:111-119.
Lillien LE, Raff MC (1990b) Analysis of the cell-cell interactions that control type-2 astrocyte development in vitro. Neuron 4:525-534.
Lillien LE, Sendtner M, Raff MC (1990) Extracellular matrix-associated molecules collaborate with ciliary neurotrophic factor to induce type-2 astrocyte development. J Cell Biol 111:635-644.
Lillien LE, Sendtner M, Rohrer H, Hughes SM, Raff MC (1988) Type-2 astrocyte development in rat brain cultures is initiated by a CNTF-like protein produced by type-1 astrocytes. Neuron 1:485-494.
Lim CP, Cao X (1999) Serine phosphorylation and negative regulation of Stat3 by JNK. J Biol Chem 274:31055-31061.
Lin LF, Doherty DH, Lile JD, Bektesh S, Collins F (1993) GDNF: a glial cell line-derived neurotrophic factor for midbrain dopaminergic neurons. Science 260:1130-1132.

Lin LF, Mismer D, Lile JD, Armes LG, Butler ET, 3rd, Vannice JL, Collins F (1989) Purification, cloning, and expression of ciliary neurotrophic factor (CNTF). Science 246:1023-1025.
Linker RA, Maurer M, Gaupp S, Martini R, Holtmann B, Giess R, Rieckmann P, Lassmann H, Toyka KV, Sendtner M, Gold R (2002) CNTF is a major protective factor in demyelinating CNS disease: a neurotrophic cytokine as modulator in neuroinflammation. Nat Med 8:620-624.
Linne ML, Jalonen TO (2014) Astrocyte-neuron interactions: from experimental research-based models to translational medicine. Progress in molecular biology and translational science 123:191-217.
Linossi EM, Babon JJ, Hilton DJ, Nicholson SE (2013) Suppression of cytokine signaling: the SOCS perspective. Cytokine Growth Factor Rev 24:241-248.
Lisman J (1994) The CaM kinase II hypothesis for the storage of synaptic memory. Trends Neurosci 17:406-412.
Lisman J, Yasuda R, Raghavachari S (2012) Mechanisms of CaMKII action in long-term potentiation. Nat Rev Neurosci 13:169-182.
Liu B, Palmfeldt J, Lin L, Colaco A, Clemmensen KKB, Huang J, Xu F, Liu X, Maeda K, Luo Y, Jaattela M (2018) STAT3 associates with vacuolar H+-ATPase and regulates cytosolic and lysosomal pH. Cell Res 28:996-1012.
Liu X, Clark AF, Wordinger RJ (2007) Expression of ciliary neurotrophic factor (CNTF) and its tripartite receptor complex by cells of the human optic nerve head. Mol Vis 13:758-763.
Luningschror P et al. (2017) Plekhg5-regulated autophagy of synaptic vesicles reveals a pathogenic mechanism in motoneuron disease. Nat Commun 8:678.
Lynch G, Larson J, Kelso S, Barrionuevo G, Schottler F (1983) Intracellular injections of EGTA block induction of hippocampal long-term potentiation. Nature 305:719-721.
Maguire EA, Frackowiak RS, Frith CD (1996a) Learning to find your way: a role for the human hippocampal formation. Proc Biol Sci 263:1745-1750.
Maguire EA, Burke T, Phillips J, Staunton H (1996b) Topographical disorientation following unilateral temporal lobe lesions in humans. Neuropsychologia 34:993-1001.
Maguire EA, Frith CD, Burgess N, Donnett JG, O'Keefe J (1998a) Knowing where things are parahippocampal involvement in encoding object locations in virtual large-scale space. J Cogn Neurosci 10:61-76.
Maguire EA, Burgess N, Donnett JG, Frackowiak RS, Frith CD, O'Keefe J (1998b) Knowing where and getting there: a human navigation network. Science 280:921-924.
Mahmoud GS, Grover LM (2006) Growth hormone enhances excitatory synaptic transmission in area CA1 of rat hippocampus. Journal of neurophysiology 95:2962-2974.
Maisonpierre PC, Belluscio L, Squinto S, Ip NY, Furth ME, Lindsay RM, Yancopoulos GD (1990) Neurotrophin-3: a neurotrophic factor related to NGF and BDNF. Science 247:1446-1451.
Malenka RC, Kauer JA, Perkel DJ, Mauk MD, Kelly PT, Nicoll RA, Waxham MN (1989) An essential role for postsynaptic calmodulin and protein kinase activity in long-term potentiation. Nature 340:554-557.
Maletic-Savatic M, Malinow R, Svoboda K (1999) Rapid dendritic morphogenesis in CA1 hippocampal dendrites induced by synaptic activity. Science 283:1923-1927.
Malinow R, Tsien RW (1990) Presynaptic enhancement shown by whole-cell recordings of long-term potentiation in hippocampal slices. Nature 346:177-180.
Manabe T, Renner P, Nicoll RA (1992) Postsynaptic contribution to long-term potentiation revealed by the analysis of miniature synaptic currents. Nature 355:50-55.
Manna T, Thrower DA, Honnappa S, Steinmetz MO, Wilson L (2009) Regulation of microtubule dynamic instability in vitro by differentially phosphorylated stathmin. J Biol Chem 284:15640-15649.
Manthorpe M, Skaper SD, Barbin G, Varon S (1982) Cholinergic neuronotrophic factors. Concurrent activities on certain nerve growth factor-responsive neurons. J Neurochem 38:415-421.
Manthorpe M, Skaper SD, Williams LR, Varon S (1986) Purification of adult rat sciatic nerve ciliary neuronotrophic factor. Brain Res 367:282-286.
Maren S (2011) Seeking a spotless mind: extinction, deconsolidation, and erasure of fear memory. Neuron 70:830-845.
Maren S, Hobin JA (2007) Hippocampal regulation of context-dependent neuronal activity in the lateral amygdala. Learn Mem 14:318-324.
Marklund U, Larsson N, Gradin HM, Brattsand G, Gullberg M (1996) Oncoprotein 18 is a phosphorylation-responsive regulator of microtubule dynamics. EMBO J 15:5290-5298.
Martel G, Uchida S, Hevi C, Chevere-Torres I, Fuentes I, Park YJ, Hafeez H, Yamagata H, Watanabe Y, Shumyatsky GP (2016) Genetic Demonstration of a Role for Stathmin in Adult Hippocampal Neurogenesis, Spinogenesis, and NMDA Receptor-Dependent Memory. The Journal of neuroscience : the official journal of the Society for Neuroscience 36:1185-1202.
Martin-Zanca D, Hughes SH, Barbacid M (1986) A human oncogene formed by the fusion of truncated tropomyosin and protein tyrosine kinase sequences. Nature 319:743-748.

Masu Y, Wolf E, Holtmann B, Sendtner M, Brem G, Thoenen H (1993) Disruption of the CNTF gene results in motor neuron degeneration. Nature 365:27-32.
Matsuzaki M, Honkura N, Ellis-Davies GC, Kasai H (2004) Structural basis of long-term potentiation in single dendritic spines. Nature 429:761-766.
Mayer ML, Westbrook GL, Guthrie PB (1984) Voltage-dependent block by Mg2+ of NMDA responses in spinal cord neurones. Nature 309:261-263.
McAllister AK, Katz LC, Lo DC (1999) Neurotrophins and synaptic plasticity. Annual review of neuroscience 22:295-318.
McKay R (1997) Stem cells in the central nervous system. Science 276:66-71.
McKee RD, Squire LR (1993) On the development of declarative memory. J Exp Psychol Learn Mem Cogn 19:397-404.
McVicker DP, Awe AM, Richters KE, Wilson RL, Cowdrey DA, Hu X, Chapman ER, Dent EW (2016) Transport of a kinesin-cargo pair along microtubules into dendritic spines undergoing synaptic plasticity. Nat Commun 7:12741.
Meier JA, Larner AC (2014) Toward a new STATe: The role of STATs in mitochondrial function. Semin Immunol 26:20-28.
Merriam EB, Lumbard DC, Viesselmann C, Ballweg J, Stevenson M, Pietila L, Hu X, Dent EW (2011) Dynamic microtubules promote synaptic NMDA receptor-dependent spine enlargement. PloS one 6:e27688.
Miller RG, Petajan JH, Bryan WW, Armon C, Barohn RJ, Goodpasture JC, Hoagland RJ, Parry GJ, Ross MA, Stromatt SC (1996) A placebo-controlled trial of recombinant human ciliary neurotrophic (rhCNTF) factor in amyotrophic lateral sclerosis. rhCNTF ALS Study Group. Ann Neurol 39:256-260.
Morris R (1984) Developments of a water-maze procedure for studying spatial learning in the rat. J Neurosci Methods 11:47-60.
Morris RG, Garrud P, Rawlins JN, O'Keefe J (1982) Place navigation impaired in rats with hippocampal lesions. Nature 297:681-683.
Morris RG, Anderson E, Lynch GS, Baudry M (1986) Selective impairment of learning and blockade of long-term potentiation by an N-methyl-D-aspartate receptor antagonist, AP5. Nature 319:774-776.
Mothet JP, Billard JM, Pollegioni L, Coyle JT, Sweedler JV (2019) Investigating brain d-serine: Advocacy for good practices. Acta physiologica 226:e13257.
Mullberg J, Oberthur W, Lottspeich F, Mehl E, Dittrich E, Graeve L, Heinrich PC, Rose-John S (1994) The soluble human IL-6 receptor. Mutational characterization of the proteolytic cleavage site. J Immunol 152:4958-4968.
Muller D, Joly M, Lynch G (1988) Contributions of quisqualate and NMDA receptors to the induction and expression of LTP. Science 242:1694-1697.
Muller S, Chakrapani BP, Schwegler H, Hofmann HD, Kirsch M (2009) Neurogenesis in the dentate gyrus depends on ciliary neurotrophic factor and signal transducer and activator of transcription 3 signaling. Stem Cells 27:431-441.
Munzberg H, Tafel J, Busing B, Hinney A, Ziegler A, Mayer H, Siegfried W, Matthaei S, Greten H, Hebebrand J, Hamann A (1998) Screening for variability in the ciliary neurotrophic factor (CNTF) gene: no evidence for association with human obesity. Exp Clin Endocrinol Diabetes 106:108-112.
Muraguchi A, Hirano T, Tang B, Matsuda T, Horii Y, Nakajima K, Kishimoto T (1988) The essential role of B cell stimulatory factor 2 (BSF-2/IL-6) for the terminal differentiation of B cells. J Exp Med 167:332-344.
Murakami M, Narazaki M, Hibi M, Yawata H, Yasukawa K, Hamaguchi M, Taga T, Kishimoto T (1991) Critical cytoplasmic region of the interleukin 6 signal transducer gp130 is conserved in the cytokine receptor family. Proc Natl Acad Sci U S A 88:11349-11353.
Murakoshi H, Wang H, Yasuda R (2011) Local, persistent activation of Rho GTPases during plasticity of single dendritic spines. Nature 472:100-104.
Murase S (2013) Signal transducer and activator of transcription 3 (STAT3) degradation by proteasome controls a developmental switch in neurotrophin dependence. J Biol Chem 288:20151-20161.
Murase S, McKay RD (2014) Neuronal activity-dependent STAT3 localization to nucleus is dependent on Tyr-705 and Ser-727 phosphorylation in rat hippocampal neurons. Eur J Neurosci 39:557-565.
Murase S, Owens DF, McKay RD (2011) In the newborn hippocampus, neurotrophin-dependent survival requires spontaneous activity and integrin signaling. J Neurosci 31:7791-7800.
Murase S, Kim E, Lin L, Hoffman DA, McKay RD (2012) Loss of signal transducer and activator of transcription 3 (STAT3) signaling during elevated activity causes vulnerability in hippocampal neurons. The Journal of neuroscience : the official journal of the Society for Neuroscience 32:15511-15520.
Murata S, Usuda N, Okano A, Kobayashi S, Suzuki T (2000) Occurrence of a transcription factor, signal transducer and activators of transcription 3 (Stat3), in the postsynaptic density of the rat brain. Brain Res Mol Brain Res 78:80-90.

Murthy VN, Schikorski T, Stevens CF, Zhu Y (2001) Inactivity produces increases in neurotransmitter release and synapse size. Neuron 32:673-682.
Nabavi S, Fox R, Proulx CD, Lin JY, Tsien RY, Malinow R (2014) Engineering a memory with LTD and LTP. Nature 511:348-352.
Nakayama AY, Harms MB, Luo L (2000) Small GTPases Rac and Rho in the maintenance of dendritic spines and branches in hippocampal pyramidal neurons. J Neurosci 20:5329-5338.
Negro A, Corona G, Bigon E, Martini I, Grandi C, Skaper SD, Callegaro L (1991a) Synthesis, purification, and characterization of human ciliary neuronotrophic factor from E. coli. Journal of neuroscience research 29:251-260.
Negro A, Tolosano E, Skaper SD, Martini I, Callegaro L, Silengo L, Fiorini F, Altruda F (1991b) Cloning and expression of human ciliary neurotrophic factor. Eur J Biochem 201:289-294.
Nemanic S, Alvarado MC, Bachevalier J (2004) The hippocampal/parahippocampal regions and recognition memory: insights from visual paired comparison versus object-delayed nonmatching in monkeys. J Neurosci 24:2013-2026.
Ng DC, Lin BH, Lim CP, Huang G, Zhang T, Poli V, Cao X (2006) Stat3 regulates microtubules by antagonizing the depolymerization activity of stathmin. J Cell Biol 172:245-257.
Ni B, Rosteck PR, Jr., Nadi NS, Paul SM (1994) Cloning and expression of a cDNA encoding a brain-specific Na(+)-dependent inorganic phosphate cotransporter. Proc Natl Acad Sci U S A 91:5607-5611.
Nicholson SE, De Souza D, Fabri LJ, Corbin J, Willson TA, Zhang JG, Silva A, Asimakis M, Farley A, Nash AD, Metcalf D, Hilton DJ, Nicola NA, Baca M (2000) Suppressor of cytokine signaling-3 preferentially binds to the SHP-2-binding site on the shared cytokine receptor subunit gp130. Proc Natl Acad Sci U S A 97:6493-6498.
Nicolas CS, Amici M, Bortolotto ZA, Doherty A, Csaba Z, Fafouri A, Dournaud P, Gressens P, Collingridge GL, Peineau S (2013) The role of JAK-STAT signaling within the CNS. Jak-Stat 2:e22925.
Nicolas CS et al. (2012) The Jak/STAT pathway is involved in synaptic plasticity. Neuron 73:374-390.
Nicoll RA (2017) A Brief History of Long-Term Potentiation. Neuron 93:281-290.
Nicoll RA, Malenka RC (1995) Contrasting properties of two forms of long-term potentiation in the hippocampus. Nature 377:115-118.
Nicoll RA, Schmitz D (2005) Synaptic plasticity at hippocampal mossy fibre synapses. Nat Rev Neurosci 6:863-876.
Nicoll RA, Kauer JA, Malenka RC (1988) The current excitement in long-term potentiation. Neuron 1:97-103.
Nimchinsky EA, Sabatini BL, Svoboda K (2002) Structure and function of dendritic spines. Annu Rev Physiol 64:313-353.
Nishi R, Berg DK (1981) Two components from eye tissue that differentially stimulate the growth and development of ciliary ganglion neurons in cell culture. J Neurosci 1:505-513.
Nowak L, Bregestovski P, Ascher P, Herbet A, Prochiantz A (1984) Magnesium gates glutamate-activated channels in mouse central neurones. Nature 307:462-465.
O'Keefe J, Dostrovsky J (1971) The hippocampus as a spatial map. Preliminary evidence from unit activity in the freely-moving rat. Brain Res 34:171-175.
Ogawa K, Matsui H, Ohtsuka S, Niwa H (2004) A novel mechanism for regulating clonal propagation of mouse ES cells. Genes Cells 9:471-477.
Okada Y, Yamazaki H, Sekine-Aizawa Y, Hirokawa N (1995) The neuron-specific kinesin superfamily protein KIF1A is a unique monomeric motor for anterograde axonal transport of synaptic vesicle precursors. Cell 81:769-780.
Oliveira AM, Hawk JD, Abel T, Havekes R (2010) Post-training reversible inactivation of the hippocampus enhances novel object recognition memory. Learn Mem 17:155-160.
Panayotatos N, Everdeen D, Liten A, Somogyi R, Acheson A (1994) Recombinant human CNTF receptor alpha: production, binding stoichiometry, and characterization of its activity as a diffusible factor. Biochemistry 33:5813-5818.
Pape HC, Pare D (2010) Plastic synaptic networks of the amygdala for the acquisition, expression, and extinction of conditioned fear. Physiol Rev 90:419-463.
Park H, Poo MM (2013) Neurotrophin regulation of neural circuit development and function. Nature reviews Neuroscience 14:7-23.
Pascalis O, Bachevalier J (1999) Neonatal aspiration lesions of the hippocampal formation impair visual recognition memory when assessed by paired-comparison task but not by delayed nonmatching-to-sample task. Hippocampus 9:609-616.
Pascalis O, Hunkin NM, Holdstock JS, Isaac CL, Mayes AR (2004) Visual paired comparison performance is impaired in a patient with selective hippocampal lesions and relatively intact item recognition. Neuropsychologia 42:1293-1300.

Pasquin S, Sharma M, Gauchat JF (2015) Ciliary neurotrophic factor (CNTF): New facets of an old molecule for treating neurodegenerative and metabolic syndrome pathologies. Cytokine Growth Factor Rev 26:507-515.
Patapoutian A, Reichardt LF (2001) Trk receptors: mediators of neurotrophin action. Curr Opin Neurobiol 11:272-280.
Patterson PH (1992) The emerging neuropoietic cytokine family: first CDF/LIF, CNTF and IL-6; next ONC, MGF, GCSF? Curr Opin Neurobiol 2:94-97.
Pavlov PI (1927) Conditioned reflexes: An investigation of the physiological activity of the cerebral cortex. Ann Neurosci 17:136-141.
Penn AC, Zhang CL, Georges F, Royer L, Breillat C, Hosy E, Petersen JD, Humeau Y, Choquet D (2017) Hippocampal LTP and contextual learning require surface diffusion of AMPA receptors. Nature 549:384-388.
Perea G, Araque A (2002) Communication between astrocytes and neurons: a complex language. J Physiol Paris 96:199-207.
Perea G, Navarrete M, Araque A (2009) Tripartite synapses: astrocytes process and control synaptic information. Trends Neurosci 32:421-431.
Perez-Alvarez A, Araque A (2013) Astrocyte-neuron interaction at tripartite synapses. Current drug targets 14:1220-1224.
Peruga I, Hartwig S, Merkler D, Thone J, Hovemann B, Juckel G, Gold R, Linker RA (2012) Endogenous ciliary neurotrophic factor modulates anxiety and depressive-like behavior. Behav Brain Res 229:325-332.
Phelps EA, LeDoux JE (2005) Contributions of the amygdala to emotion processing: from animal models to human behavior. Neuron 48:175-187.
Phillips RG, LeDoux JE (1992) Differential contribution of amygdala and hippocampus to cued and contextual fear conditioning. Behav Neurosci 106:274-285.
Pilli S, Zawadzki RJ, Telander DG (2014) The dose-dependent macular thickness changes assessed by fd-oct in patients with retinitis pigmentosa treated with ciliary neurotrophic factor. Retina 34:1384-1390.
Pitkanen A, Pikkarainen M, Nurminen N, Ylinen A (2000) Reciprocal connections between the amygdala and the hippocampal formation, perirhinal cortex, and postrhinal cortex in rat. A review. Ann N Y Acad Sci 911:369-391.
Porter JT, McCarthy KD (1996) Hippocampal astrocytes in situ respond to glutamate released from synaptic terminals. J Neurosci 16:5073-5081.
Porter JT, McCarthy KD (1997) Astrocytic neurotransmitter receptors in situ and in vivo. Prog Neurobiol 51:439-455.
R von Collenberg C (2015) Neurotrophic factor-dependent signaling associated with fear learning and extinction. Master thesis, Institute for Clinical Neurobiology, University of Würzburg.
R von Collenberg C, Schmitt D, Rulicke T, Sendtner M, Blum R, Buchner E (2019) An essential role of the mouse synapse-associated protein Syap1 in circuits for spontaneous motor activity and rotarod balance. Biol Open 8.
Rao MS, Landis SC, Patterson PH (1990) The cholinergic neuronal differentiation factor from heart cell conditioned medium is different from the cholinergic factors in sciatic nerve and spinal cord. Dev Biol 139:65-74.
Reger ML, Hovda DA, Giza CC (2009) Ontogeny of Rat Recognition Memory measured by the novel object recognition task. Dev Psychobiol 51:672-678.
Rizzoli SO (2014) Synaptic vesicle recycling: steps and principles. EMBO J 33:788-822.
Rolls ET (2013) The mechanisms for pattern completion and pattern separation in the hippocampus. Front Syst Neurosci 7:74.
Rose-John S (2018) Interleukin-6 Family Cytokines. Cold Spring Harbor perspectives in biology 10.
Rose-John S, Heinrich PC (1994) Soluble receptors for cytokines and growth factors: generation and biological function. Biochem J 300 (Pt 2):281-290.
Rose TM, Bruce AG (1991) Oncostatin M is a member of a cytokine family that includes leukemia-inhibitory factor, granulocyte colony-stimulating factor, and interleukin 6. Proc Natl Acad Sci U S A 88:8641-8645.
Rothaug M, Becker-Pauly C, Rose-John S (2016) The role of interleukin-6 signaling in nervous tissue. Biochim Biophys Acta 1863:1218-1227.
Rubin CI, Atweh GF (2004) The role of stathmin in the regulation of the cell cycle. J Cell Biochem 93:242-250.
Rudge JS, Davis GE, Manthorpe M, Varon S (1987) An examination of ciliary neuronotrophic factors from avian and rodent tissue extracts using a blot and culture technique. Brain Res 429:103-110.
Rudge JS, Alderson RF, Pasnikowski E, McClain J, Ip NY, Lindsay RM (1992) Expression of Ciliary Neurotrophic Factor and the Neurotrophins-Nerve Growth Factor, Brain-Derived Neurotrophic Factor and Neurotrophin 3-in Cultured Rat Hippocampal Astrocytes. Eur J Neurosci 4:459-471.

Ruediger S, Vittori C, Bednarek E, Genoud C, Strata P, Sacchetti B, Caroni P (2011) Learning-related feedforward inhibitory connectivity growth required for memory precision. Nature 473:514-518.
Saadat S, Sendtner M, Rohrer H (1989) Ciliary neurotrophic factor induces cholinergic differentiation of rat sympathetic neurons in culture. J Cell Biol 108:1807-1816.
Sahay A, Hen R (2007) Adult hippocampal neurogenesis in depression. Nat Neurosci 10:1110-1115.
Sahay A, Wilson DA, Hen R (2011) Pattern separation: a common function for new neurons in hippocampus and olfactory bulb. Neuron 70:582-588.
Sakimura K, Kutsuwada T, Ito I, Manabe T, Takayama C, Kushiya E, Yagi T, Aizawa S, Inoue Y, Sugiyama H, et al. (1995) Reduced hippocampal LTP and spatial learning in mice lacking NMDA receptor epsilon 1 subunit. Nature 373:151-155.
Sala D, Cunningham TJ, Stec MJ, Etxaniz U, Nicoletti C, Dall'Agnese A, Puri PL, Duester G, Latella L, Sacco A (2019) The Stat3-Fam3a axis promotes muscle stem cell myogenic lineage progression by inducing mitochondrial respiration. Nature Communications 10.
Santello M, Cali C, Bezzi P (2012) Gliotransmission and the tripartite synapse. Adv Exp Med Biol 970:307-331.
Schatzle P, Esteves da Silva M, Tas RP, Katrukha EA, Hu HY, Wierenga CJ, Kapitein LC, Hoogenraad CC (2018) Activity-Dependent Actin Remodeling at the Base of Dendritic Spines Promotes Microtubule Entry. Curr Biol 28:2081-2093 e2086.
Schikorski T, Stevens CF (2001) Morphological correlates of functionally defined synaptic vesicle populations. Nat Neurosci 4:391-395.
Schmalbruch H, Jensen HJ, Bjaerg M, Kamieniecka Z, Kurland L (1991) A new mouse mutant with progressive motor neuronopathy. J Neuropathol Exp Neurol 50:192-204.
Schwartzkroin PA, Wester K (1975) Long-lasting facilitation of a synaptic potential following tetanization in the in vitro hippocampal slice. Brain Res 89:107-119.
Schweizer U, Gunnersen J, Karch C, Wiese S, Holtmann B, Takeda K, Akira S, Sendtner M (2002) Conditional gene ablation of Stat3 reveals differential signaling requirements for survival of motoneurons during development and after nerve injury in the adult. J Cell Biol 156:287-297.
Selvaraj BT, Frank N, Bender FL, Asan E, Sendtner M (2012) Local axonal function of STAT3 rescues axon degeneration in the pmn model of motoneuron disease. The Journal of cell biology 199:437-451.
Sendtner M, Kreutzberg GW, Thoenen H (1990) Ciliary neurotrophic factor prevents the degeneration of motor neurons after axotomy. Nature 345:440-441.
Sendtner M, Stockli KA, Thoenen H (1992a) Synthesis and localization of ciliary neurotrophic factor in the sciatic nerve of the adult rat after lesion and during regeneration. J Cell Biol 118:139-148.
Sendtner M, Arakawa Y, Stockli KA, Kreutzberg GW, Thoenen H (1991) Effect of ciliary neurotrophic factor (CNTF) on motoneuron survival. J Cell Sci Suppl 15:103-109.
Sendtner M, Carroll P, Holtmann B, Hughes RA, Thoenen H (1994) Ciliary neurotrophic factor. Journal of neurobiology 25:1436-1453.
Sendtner M, Schmalbruch H, Stockli KA, Carroll P, Kreutzberg GW, Thoenen H (1992e) Ciliary neurotrophic factor prevents degeneration of motor neurons in mouse mutant progressive motor neuronopathy. Nature 358:502-504.
Sendtner M, Gotz R, Holtmann B, Escary JL, Masu Y, Carroll P, Wolf E, Brem G, Brulet P, Thoenen H (1996) Cryptic physiological trophic support of motoneurons by LIF revealed by double gene targeting of CNTF and LIF. Curr Biol 6:686-694.
Sheng M, Greenberg ME (1990) The regulation and function of c-fos and other immediate early genes in the nervous system. Neuron 4:477-485.
Shimazaki T, Shingo T, Weiss S (2001) The ciliary neurotrophic factor/leukemia inhibitory factor/gp130 receptor complex operates in the maintenance of mammalian forebrain neural stem cells. J Neurosci 21:7642-7653.
Shuai K (1994) Interferon-activated signal transduction to the nucleus. Curr Opin Cell Biol 6:253-259.
Shuai K, Horvath CM, Huang LH, Qureshi SA, Cowburn D, Darnell JE, Jr. (1994) Interferon activation of the transcription factor Stat91 involves dimerization through SH2-phosphotyrosyl peptide interactions. Cell 76:821-828.
Sidenstein SC, D'Este E, Bohm MJ, Danzl JG, Belov VN, Hell SW (2016) Multicolour Multilevel STED nanoscopy of Actin/Spectrin Organization at Synapses. Sci Rep 6:26725.
Sieving PA, Caruso RC, Tao W, Coleman HR, Thompson DJS, Fullmer KR, Bush RA (2006) Ciliary neurotrophic factor (CNTF) for human retinal degeneration: Phase I trial of CNTF delivered by encapsulated cell intraocular implants. P Natl Acad Sci USA 103:3896-3901.
Silva AJ, Kogan JH, Frankland PW, Kida S (1998) CREB and memory. Annu Rev Neurosci 21:127-148.
Simpson RJ, Hammacher A, Smith DK, Matthews JM, Ward LD (1997) Interleukin-6: structure-function relationships. Protein Sci 6:929-955.

Sivadasan R, Hornburg D, Drepper C, Frank N, Jablonka S, Hansel A, Lojewski X, Sterneckert J, Hermann A, Shaw PJ, Ince PG, Mann M, Meissner F, Sendtner M (2016) C9ORF72 interaction with cofilin modulates actin dynamics in motor neurons. Nature neuroscience 19:1610-1618.

Sivakumaran MH, Mackenzie AK, Callan IR, Ainge JA, O'Connor AR (2018) The Discrimination Ratio derived from Novel Object Recognition tasks as a Measure of Recognition Memory Sensitivity, not Bias. Sci Rep 8:11579.

Smith AG, Heath JK, Donaldson DD, Wong GG, Moreau J, Stahl M, Rogers D (1988) Inhibition of pluripotential embryonic stem cell differentiation by purified polypeptides. Nature 336:688-690.

Sobel A, Boutterin MC, Beretta L, Chneiweiss H, Doye V, Peyro-Saint-Paul H (1989) Intracellular substrates for extracellular signaling. Characterization of a ubiquitous, neuron-enriched phosphoprotein (stathmin). J Biol Chem 264:3765-3772.

Song H, Stevens CF, Gage FH (2002) Astroglia induce neurogenesis from adult neural stem cells. Nature 417:39-44.

Spiers HJ, Burgess N, Hartley T, Vargha-Khadem F, O'Keefe J (2001a) Bilateral hippocampal pathology impairs topographical and episodic memory but not visual pattern matching. Hippocampus 11:715-725.

Spiers HJ, Burgess N, Maguire EA, Baxendale SA, Hartley T, Thompson PJ, O'Keefe J (2001b) Unilateral temporal lobectomy patients show lateralized topographical and episodic memory deficits in a virtual town. Brain 124:2476-2489.

Squire LR, Zola SM (1996) Structure and function of declarative and nondeclarative memory systems. Proc Natl Acad Sci U S A 93:13515-13522.

Stahl N, Yancopoulos GD (1993) The alphas, betas, and kinases of cytokine receptor complexes. Cell 74:587-590.

Stahl N, Farruggella TJ, Boulton TG, Zhong Z, Darnell JE, Jr., Yancopoulos GD (1995) Choice of STATs and other substrates specified by modular tyrosine-based motifs in cytokine receptors. Science 267:1349-1353.

Stepanova T, Slemmer J, Hoogenraad CC, Lansbergen G, Dortland B, De Zeeuw CI, Grosveld F, van Cappellen G, Akhmanova A, Galjart N (2003) Visualization of microtubule growth in cultured neurons via the use of EB3-GFP (end-binding protein 3-green fluorescent protein). J Neurosci 23:2655-2664.

Stewart CL, Kaspar P, Brunet LJ, Bhatt H, Gadi I, Kontgen F, Abbondanzo SJ (1992) Blastocyst implantation depends on maternal expression of leukaemia inhibitory factor. Nature 359:76-79.

Stockli KA, Lottspeich F, Sendtner M, Masiakowski P, Carroll P, Gotz R, Lindholm D, Thoenen H (1989) Molecular cloning, expression and regional distribution of rat ciliary neurotrophic factor. Nature 342:920-923.

Stockli KA, Lillien LE, Naher-Noe M, Breitfeld G, Hughes RA, Raff MC, Thoenen H, Sendtner M (1991) Regional distribution, developmental changes, and cellular localization of CNTF-mRNA and protein in the rat brain. J Cell Biol 115:447-459.

Stoppini L, Buchs PA, Muller D (1991) A simple method for organotypic cultures of nervous tissue. J Neurosci Methods 37:173-182.

Taga T, Kishimoto T (1997) Gp130 and the interleukin-6 family of cytokines. Annu Rev Immunol 15:797-819.

Taga T, Hibi M, Hirata Y, Yamasaki K, Yasukawa K, Matsuda T, Hirano T, Kishimoto T (1989a) Interleukin-6 triggers the association of its receptor with a possible signal transducer, gp130. Cell 58:573-581.

Taga T, Hibi M, Hirata Y, Yawata H, Natsuka S, Yasukawa K, Totsuka T, Yamasaki K, Hirano T, Kishimoto T (1989d) Interleukin-6 receptor and a unique mechanism of its signal transduction. Cold Spring Harb Symp Quant Biol 54 Pt 2:713-722.

Takahashi R (1995) [Deficiency of human ciliary neurotropic factor (CNTF) is not causally related to amyotrophic lateral sclerosis (ALS)]. Rinsho Shinkeigaku 35:1543-1545.

Takahashi R, Kawamura K, Hu J, Hayashi M, Deguchi T (1996) Ciliary neurotrophic factor (CNTF) genotypes and CNTF contents in human sciatic nerves as measured by a sensitive enzyme-linked immunoassay. J Neurochem 67:525-529.

Takahashi R, Yokoji H, Misawa H, Hayashi M, Hu J, Deguchi T (1994) A null mutation in the human CNTF gene is not causally related to neurological diseases. Nature genetics 7:79-84.

Takeda K, Noguchi K, Shi W, Tanaka T, Matsumoto M, Yoshida N, Kishimoto T, Akira S (1997) Targeted disruption of the mouse Stat3 gene leads to early embryonic lethality. Proc Natl Acad Sci U S A 94:3801-3804.

Talcott KE, Ratnam K, Sundquist SM, Lucero AS, Lujan BJ, Tao W, Porco TC, Roorda A, Duncan JL (2011) Longitudinal Study of Cone Photoreceptors during Retinal Degeneration and in Response to Ciliary Neurotrophic Factor Treatment. Invest Ophth Vis Sci 52:2219-2226.

Thoenen H (1995) Neurotrophins and neuronal plasticity. Science 270:593-598.

Thoenen H, Sendtner M (2002) Neurotrophins: from enthusiastic expectations through sobering experiences to rational therapeutic approaches. Nature Neuroscience 5:1046-1050.

Thome J, Kornhuber J, Baumer A, Rosler M, Beckmann H, Riederer P (1996a) CNTF and endogenous psychoses? Nature genetics 12:123.
Thome J, Kornhuber J, Baumer A, Rosler M, Beckmann H, Riederer P (1996c) Association between a null mutation in the human ciliary neurotrophic factor (CNTF) gene and increased incidence of psychiatric diseases? Neurosci Lett 203:109-110.
Thome J, Durany N, Harsanyi A, Foley P, Palomo A, Kornhuber J, Weijers HG, Baumer A, Rosler M, Cruz-Sanchez FF, Beckmann H, Riederer P (1996e) A null mutation allele in the CNTF gene and schizophrenic psychoses. Neuroreport 7:1413-1416.
Tovote P, Fadok JP, Luthi A (2015) Neuronal circuits for fear and anxiety. Nat Rev Neurosci 16:317-331.
Uchida S, Shumyatsky GP (2015) Deceivingly dynamic: Learning-dependent changes in stathmin and microtubules. Neurobiol Learn Mem 124:52-61.
Uchida S, Martel G, Pavlowsky A, Takizawa S, Hevi C, Watanabe Y, Kandel ER, Alarcon JM, Shumyatsky GP (2014) Learning-induced and stathmin-dependent changes in microtubule stability are critical for memory and disrupted in ageing. Nat Commun 5:4389.
van Adel BA, Kostic C, Deglon N, Ball AK, Arsenijevic Y (2003) Delivery of ciliary neurotrophic factor via lentiviral-mediated transfer protects axotomized retinal ganglion cells for an extended period of time. Hum Gene Ther 14:103-115.
van Groen T, Wyss JM (1990) Extrinsic projections from area CA1 of the rat hippocampus: olfactory, cortical, subcortical, and bilateral hippocampal formation projections. The Journal of comparative neurology 302:515-528.
van Hagen BT, van Goethem NP, Lagatta DC, Prickaerts J (2015) The object pattern separation (OPS) task: a behavioral paradigm derived from the object recognition task. Behavioural brain research 285:44-52.
Volterra A, Meldolesi J (2005) Astrocytes, from brain glue to communication elements: the revolution continues. Nat Rev Neurosci 6:626-640.
Voronin LL (1993) On the quantal analysis of hippocampal long-term potentiation and related phenomena of synaptic plasticity. Neuroscience 56:275-304.
Watkins JC, Jane DE (2006) The glutamate story. Br J Pharmacol 147 Suppl 1:S100-108.
Wegrzyn J et al. (2009) Function of Mitochondrial Stat3 in Cellular Respiration. Science 323:793-797.
Weis J, Lie DC, Ragoss U, Zuchner SL, Schroder JM, Karpati G, Farruggella T, Stahl N, Yancopoulos GD, DiStefano PS (1998) Increased expression of CNTF receptor alpha in denervated human skeletal muscle. Journal of neuropathology and experimental neurology 57:850-857.
Wen R, Tao W, Li YW, Sieving PA (2012) CNTF and retina. Prog Retin Eye Res 31:136-151.
Wen Z, Zhong Z, Darnell JE, Jr. (1995) Maximal activation of transcription by Stat1 and Stat3 requires both tyrosine and serine phosphorylation. Cell 82:241-250.
Wilhelm BG, Mandad S, Truckenbrodt S, Krohnert K, Schafer C, Rammner B, Koo SJ, Classen GA, Krauss M, Haucke V, Urlaub H, Rizzoli SO (2014) Composition of isolated synaptic boutons reveals the amounts of vesicle trafficking proteins. Science 344:1023-1028.
Williams LR, Manthorpe M, Barbin G, Nieto-Sampedro M, Cotman CW, Varon S (1984) High ciliary neuronotrophic specific activity in rat peripheral nerve. Int J Dev Neurosci 2:177-180.
Williams RL, Hilton DJ, Pease S, Willson TA, Stewart CL, Gearing DP, Wagner EF, Metcalf D, Nicola NA, Gough NM (1988) Myeloid leukaemia inhibitory factor maintains the developmental potential of embryonic stem cells. Nature 336:684-687.
Wilson MA, Tonegawa S (1997) Synaptic plasticity, place cells and spatial memory: study with second generation knockouts. Trends Neurosci 20:102-106.
Winters BD, Saksida LM, Bussey TJ (2008) Object recognition memory: neurobiological mechanisms of encoding, consolidation and retrieval. Neurosci Biobehav Rev 32:1055-1070.
Wittchen HU, Jacobi F, Rehm J, Gustavsson A, Svensson M, Jonsson B, Olesen J, Allgulander C, Alonso J, Faravelli C, Fratiglioni L, Jennum P, Lieb R, Maercker A, van Os J, Preisig M, Salvador-Carulla L, Simon R, Steinhausen HC (2011) The size and burden of mental disorders and other disorders of the brain in Europe 2010. Eur Neuropsychopharmacol 21:655-679.
Wolosker H, Balu DT, Coyle JT (2016) The Rise and Fall of the d-Serine-Mediated Gliotransmission Hypothesis. Trends in neurosciences 39:712-721.
Xu B, Dube MG, Kalra PS, Farmerie WG, Kaibara A, Moldawer LL, Martin D, Kalra SP (1998) Anorectic effects of the cytokine, ciliary neurotropic factor, are mediated by hypothalamic neuropeptide Y: comparison with leptin. Endocrinology 139:466-473.
Yang Y, Ge W, Chen Y, Zhang Z, Shen W, Wu C, Poo M, Duan S (2003) Contribution of astrocytes to hippocampal long-term potentiation through release of D-serine. Proceedings of the National Academy of Sciences of the United States of America 100:15194-15199.
Yau KW, Schatzle P, Tortosa E, Pages S, Holtmaat A, Kapitein LC, Hoogenraad CC (2016) Dendrites In Vitro and In Vivo Contain Microtubules of Opposite Polarity and Axon Formation Correlates with Uniform Plus-End-Out Microtubule Orientation. J Neurosci 36:1071-1085.

Yivgi-Ohana N, Sher N, Melamed-Book N, Eimerl S, Koler M, Manna PR, Stocco DM, Orly J (2009) Transcription of steroidogenic acute regulatory protein in the rodent ovary and placenta: alternative modes of cyclic adenosine 3', 5'-monophosphate dependent and independent regulation. Endocrinology 150:977-989.

Yuste R, Bonhoeffer T (2001) Morphological changes in dendritic spines associated with long-term synaptic plasticity. Annu Rev Neurosci 24:1071-1089.

Zakharenko SS, Zablow L, Siegelbaum SA (2001) Visualization of changes in presynaptic function during long-term synaptic plasticity. Nat Neurosci 4:711-717.

Zearfoss NR, Alarcon JM, Trifilieff P, Kandel E, Richter JD (2008) A molecular circuit composed of CPEB-1 and c-Jun controls growth hormone-mediated synaptic plasticity in the mouse hippocampus. J Neurosci 28:8502-8509.

Zhang JM, An J (2007) Cytokines, inflammation, and pain. Int Anesthesiol Clin 45:27-37.

Zhang K, Hopkins JJ, Heier JS, Birch DG, Halperin LS, Albini TA, Brown DM, Jaffe GJ, Tao W, Williams GA (2011) Ciliary neurotrophic factor delivered by encapsulated cell intraocular implants for treatment of geographic atrophy in age-related macular degeneration. Proceedings of the National Academy of Sciences of the United States of America 108:6241-6245.

Zhong Z, Wen Z, Darnell JE, Jr. (1994) Stat3: a STAT family member activated by tyrosine phosphorylation in response to epidermal growth factor and interleukin-6. Science 264:95-98.

Zola-Morgan S, Squire LR, Amaral DG (1986) Human amnesia and the medial temporal region: enduring memory impairment following a bilateral lesion limited to field CA1 of the hippocampus. J Neurosci 6:2950-2967.

Zola SM, Squire LR, Teng E, Stefanacci L, Buffalo EA, Clark RE (2000) Impaired recognition memory in monkeys after damage limited to the hippocampal region. J Neurosci 20:451-463.

6 Appendix

6.1 Supplementary data

Table 11 Supplementary table S1: Entries in anxiety-related behavioral paradigms

			male		female	
cohort	experiment	# entries into	wt	*Cntf* $^{-/-}$	wt	*Cntf* $^{-/-}$
1	DL	light	28.57 ± 6.554	28.20 ± 10.55	-	-
2	OF	center	16.13 ± 2.949	16.00 ± 3.00	14.80 ± 5.167	11.00 ± 4.690
	DL	light	32.43 ± 3.409	29.33 ± 6.506	24.00 ± 7.874	26.25 ± 9.639
	EPM	open arms	6.833 ± 2.483	6.00 ± 1.732	7.60 ± 2.408	10.75 ± 4.272
3	OF	center	12.20 ± 2.557	10.33 ± 1.045	14.4 ± 2.926	13.00 ± 2.799
	EPM	open arms	13.33 ± 3.615*	6.833 ± 2.563*	12.40 ±4.099	11.00 ±6.782

* p = 0.013, Mann Whitney

Table 12 Supplementary table S2: Statistical analysis

Fig. 8 B					
Unpaired t-test	Sig. diff?	t, df	Summary	One/ two-tailed P value?	P value
wt vs. ko	No	t = 1,170 df = 27	ns	Two-tailed	0,2523
One sample t-test	Sig. diff?	t, df	Summary	One/ two-tailed P value?	P value
wt vs. 0	Yes	t = 3,892, df = 17	**	Two-tailed	0,0012
wt vs. 0	No	1,116, 10	ns	Two-tailed	0,2903
Fig. 8 C					
One sample t-test	Sig. diff?	t, df	Summary	One/ two-tailed P value?	P value
wt vs. 50%	Yes	t = 3,892, df = 17	**	Two-tailed	0,0012
wt vs. 50%	No	t = 1,116, df = 10	ns	Two-tailed	0,2903
Fig. 9 A					
ANOVA table	SS	DF	MS	F (DFn, DFd)	P value
Interaction	298,9	4	74,74	F (4, 84) = 0,6728	P = 0,6127
Run	18104	4	4526	F (4, 84) = 40,75	P < 0,0001
Genotype	121,0	1	121,0	F (1, 21) = 0,3752	P = 0,5467
ANOVA table	SS	DF	MS	F (DFn, DFd)	P value
Interaction	804,0	4	201,0	F (4, 48) = 1,965	P = 0,1150
Run	14101	4	3525	F (4, 48) = 31,45	P < 0,0001
Cohort 2 vs. 3 wt	414,1	1	414,1	F (1, 12) = 1,798	P = 0,2048
ANOVA table	SS	DF	MS	F (DFn, DFd)	P value
Interaction	637,7	4	159,4	F (4, 28) = 1,499	P = 0,2294
Run	6346	4	1586	F (4, 28) = 14,91	P < 0,0001
Cohort 2 vs. 3 ko	156,2	1	156,2	F (1, 7) = 0,3181	P = 0,5904
Fig. 9 B					
ANOVA table	SS	DF	MS	F (DFn, DFd)	P value
Interaction	194,2	4	48,54	F (4, 68) = 0,3948	P = 0,8117
Run	8634	4	459,4	F (4, 68) = 17,65	P < 0,0001
Genotype	459,4	1	459,4	F (1, 17) = 1,131	P = 0,3024
ANOVA table	SS	DF	MS	F (DFn, DFd)	P value
Interaction	616,0	4	154,0	F (4, 36) = 1,074	P = 0,3836
Run	4629	4	1157	F (4, 36) = 8,072	P < 0,0001
Cohort 2 vs. 3 wt	600,3	1	600,3	F (1, 9) = 2,241	P = 0,1685
ANOVA table	SS	DF	MS	F (DFn, DFd)	P value
Interaction	215,1	4	53,79	F (4, 24) = 0,5454	P = 0,7040
Run	4304	4	1076	F (4, 24) = 10,91	P < 0,0001
Cohort 2 vs. 3 ko	704,3	1	704,3	F (1, 6) = 1,326	P = 0,2934
Fig. 9 C					
ANOVA table	SS	DF	MS	F (DFn, DFd)	P value
Interaction	11,99	3	3,996	F (3, 84) = 0,2876	P = 0,8343
Quadrant	1781	3	593,8	F (3, 84) = 42,73	P < 0,0001
Genotype	0,1753	1	0,1753	F (1, 84) = 0,01261	P = 0,9109
ANOVA table	SS	DF	MS	F (DFn, DFd)	P value
Interaction	61,38	3	20,46	F (3, 48) = 1,284	P = 0,2904
Quadrant	1029	3	342,9	F (3, 48) = 21,52	P < 0,0001
Cohort 2 vs. 3 wt	1,585	1	1,585	F (1, 48) = 0,09953	P = 0,7538
ANOVA table	SS	DF	MS	F (DFn, DFd)	P value
Interaction	10,41	3	3,469	F (3, 28) = 0,2953	P = 0,8284
Quadrant	786,8	3	262,3	F (3, 28) = 22,33	P < 0,0001
Cohort 2 vs. 3 ko	0,3744	1	0,3744	F (1, 28) = 0,03187	P = 0,8596
Fig. 9 D					
ANOVA table	SS	DF	MS	F (DFn, DFd)	P value

Interaction	18,56	3	6,187	F (3, 76) = 0,3002	P = 0,8251
Quadrant	787,9	3	262,6	F (3, 76) = 12,74	P < 0,0001
Genotype	0,02226	1	0,02226	F (1, 76) = 0,001080	P = 0,9739
ANOVA table	SS	DF	MS	F (DFn, DFd)	P value
Interaction	10,58	3	3,526	F (3, 44) = 2390	P = 0,8687
Quadrant	640,3	3	313,4	F (3, 44) = 14,46	P < 0,0001
Cohort 2 vs. 3 wt	0,5167	1	0,5167	F (1, 44) = 0,03502	P = 0,8524
ANOVA table	SS	DF	MS	F (DFn, DFd)	P value
Interaction	71,73	3	23,91	F (3, 24) = 0,6886	P = 0,5679
Quadrant	254,3	3	84,76	F (3, 24) = 2,441	P = 0,0889
Cohort 2 vs. 3 ko	0,6492	1	0,6492	F (1, 24) = 0,01870	P = 0,8924
Fig. 12					
ANOVA table	SS	DF	MS	F (DFn, DFd)	P value
Interaction	1716	4	429,1	F (4, 52) = 6,665	P = 0,0002
Phase	9714	4	2429	F (4, 52) = 37,73	P < 0,0001
Cohort	2574	1	2574	F (1, 13) = 7,868	P = 0,0149
Tukey's multiple comp	Mean Diff.	95% CI of diff.	Significant?	Summary	Adjusted P Value
cohort 1 vs. 2 (after)	26,99	12,18 to 41,80	Yes	****	< 0,0001
cohort 1 vs 2 (B tone)	17,55	2,738 to 32,35	Yes	*	< 0,0128
Fig. 12 B					
ANOVA table	SS	DF	MS	F (DFn, DFd)	P value
Interaction	556,2	4	139,0	F (4, 60) = 1,910	P = 0,1205
Phase	13987	4	3497	F (4, 60) = 48,03	P < 0,0001
Genotype	479,6	1	479,6	F (1, 15) = 1,608	P = 0,2241
Tukey's multiple comp	Mean Diff.	95% CI of diff.	Significant?	Summary	Adjusted P Value
before vs. after (wt)	-37,01	-49,84 to -24,19	Yes	****	< 0,0001
B vs. B tone (wt)	-25,72	-38,55 to -12,89	Yes	****	< 0,0001
A vs. B (wt)	-3,348	-16,18 to 9,480	No	ns	0,9477
before vs. after (ko)	-27,27	-38,00 to -16,54	Yes	****	< 0,0001
B vs. B tone (ko)	-15,67	-26,40 to -4,935	Yes	**	0,0011
A vs. B (ko)	-5,734	-16,47 to 4,998	No	ns	0,5649
Fig. 13 B					
ANOVA table	SS	DF	MS	F (DFn, DFd)	P value
Interaction	215,5	3	71,83	F (3, 30) = 0,6803	P = 0,5710
Phase	7513	3	2504	F (3, 30) = 23,72	P < 0,0001
Genotype	35,46	1	35,46	F (1, 10) = 0,1333	P = 0,7227
Tukey's multiple comp	Mean Diff.	95% CI of diff.	Significant?	Summary	Adjusted P Value
before vs. after (wt)	-15,10	-31,23 to 1,027	No	ns	0,0729
B vs. B tone (wt	-31,56	-47,69 to -15,43	Yes	****	< 0,0001
before vs. after (ko)	-10,04	-26,17 to 6,086	No	ns	0,3448
B vs. B tone (ko)	-25,36	-41,49 to -9,231	Yes	***	0,0010
Fig. 13 D					
ANOVA table	SS	DF	MS	F (DFn, DFd)	P value
Interaction	1093	3	364,3	F (3, 15) = 4,756	P = 0,0159
Phase	6123	3	2041	F (3, 15) = 11,51	P = 0,0004
Genotype	1445	1	1445	F (1, 5) = 8,770	P = 0,0315
Tukey's multiple comp	Mean Diff.	95% CI of diff.	Significant?	Summary	Adjusted P Value
E1 early vs. late (wt)	13,69	-0,8697 to 28,26	No	ns	0,0688
E2 early vs. late (wt)	29,97	15,41 to 44,54	Yes	***	0,0001
E1 early vs. late (ko)	28,75	14,19 to 43,31	Yes	***	0,0002
E2 early vs. late (ko)	17,75	3,186 to 32,31	Yes	*	0,0148
wt vs. ko (early E1)	-25,14	-45,61 to -4,672	Yes	*	0,0106
B tone vs. late E2 (wt)	21,69	-2,068 to 45,46	No	ns	0,0735
B tone vs. late E2 (ko)	13,03	-10,73 to 36,79	No	ns	0,3284
Fig. 13 F					
ANOVA table	SS	DF	MS	F (DFn, DFd)	P value
Interaction	17,51	1	17,51	F (1, 10) = 0,04333	P = 0,8393
Phase	1144	1	1144	F (1, 10) = 2,830	P = 0,1235
Genotype	1418	1	1418	F (1, 10) = 2,897	P = 0,1196
Sidak's multiple comp.	Mean Diff.	95% CI of diff.	Significant?	Summary	Adjusted P Value
A vs. A tone (wt)	-12,10	-42,58 to 18,39	No	ns	0,5401
A vs. A tone (ko)	-15,51	-46,00 to 14,97	No	ns	0,3774
late E2 vs. A (wt)	-3,528	-19,64 to 12,59	No	ns	0,8220
late E2 vs. A (ko)	-6,750	-22,87 to 9,366	No	ns	0,5059
Fig. 14 B					
ANOVA table	SS	DF	MS	F (DFn, DFd)	P value
Interaction	1038	4	259,4	F (4, 60) = 1,150	P = 0,3420
Phase	13979	4	3495	F (4, 60) = 15,49	P < 0,0001
Genotype	837,8	1	837,8	F (1, 15) = 2,540	P = 0,1318
Tukey's multiple comp	Mean Diff.	95% CI of diff.	Significant?	Summary	Adjusted P Value
before vs. after (wt)	-28,81	-48,73 to -8,901	Yes	**	0,0013

before vs. retr. (wt)	-39,17	-59,08 to -19,25	Yes	****	< 0,0001
retr. vs. late E (wt)	13,72	-6,191 to 33,64	No	ns	0,3089
late E vs. rec. (wt)	-5,231	-25,14 to 14,68	No	ns	0,9465
before vs. after (ko)	-27,75	-48,87 to -6,632	Yes	**	0,0042
before vs. retr. (ko)	-38,33	-59,45 to -17,20	Yes	****	< 0,0001
retr. vs. late E (ko)	28,52	7,400 to 49,64	Yes	**	0,0031
late E vs. rec. (ko)	-6,771	-27,89 to 14,35	No	ns	0,8952
Fig. 15					
Mann-Whitney	Sig. diff?	Sum ranks A, B	Summary	Exact or approximate?	P value
1 vs. 2 (time wt m)	Yes	70 , 21	*	Exact	0,0451
1 vs. 2 (time wt fem)	Yes	40 , 15	**	Exact	0,0079
1 vs. 2 (time ko fem)	Yes	26 , 10	*	Exact	0,0286
Fig. 16 A, E					
Mann-Whitney	Sig. diff?	Sum ranks A, B	Summary	Exact or approximate?	P value
1 vs. 2 (dist. wt m)	No	58 , 62	ns	Exact	0,8454
1 vs. 2 (time wt m)	No	64 , 56	ns	Exact	0,3916
1 vs. 2 (dist. ko m)	No	70 , 21	ns	Exact	> 0,9999
1 vs. 2 (time ko m)	No	74 , 17	ns	Exact	0,4965
Unpaired t-test	Sig. diff?	t, df	Summary	One/ two-tailed P value?	P value
wt vs. ko (time)	No	t=0,5927 df=26	ns	Two-tailed	0,5585
wt vs. ko (distance)	Yes	t=2,795 df=26	**	Two-tailed	0,0096
Fig. 17					
Mann-Whitney	Sig. diff?	Sum ranks A, B	Summary	Exact or approximate?	P value
1 vs. 2 (dist. m wt)	Yes	57 , 21	**	Exact	0,0022
1 vs. 2 (time fem wt)	Yes	40 , 15	**	Exact	0,0079
Fig. 20 D					
Unpaired t-test	Sig. diff?	t, df	Summary	One/ two-tailed P value?	P value
wt vs. ko (ctrl)	Yes	t=4,157 df=28	***	Two-tailed	0,0003
Fig. 20 E					
Wilcoxon	Sig. diff?	Sum of ranks	Summary	One/ two-tailed P value?	P value
ctrl vs. Cntf (wt)	No	14,00 , -64,00	ns	Two-tailed	0,0522
Fig. 20 F					
Paired t-test	Sig. diff?	t, df	Summary	One/ two-tailed P value?	P value
ctrl vs. Cntf (ko)	Yes	t=3,095 df=8	*	Two-tailed	0,0148
Fig. 20 G					
Paired t-test	Sig. diff?	t, df	Summary	One/ two-tailed P value?	P value
ctrl vs. BSA (wt)	No	t=0,3976 df=9	ns	Two-tailed	0,7002
Fig. 20 H					
Mann-Whitney	Sig. diff?	Sum ranks A, B	Summary	Exact or approximate?	P value
ctrl vs. BSA (ko)	No	51 , 54	ns	Two-tailed	0,9015
Fig. 21 C					
Paired t-test	Sig. diff?	t, df	Summary	One/ two-tailed P value?	P value
ctrl vs. LTP (wt)	Yes	t=3,480 df=10	**	Two-tailed	0,0059
Fig. 21 D					
Paired t-test	Sig. diff?	t, df	Summary	One/ two-tailed P value?	P value
ctrl vs. LTP (ko)	Yes	t=5,544 df=4	**	Two-tailed	0,0052
Fig. 21 E					
Tukey's multiple comp	Mean Diff.	95% CI of diff.	Significant?	Summary	Adjusted P Value
ctrl vs. LTP	0,2541	-0,1916 to 0,6998	No	ns	0,2779
ctrl vs. LTPCntf	0,3653	-0,0106 to 0,7412	No	ns	0,0560
CNTF vs. LTPCntf	0,1112	-0,0747 to 0,2972	No	ns	0,2500
Fig. 21 F					
Tukey's multiple comp	Mean Diff.	95% CI of diff.	Significant?	Summary	Adjusted P Value
ctrl vs. LTP	-0,09775	-0,4035 to 0,2080	No	ns	0,6142
ctrl vs. LTPCntf	-0,08628	-0,3705 to 0,1979	No	ns	0,6421
CNTF vs. LTPCntf	0,01147	-0,2719 to 0,2948	No	ns	0,9915
Fig. 23 C, D					
1way ANOVA	SS	DF	MS	F (DFn, DFd)	P value
pStat3/vGluT/Phall	1,017	3	0,3391	F (3, 48) = 72,22	P < 0,0001
Tukey's multiple comp	Mean Diff.	95% CI of diff.	Significant?	Summary	Adjusted P Value
vGlut vs. Phall (wt)	-0,2811	-0,3588 to -0,2033	Yes	****	< 0,0001
vGlut vs. Phall (ko)	-0,2747	-0,3413 to -0,2081	Yes	****	< 0,0001
Fig. 23 G					
KruskalWallis ANOVA	Sig. diff?	KW statistic	Summary	Exact or approximate?	P value
pre vs. post (wt, ko)	Yes	99,51	****	approximate	< 0,0001
Dunn's multiple comp.		Mean rank diff,	Significant?	Summary	Adjusted P Value
pre vs. post (wt)		73,74	Yes	****	< 0,0001
pre vs. post (ko)		76,69	Yes	****	< 0,0001
wt vs. ko (pre)		-6,908	No	ns	> 0,9999
wt vs. ko (post)		-3,957	No	ns	> 0,9999

Fig. 23 H					
Mann-Whitney	Sig. diff?	Sum ranks A, B	Summary	Exact or approximate?	P value
wt vs. ko (pre/post)	Yes	1114 , 1661	*	Exact	0,0103
Fig. 25 A					
KruskalWallis ANOVA	Sig. diff?	KW statistic	Summary	Exact or approximate?	P value
spine vs. astro (wt,ko)	Yes	48,96	****	approximate	< 0,0001
Dunn's multiple comp.		Mean rank diff,	Significant?	Summary	Adjusted P Value
wt vs. ko (spine)		95,02	Yes	*	0,0436
wt vs. ko (astro)		207,5	Yes	****	< 0,0001
presyn vs. astro (wt)		-147,6	Yes	***	0,0009
presyn vs. astro (ko)		-35,15	No	ns	> 0,9999
Fig. 25 B					
KruskalWallis ANOVA	Sig. diff?	KW statistic	Summary	Exact or approximate?	P value
presyn vs.astro(wt,ko)	Yes	115,8	****	approximate	< 0,0001
Dunn's multiple comp.		Mean rank diff,	Significant?	Summary	Adjusted P Value
wt vs. ko (spine)		2,541	No	ns	> 0,9999
wt vs. ko (astro)		232,4	Yes	****	< 0,0001
presyn vs. astro (wt)		-353,8	Yes	****	< 0,0001
presyn vs. astro (ko)		-124,0	Yes	**	0,0018
Fig. 25 C					
Linear regression	R Square	Sign. from zero?	F	DFn, DFd	P value
wt presynapses	0,8432	Yes	2609	1,000, 485,0	< 0,0001
Fig. 25 D					
Linear regression	R Square	Sign. from zero?	F	DFn, DFd	P value
ko presynapses	0,8034	Yes	2783	1,000, 681,0	< 0,0001
Fig. 25 E					
Linear regression	R Square	Sign. from zero?	F	DFn, DFd	P value
wt astro	0,7682	Yes	1524	1,000, 460,0	< 0,0001
Fig. 25 F					
Linear regression	R Square	Sign. from zero?	F	DFn, DFd	P value
ko astro	0,8076	Yes	2283	1,000, 544,0	< 0,0001

SS = sum of squares, CI = confidence interval, DF = degrees of freedom, MS = mean square, DFn = degrees of freedom numerator, DFd = degrees of freedom denominator, P = probability value, ko = *Cntf* $^{-/-}$

6.2 List of tables

6.3 List of figures

6.4 Abbreviations

°C	degree celsius
µm	micrometer
ACSF	artificial cerebrospinal fluid
AMPA	α-amino-3-hydroxy-5-methyl-4-isoxazolepropionic acid
AMPAR	α-amino-3-hydroxy-5-methyl-4-isoxazolepropionic acid receptor
BME	basal medium eagle
Bdnf	brain derived neurotrophic factor
BSA	bovine serum albumin
CA1	cornu ammonis 1
CA3	cornu ammonis 3
CD-1	cardiotrophin 1
CLC	cardiotrophin like cytokine
cm	centimeter
Cntf	ciliary neurotrophic factor
CntfRα	ciliary neurotrophic factor receptor α
CNS	central nerve system
Creb	cAMP response element-binding protein
CS	conditioned stimulus
CPEB-1	cytoplasmic polyadenylation element binding protein 1
DG	dentate gyrus
DL	dark light
DNA	deoxyribonucleic acid
dNTP	deoxyribose nucleoside triphosphate
DR	discrimination ratio
DTT	dithiothreito
EDTA	ethylenediaminetetraacetic acid
EPM	elevated plus maze
EPSP	Excitatory postsynaptic potential
FC	fear conditioning
Gapdh	glyceraldehyde-3-phosphate dehydrogenase
Gfap	glial fibrillary acidic protein
GH	growth hormone
GluA2	glutamate receptor ionotropic AMPA2
GTPase	nucleotide guanosine triphosphate hydrolase enzyme
h	hour
HBSS	Hank's buffered salt solution
H_20	water
HP	hot plate
Il-6	internleukin 6

Il-6R	internleukin 6 receptor
Il-11	internleukin 11
IR	immunoreactivity
Jak	janus kinase
Kif5	kinesin related protein 5
Lif	leukemia inhibitory factor
LifRß	leukemia inhibitory factor receptor β
LMD	laser micro dissection
LTP	long term potentiation
LV	lateral ventricle
min	minute
mm	millimeter
MWM	Morris water maze
NB	Neurobasal medium
NGF	neurotrophic growth factor
NMDA	*N*-methyl-d-aspartate
NMDAR	*N*-methyl-d-aspartate receptor
NOR	novel object recognition
Nt3	neurotrophic factor 3
Nt4	neurotrophic factor 4
OF	open field
OSM	oncostatin M
PBS	phosphate buffered saline
PCR	polmerase chain reaction
pCreb	phosphorylated cAMP response element-binding protein
pStat3	phosphorylated signal transducer and activator 3
RGB	red/green/blue
RNA	ribonucleic acid
RT	reverse transcriptase
SDS	sodium dodecyl sulfate
s	second
Socs	suppressor of cytokine signaling
Stat3	signal transducer and activator 3
TAE	tris, acetic acid, EDTA
TBS	tris buffered saline
TBST	tris buffered saline with tween
TEMED	tetramethylethylenediamine
Trk	tyrosine receptor kinase
US	unconditioned stimulus
vGluT	vesicular glutamate transporter

6.5 Affidavit / *Eidesstattliche Erklärung gemäß ASPO vom 05.08. 2009 § 23 Abs. 10*

Affidavit

I hereby confirm that my thesis entitled **"The role of Ciliary Neurotrophic Factor in hippocampal synaptic plasticity and learning"** is the result of my own work. I did not receive any help or support from commercial consultants. All sources and/or and materials applied are listed and specified in the thesis.

Furthermore, I confirm that this thesis has not yet been submitted as part of another examination process neither in identical nor in similar form.

Place, Date Signature

Eidesstattliche Erklärung

Hiermit erkläre ich an Eides statt, dass ich die Dissertation mit dem Titel **„Die Rolle von Ciliary Neurotrophic Factor bei hippocampaler synaptischer Plastizität und Lernen"** eigenständig, d.h. insbesondere selbstständig und ohne Hilfe eines kommerziellen Promotionspartners angefertigt und keine anderen als die von mir angegebenen Quellen und Hilfsmittel verwendet zu haben.

Ich erkläre außerdem, dass die Dissertation weder in gleicher noch in ähnlicher Form bereits in einem anderen Prüfungsverfahren vorgelegen hat.

Ort, Datum Unterschrift